



Joy's Law, Anti-Hale Classifications, and the Evolution of Emerging Sunspot Regions

A Thesis submitted by

Bruce H. McClintock, B.Sc., M.A.

For the award of

Doctor of Philosophy

2016

Abstract

This thesis aims to use analysis of the time dependence of sunspot locations and other physical characteristics to provide an improved empirical basis for understanding solar magnetic fields. Bipolar active regions in both hemispheres tend to be tilted with respect to the East–West Equator of the Sun in accordance with Joy’s law, which describes the average tilt angle as a function of latitude. We recommend a revision of Joy’s law towards a weaker dependence on latitude (slope of 0.13–0.26) and without forcing the tilt to zero at the Equator. We determine that the hemispheric mean tilt value of active regions varies with each solar cycle but mean tilt angles do not show a dependence on longitude for any hemisphere or cycle. We also explore the visual representation of magnetic tilt angles on a traditional butterfly diagram to show that the average latitude of anti-Hale regions does not differ from the average latitude of all regions in both hemispheres. The distribution of anti-Hale sunspot tilt angles is broadly distributed between 0 and 360° with a weak preference for east-west alignment 180° from their expected Joy’s law angle. Anti-Hale sunspots display a log-normal size distribution similar to that of all sunspots, indicating no preferred size for anti-Hale spots. In addition, we report that $8.4\% \pm 0.8\%$ of all bipolar sunspot regions are misclassified as Hale in traditional catalogues. This percentage is slightly higher for groups within 5° of the Equator due to the misalignment of the magnetic and heliographic equators. We also investigate bipolar sunspot regions and how tilt angle and footpoint separation vary during emergence and decay, finding that within ± 48 hours of the time of peak umbral area, large regions steadily increase in tilt angle, midsize regions are nearly constant, and small regions show evidence of negative tilt during emergence. A period of growth in footpoint separation occurs over a 72-hour period for all of the regions from roughly 40 to 70 Mm. The smallest bipoles are outliers in that they do not obey Joy’s law and have a much smaller footpoint separation. We confirm previous research that the sunspots appear to be two distinct populations, where the smallest spots are potentially supergranular precursors to the more familiar flux tube sunspots. In summary, this thesis has revealed increased complexity in sunspot behavior compared to previous studies and demonstrates that analysis of sunspot observations continues to provide an empirical basis for improved models of small-scale solar flux tubes and the underlying magnetic dynamo.

Certification of Thesis

This thesis is entirely the work of Bruce H. McClintock, except where otherwise acknowledged. The work is original and has not previously been submitted for any other award, except where acknowledged.

Student and supervisors signatures of endorsement are held at USQ.

Acknowledgements

First, I would like to thank the members of the independent thesis examiners committee for volunteering their time to review my research. I thank Stephen Marsden and the University of Southern Queensland staff for their supervision and guidance through the entire process.

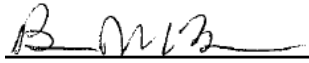
This research work was enabled by NASA contract NAS5-02139 (HMI/SDO) to Stanford University and supported by the HMI science team. Thanks to Tünde Baranyi along with the scientists and staff at Debrecen Heliophysical Observatory for their published data sets. The work of many at Mt. Wilson Observatory over the last century significantly informed my research and is much appreciated. Many thanks to Jing Li and Roger Ulrich for graciously sharing reduced data sets from their own research.

I have the utmost respect and appreciation for my supervisor, Aimee Norton, who always knew what to do to ensure my success. She has been a patient mentor and dedicated advocate on my behalf. I am so thankful for the time and effort she invested in me.

A debt of gratitude to my family for their love, support and understanding over the past few years. Special thanks to my mother for fostering my curiosity and desire for knowledge. And a dedication to my father who taught me the confidence and self-reliance necessary to complete this endeavor.

Statement of Authorship

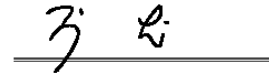
Each author certifies by signature that the stated contributions to the publications listed are accurate and permission is granted to include the publications in the thesis.



Bruce McClintock



Aimee Norton



Jing Li

.....

MCCLINTOCK, B. H., & NORTON, A. A. (2013). Recovering Joy's law as a function of solar cycle, hemisphere, and longitude. *Solar Physics*, **287**, 215-227.

Authors	Contributions	pct.
Bruce McClintock	Reviewed previous research; analyzed and interpreted data; wrote a majority of the manuscript; acted as corresponding author	60%
Aimee Norton	Suggested topic, references to review; supervised development of topic and data interpretation; wrote portions of manuscript	40%

MCCLINTOCK, B. H., NORTON, A. A., & LI, J. (2014). Re-examining sunspot tilt angle to include anti-Hale statistics. *The Astrophysical Journal*, **797**, 130.

Authors	Contributions	pct.
Bruce McClintock	Reviewed previous research; analyzed and interpreted data; wrote a majority of the manuscript; acted as corresponding author	70%
Aimee Norton	Suggested topic, references for literature review; supervised progress; evaluated manuscript for publication	20%
Jing Li	Reduced raw data to viable data sets; suggested minor revisions to final draft for publication	10%

MCCLINTOCK, B. H., & NORTON, A. A. (2016). Tilt Angle and Footpoint Separation of Small and Large Bipolar Sunspot Regions Observed with HMI. *The Astrophysical Journal*, **818**, 7.

Authors	Contributions	pct.
Bruce McClintock	Selected topic and reviewed previous research; analyzed and interpreted data; wrote the manuscript; acted as corresponding author	90%
Aimee Norton	Supervised overall progress	10%

Table of Contents

Abstract	i
Certification of Thesis	ii
Acknowledgements	iii
Statement of Authorship	iv
1 Introduction	1
1.1 Motivation	1
1.2 An Astrophysical Dynamo	2
1.3 Sunspot Cycle	7
1.4 Sunspot Observations	10
1.5 Joy's Law	12
1.6 Potential Causes of Joy's Law	14
1.7 Statement of Thesis Objectives	15
2 Recovering Joy's Law as a Function of Solar Cycle, Hemisphere, and Longitude	16
2.1 Data	17
2.2 Recovering Joy's Law	18
2.3 Joy's Law as a Function of Hemisphere	22
2.4 Joy's Law as a Function of Longitude: Searching for Evidence of a Tipped Toroidal Field in Tilt Angle Data	26
2.5 Discussion	28
3 Re-Examining Sunspot Tilt Angle to Include Anti-Hale Statistics	30
3.1 Data	33
3.2 Adding Tilt Angle to Butterfly Diagrams	34
3.3 Anti-Hale Regions	42
3.4 Equatorial Regions	47
3.5 Other Efforts to Include Tilt Angle in Butterfly Diagrams	48

3.6 Discussion.....	50
4 Tilt Angle and Footpoint Separation of Small and Large Bipolar Sunspot Regions Observed with HMI	54
4.1 Data.....	56
4.2 Bipolar Sunspot Behavior during Emergence and Decay	57
4.3 Very Small Bipolar Sunspot Regions.....	62
4.4 Discussion.....	64
5 Conclusion	66
5.1 Summary.....	66
5.2 Overall Findings	68
5.3 Future Research	69
Bibliography	71
Publications	80

1 Introduction

This chapter introduces fundamental concepts in support of the subsequent research as well as the motivation for this work (1.1). A general overview of magnetic field production by the astrophysical dynamo (1.2) in the Sun is provided. The general features of the sunspot cycle (1.3) are discussed as well as relevant sunspot observations (1.4). We address the importance of Joy's law (1.5), potential causes of Joy's law (1.6), and how it relates to the generation of magnetic fields in the Sun. The introduction concludes with a statement of the thesis objectives (1.7).

1.1 Motivation

The prevailing theory of the solar dynamo has toroidal magnetic fields generated at the tachocline between the radiative and convective zones becoming buoyant and rising through the convective zone as flux loops, forming bipolar sunspot groups when the loops break the surface. The tilt angles of these groups with respect to the Equator varies as a function of latitude (Joy's law) and was observed daily over several solar cycles at Mount Wilson Observatory (MWO). To investigate whether the Northern and Southern hemispheres of the Sun host dynamo processes that are independent of each other, we look at the MWO data for variations in Joy's law between hemispheres across solar cycles. We also search for a dependence of tilt angle on longitude as it relates to the origins of the toroidal field lines at depth.

Solar cycles are typically reported as ending on a single date, presenting a problem with assigning late-cycle (or early-cycle) active regions to a particular cycle. During the transitional time between cycles, high latitude active regions are still emerging while activity from the previous solar cycle continues near the Equator. We separate the distinct cycles as a function of time and latitude so that new cycle sunspot groups appearing at high latitudes are not incorrectly identified as anti-Hale. Similar problems with hemispheric classifications have been observed as far back as Solar Cycle 12 by Maunder & Maunder (1904), where sunspot production from one hemisphere appears to cross the Equator. We distinguish between heliographic and magnetic equators by defining the magnetic equator in a similar fashion to Zolotova et al. (2009) as the difference in sunspot group latitudes between the hemispheres. Using tilt angle measurements that include polarity, collected by Li and Ulrich (2012), we explore whether a percentage of anti-Hale sunspot regions near the Equator are due

to Northern (Southern) polarity spot groups appearing below (above) the heliographic equator.

Joy's law is inherently noisy and overall trends in tilt angle are difficult to observe for individual active regions. However, the evolution of tilt angle for a particular active region from early emergence through the decay period provides insight into the magnetic field formation and distribution associated with these regions. Images taken by the Helioseismic and Magnetic Imager (HMI) on board NASA's Solar Dynamics Observatory were used to calculate bipolar sunspot tilt angles for HMI - Debrecen Data (HMIDD), which we used to identify NOAA regions with umbral signatures to record tilt angle and footpoint separation measurements. Peak umbral area establishes the end of emergence and the beginning of sunspot decay for each region, serving as a universal reference point common to all of the active regions. We look for trends in tilt angle and footpoint separation during the emergence and decay periods, keeping in mind the physical processes such as convection that could compete with or influence the flux emergence process. Correlations between tilt angle behavior of an active region with parameters such as sunspot size and total magnetic flux can provide insight into the forces that determine Joy's law.

1.2 An Astrophysical Dynamo

The existence of the Sun's magnetic field was discovered by observing the spectra of sunspots (Hale 1908). The production of magnetic fields in celestial bodies is believed to originate from an astrophysical dynamo. A dynamo can be described as a process that converts the mechanical energy of an electrically conductive fluid into a magnetic field. The solar dynamo is considered to be a convective dynamo, in that motions due to turbulent convection regenerate and amplify magnetic fields (Miesch 2012). A strong magnetic field is thought to be housed in the tachocline region, the relatively thin layer between the radiative zone and the convective zone that has a large shear profile (Gilman 2000).

Faraday's law maintains that if an electrically conductive material is moved through a pre-existing magnetic field, then an electric current is produced in the material. By Ampere's law, an electric current produces a magnetic field around the current. Moving conductive fluid through a magnetic field creates an electric current in the fluid which in turn induces a magnetic field. By moving the electrically conductive plasma in the Sun through a seed magnetic field, additional magnetic flux is created. Magnetic fields are strengthened by the twisting, stretching, and folding that occur as a result of rotational dynamics and convective zone turbulence. For a complete treatment of the nonlinear equations describing the solar dynamo, see Deluca and Gilman (1986a, 1986b).

Observations of rotational rates (Ω) with respect to latitude, as seen in Figure 1.1, have indicated differential rotation in the convective zone. Figure 1.2 shows the radiative zone rotates essentially as a solid body. The equatorial region of the

convective zone rotates the fastest, with Ω ranging from about 25 days at the equator to 35 days in the polar regions. Rotation rates in the convective zone do not appear to change significantly with depth, remaining nearly constant at each latitude. The entire radiative zone takes approximately 27 days to complete a rotation. It has been difficult to observe the rotation of the solar core, but research using fluctuations in neutrino output and solar brightness suggests a rotation rate of approximately 25 days (Sturrock 2008).

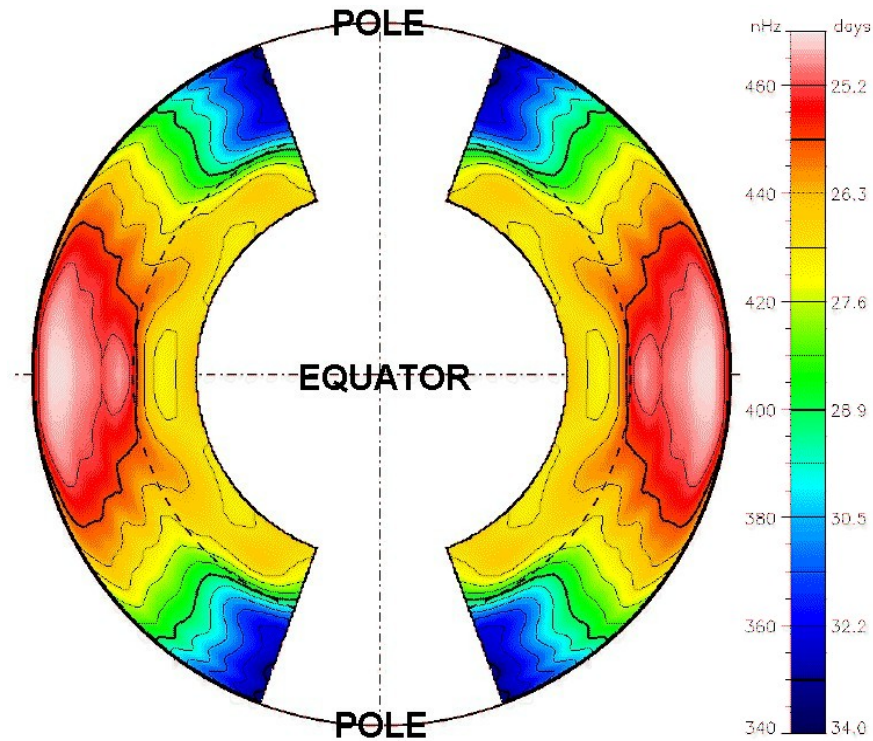


Figure 1.1: Sidereal rotation rates inside the Sun. The color key on the right indicates the rotation rate in nanohertz and the corresponding period in days. The approximate base of the convection zone is indicated by the dashed line at approximately $r = 0.7R$. Image by M. J. Thompson obtained from Marshall Space Flight Center/NASA at <http://solarscience.msfc.nasa.gov/Helioseismology.shtml>

The abrupt transition from differential rotation to solid body rotation (see Figure 1.2) between the convective and radiative zones is a layer of high shear and is believed to be the region where magnetic field re-generation occurs in the Sun. As the convective zone moves past the radiative zone at different speeds, a shearing of the electrically conductive plasma occurs. This shearing in the tachocline amplifies and possibly regenerates the magnetic fields in the plasma through stretching (Ossendrijver 2003).

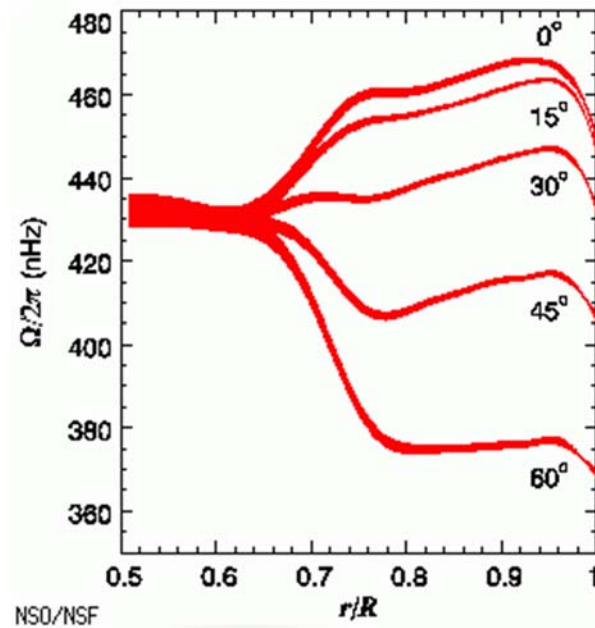
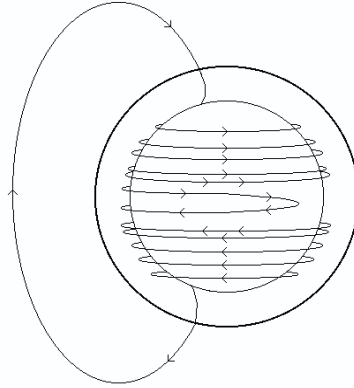


Figure 1.2: Rotational rates at various latitudes where r/R is a percentage of the solar radius, based on GONG data from 1995-2009. Surface-like differential rotation persists through the bulk of the convection zone ($> 0.70 r/R$), with a transition near the base of the convection zone to a flow that is consistent with latitudinally independent rotation. Graph courtesy of NSF's National Solar Observatory.

A model describing the process of magnetic field regeneration in the Sun was proposed by Babcock (1961) and later amended by Leighton (1969). The magnetic field of the Sun is described in relation to the rotational axis geometry of the Sun. At solar minimum, the dipole magnetic poles of the Sun are in close proximity to the rotational poles of the Sun. Magnetic field lines that are primarily N-S in direction, such as those that stretch from one pole to the other are called poloidal field lines. These lines follow the classical model of a magnetic dipole.

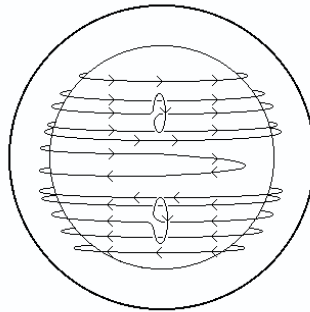
The model proposes that poloidal magnetic fields are stretched near the equator by differential rotation. Beyond the Sun's radiative zone, the Sun does not rotate as a solid body, with the equatorial region rotating faster than the polar regions. The poloidal field lines are pulled in the direction of the equatorial rotation by the shearing effect of differential rotation and are eventually wrapped in the E-W direction around the Sun (see Figure 1.3). Magnetic field lines that are primarily in the E-W direction are called toroidal and wrap around the Sun in the same direction as rotation. A large reservoir of toroidal magnetic field, believed to be the source of sunspots, is thought to exist at the base of the convection zone of the Sun. The conversion of poloidal magnetic field lines to a toroidal orientation by way of differential rotation is called the omega-effect.



The ω -effect

Figure 1.3: Arrowed lines indicate toroidal magnetic field lines at depth, wrapped around the Sun by differential rotation. The ω -effect transforms a poloidal field into a toroidal field. Obtained from <http://solarscience.msfc.nasa.gov/dynamo.shtml>

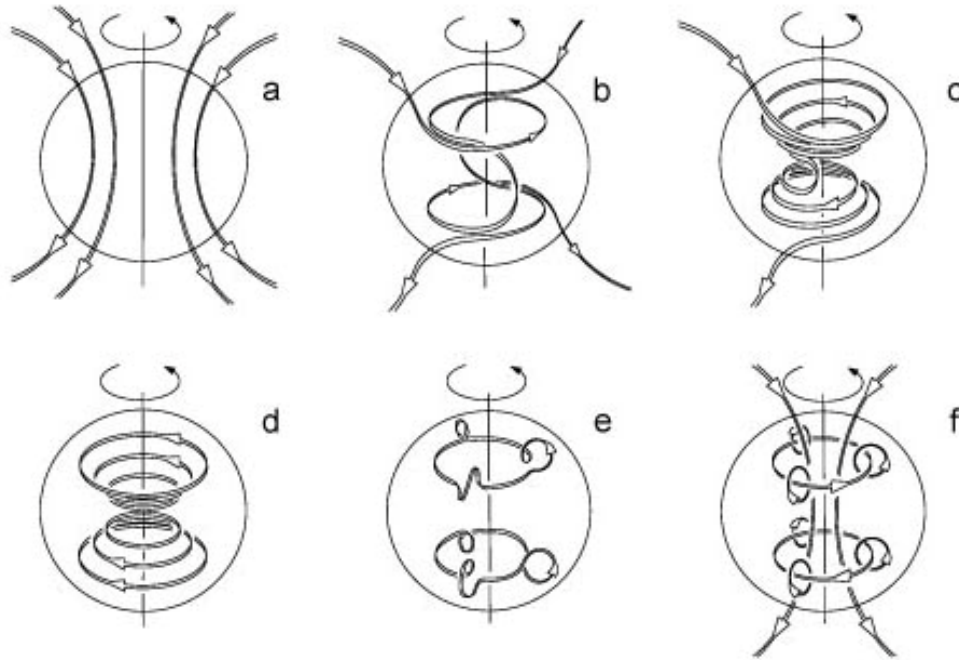
A second process introduced or furthered by Parker (1955), called the alpha-effect, is thought to convert portions of the toroidal magnetic fields back to poloidal fields. Magnetic flux tubes are believed to be stored and strengthened in or near the tachocline, the boundary between the convective zone and the radiative zone of the Sun. Flux tubes rise through the turbulent convective zone toward the solar surface due to magnetic buoyancy. As the middle span of these tubes rises faster than the “anchored” ends of the tube, a loop forms (see Figure 1.4). Sunspots are formed when the loop, tilted with respect to a line of constant latitude by the Coriolis force, breaks through the surface of the Sun. The magnetic field “frozen” in the tube has now been tilted and redirected away from the Sun in a poloidal direction.



The α -effect

Figure 1.4: Toroidal magnetic field lines are twisted into loops and rise toward the solar surface due to the magnetic buoyancy. The α -effect transforms a toroidal field into a poloidal field. Obtained from <http://solarscience.msfc.nasa.gov/dynamo.shtml>

The omega-effect and alpha-effect can be combined to describe a closed system of magnetic field regeneration. A diagram of converting poloidal fields to a toroidal orientation then back to poloidal emerges in Figure 1.5. The diagram represents the evolution of the magnetic field over one solar cycle, with the polarity of the global field reversed at the end of the cycle. Additional processes may have an effect on magnetic field generation in the Sun, such as magnetic pumping by the turbulent convective zone and the transport of magnetic flux by meridional circulation (Dikpati 2005).



Love, J. J., 1999. *Astronomy & Geophysics*, 40, 6.14-6.19.

Figure 1.5: The alpha-omega cycle of converting poloidal magnetic fields to toroidal fields, then back to a poloidal orientation (Love 1999).

At a glance, it would be easy to assume that the largest magnetic events on the solar surface are the foremost contributor to the global magnetic landscape. However, small scale magnetic activity contributes greatly to the global flux balance, where the flux emergence rate decreases as the scale size of bipolar active regions increases (Harvey & Zwaan 1993). The size distribution of bipolar active regions with sunspots does not vary significantly from the distribution without sunspots (Harvey & Zwaan 1993). Parnell et al. (2009) find a single power law across all observable scales of flux as an indication of a singular mechanism at work distributing magnetic activity across all scales. This can be attributed to either to a solar dynamo producing flux the same

way on all scales or an environmental factor acting on flux after it is produced. The impact of small-scale dynamos within the context of solar magnetic field formation at the global level (Karak & Brandenburg 2015) must be considered as part of the paradigm.

1.3 Sunspot Cycle

Sunspots are dark patches on the surface of the Sun with a life span ranging from a few hours to several months. The invention of the telescope 400 years ago made it possible to consistently observe the location and number of sunspots. A pattern emerged, with sunspot appearances concentrated between the mid-latitudes and the equator. It was also discovered that the number of sunspot occurrences varied over time.

Approximately every 11 years, the Sun reaches solar minimum. The Sun is much quieter during this time with respect to sunspot activity and other magnetic phenomena. After solar minimum, the following occurs:

- 1) Sunspots start to appear in bands located around 30° latitude in both hemispheres.
- 2) As time progresses, the average position of the sunspot bands moves to lower latitudes, closer to the equator, in each hemisphere. The Sun reaches its maximum output of sunspots during this time.
- 3) The number of sunspots slowly declines after solar maximum. New sunspots appear increasingly closer to the equator.
- 4) Eventually, the number of sunspots observed reaches zero or nearly zero, returning the Sun to solar minimum again.

This reoccurring period of sunspot activity is commonly referred to as the sunspot cycle or the solar cycle, although a full solar cycle is 22 years as explained below. Sunspot activity can be plotted as a function of time, presented in Figure 1.6 as a “butterfly” diagram or as a frequency distribution:

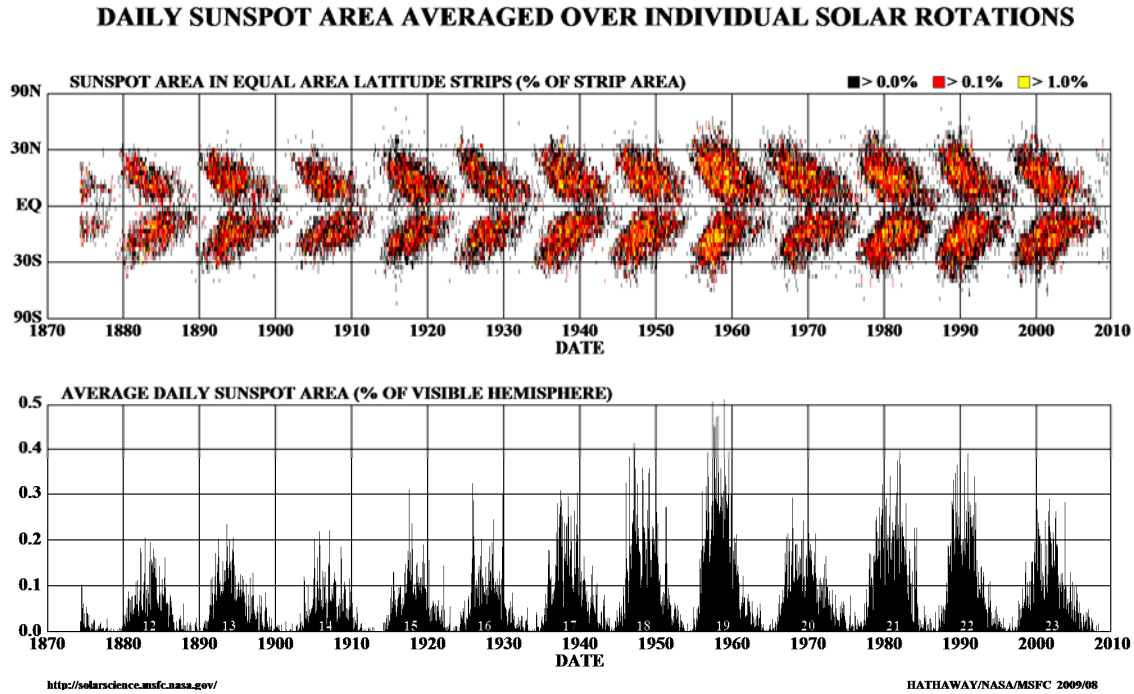


Figure 1.6: The percent of solar surface covered by sunspots as a function of latitude shown in time (top) and the total percent in time (below). Obtained from Marshall Space Flight Center/NASA at solarscience.msfc.nasa.gov

Once Hale discovered the existence of magnetic fields in sunspots, other patterns were observed within the solar cycle (Hale et al. 1919). Sunspots often appeared in groups with a pairing of opposing magnetic charges in portions of the group. If a leading sunspot in a pair, with respect to rotation, was positively charged in the northern hemisphere then almost all leading sunspots in the northern hemisphere were positively charged for that cycle. The orientation of polarity was consistently the opposite in the southern hemisphere for the entire solar cycle. Sunspot polarity led observers to believe that the magnetic field in the Sun was systematically organized on a global scale.

At or near every solar maximum the polar fields reverse polarities (see Figure 1.7). This combined with the change of leading spot polarity in each hemisphere from one sunspot cycle to the next gives rise to an average magnetic solar cycle of 22 years. This further strengthened the argument for a global structuring of the magnetic field. It is also fundamental to dynamo theory, as any model must describe not only the orientation of polarities in the hemispheres but the switching of polarities between consecutive solar cycles. Thus, the total solar cycle is 22 years in average duration to complete the polarity reversals of both the polar and equatorial (sunspot) fields.

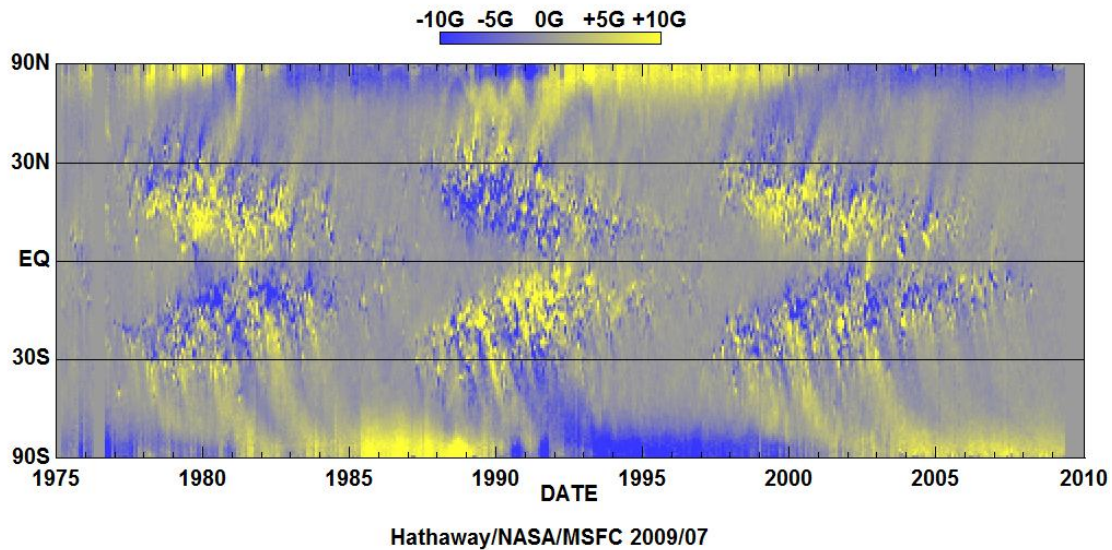


Figure 1.7: A butterfly diagram illustrating the reversal of magnetic polarity over consecutive solar cycles. Image by D. Hathaway courtesy of NASA.

The alpha-omega model describes the regeneration of toroidal magnetic fields into poloidal fields. Coupling Hale’s polarity law with Joy’s law (see section 1.4) within this construct facilitates the reversed polarity of the global field in the next cycle. For current research on surface flux transport models, see Sun et al. (2015); Miesch & Teweldebirhan (2015). However, any dynamo model must include the not insignificant percentage of bipolar active regions that exhibit anti-Hale tendencies. In fact, the behavior of anti-Hale activity can be used as a diagnostic of the role small-scale dynamos play in that regard. This small but consistent percentage of anti-Hale sunspot groups have a density independent of the phase of the solar cycle (Sokoloff et al. 2015). The prospect of multiple dynamos at various scales responsible for magnetic activity on the solar surface should be explored further.

While the sunspot cycle, and how the Sun generates magnetic fields, may seem like a purely academic topic that is of no interest to humanity other than for the advance of our astronomical knowledge – this is not the case. The Earth, and everything else in the solar system, is embedded in the heliosphere, which is structured not only by the Sun’s electromagnetic radiation but also by the solar wind. The solar wind is comprised of charged particles and bubbles of plasma that escape the Sun during solar storms such as highly energetic flares or coronal mass ejections (CMEs). The magnetic fields on the solar surface are the primary driver of these solar storms. In addition, the structure of the solar wind density, velocity, and temperature is determined by the source region from which that solar wind originates on the solar surface. The solar wind speeds and compositions have been sampled by instruments on the Ulysses spacecraft that orbited the Sun in order to sample it at all solar latitudes (McComas et al., 2000). For example, the slow solar wind originates from near the Equatorial regions of the Sun where sunspots form and bipolar magnetic regions form

closed magnetic loop systems. Meanwhile, the fast solar wind originates from the polar regions where the magnetic fields are unipolar.

An increasingly important aspect of solar physics research is the ability of researchers to predict solar storms in advance so that communications satellites, astronauts, and air traffic in polar routes can protect and shield equipment and humans from bursts of high radiation that result from these impulsive events. This subspecialty of predictive science began during the US involvement in the Gulf War when crucial military communications were lost due to the charged particles from a solar storm interfering with radio contact between commanders and troops and subsequently led to loss of life. To see an example of near-real-time space weather prediction, visit the <http://spaceweather.com/> site to see what percent chance the forecasters have given for a geomagnetic storm to occur based on the current solar wind stream and sunspot / magnetic activity on the solar disk. Therefore, the Sun's magnetic field directly affects our increasingly technology-dependent human society, with much of our technology existing in low Earth orbit where solar radiation is highly variable. While the topic of my research, Joy's law, is only one aspect of the solar magnetic fields, it is a systematic observation that provides crucial insight into how the Sun generates and maintains its electromagnetic dynamo.

1.4 Sunspot Observations

If it were possible to view sunspots as isolated objects, they would still radiate with nearly the same intensity as the Sun. Sunspots only appear dark in contrast with the hotter, and therefore brighter, solar photosphere. A sunspot is characterized by a dark center called the umbra and a brighter filamentary ring around the umbra called the penumbra. On occasion, the penumbra of a sunspot will appear to stretch across the umbra, creating a light bridge, indicated in the white box in Figure 1.8.

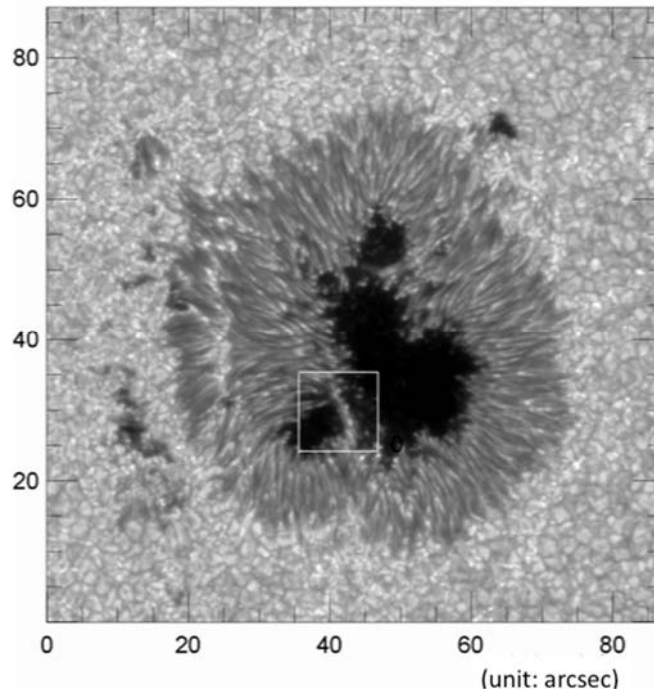


Figure 1.8: A sunspot observed with the Hinode Solar Optical Telescope. A bright filamentary structure at the center of the square is a "light bridge". Obtained from <http://darts.jaxa.jp/month/200908/200908.html.en> (JAXA/NAOJ).

Sunspots usually appear in pairs or groups but are observed as individual spots as well. Sunspot diameters range from approximately 3.5 Mm to as large as 60 Mm, however most sunspots trend toward smaller diameters (Solanki 2003). Penumbrae almost always materialize around sunspots of diameter 3.5 Mm or larger, distinguishing them from pores - smaller spots without penumbrae (Bray & Loughhead 1964). Analyses of umbral surface areas yield percentages between 15% and 25% of the total sunspot area with the remaining area attributed to the penumbra (Solanki 2003). Sunspots are not two-dimensional phenomena but descriptions will be limited as such for our purposes here.

The orientation of the magnetic field within a sunspot is approximately radial at center, becoming more horizontal at the perimeter. A comprehensive review of sunspot observations made over the last several sunspot cycles calibrated data collected by multiple observers. Distributions of maximum field strength per solar cycle indicated very few spots observed above 4000 G in a particular cycle, although a 6100 G field was recorded (Livingston et al. 2006). Field strength decreases away from the center to 700-1000 G near the outer edge of the penumbra.

Sunspots appear significantly darker than all other features on the surface due to temperature differences. It has been determined that umbrae are 1000 K to 1900 K cooler than the quiet Sun, but the change is less dramatic in the penumbra where

temperatures are only slightly cooler than the normal solar photosphere (Solanki 2003). The strong magnetic field within a spot directly affects the temperature by inhibiting heat transport from the convective zone.

Obtaining long-term, systematic observations of the Sun's magnetic field are crucial, of course, in order to study Joy's law and aggregate sunspot behavior. Daily, or near-daily, observations of magnetic fields began at Mount Wilson Solar Observatory (MWO) in California in 1966 and were discontinued in 2013 (Ulrich & Tran, 2013). The National Solar Observatory facilities in Arizona began taking photospheric observations of the full solar disk in the 1970's at the Kitt Peak National Observatory (Hathaway, 2010). Maps from these measurements cover the time period from early-1975 to mid-2003. The National Solar Observatory's Synoptic Optical Long-term Investigations of the Sun (SOLIS) facility (Keller, 1998) is another ground-based telescope that has consistently obtained full-disk observations of solar magnetism from the mid 2000's onward.

Space-based telescopes have provided near-continuous coverage of the solar disk including observations of magnetic field data, such as the Michelson Doppler Imager (MDI) on the Solar and Heliospheric Observatory (SOHO) mission (Scherrer et al., 1995) from 1995 – 2010. The Solar Dynamics Observatory (SDO) spacecraft hosts a new generation of instrument, called the Helioseismic and Magnetic Imager (HMI) (Scherrer et al., 2012), that began providing high cadence maps of solar magnetism in 2010. The telescopes and observatories described here are some of the most frequently used modern facilities that have created extensive databases for studying sunspots.

1.5 Joy's Law

Sunspots represent magnetic activity on the surface of the Sun and frequently appear as bipolar groups. The tilt angle of bipolar sunspot groups is defined as the angle of the line connecting the centroids of each polarity with the E-W line along constant latitude. Tilt is typically reported as positive when the leading sunspot is closer to the equator, in either hemisphere, than the following spot, as seen in Figure 1.9. This example is indicative of the expected bipolar sunspot behavior in the Northern hemisphere, although not exclusively so.

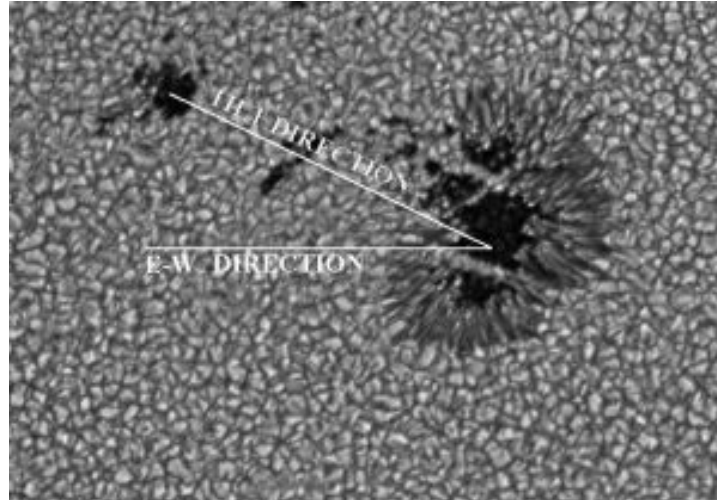


Figure 1.9: An angle between the line connecting two magnetically opposed sunspots and the EW line. According to Joy's law, this angle varies with latitude and the leading sunspot with respect to rotation is nearer the equator. Obtained from http://solarscience.msfc.nasa.gov/images/joy's_law.jpg

Joy studied drawings made by Carrington and Spörer in the 1800's and discovered that tilt angle changed with the latitudinal location of the pair, regardless of hemisphere (Hale et al. 1919). Statistical analysis of the relationship between tilt angle and latitude revealed a linear dependency (Figure 1.10).

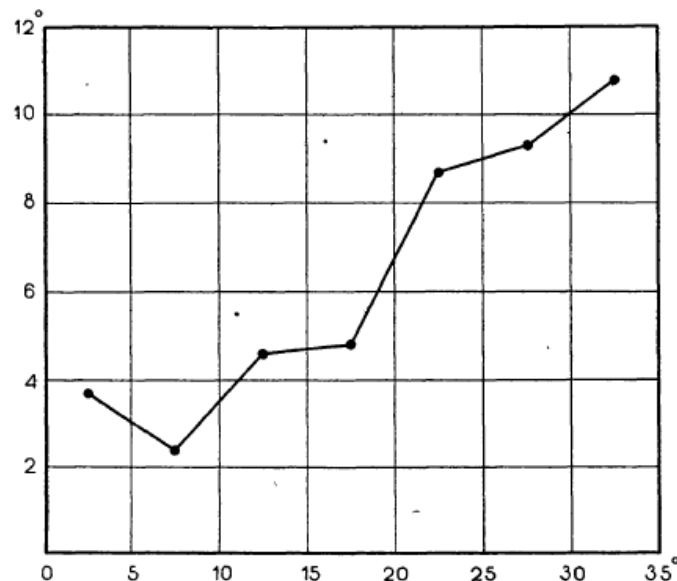


Figure 1.10: Summary of a statistical study of the bipolar sunspot drawings of Carrington and Spörer. A linear dependency of tilt angle (y-axis) as a function of latitude (x-axis) can be seen. (Hale et al. 1919)

Now known as Joy's law, the variation in tilt angle as a function of latitude is integral to understanding the solar magnetic dynamo. Any model describing the mechanism producing and regenerating the global magnetic field in the Sun must include Joy's law. The cause of Joy's law remains a subject of significant study as no definite consensus has been reached on its origins. It is clear that Joy's law, coupled with the polarity orientations discovered by Hale's research, is a strong indication of an organized, global magnetic field generator at work in the Sun.

1.6 Potential Causes of Joy's Law

The discovery of Joy's law brought more order to the appearance of sunspots; however the true cause or causes of the tilt remains in question. Babcock (1961) suggested that tilt is a result of the omega-effect, since differential rotation would spiral magnetic fields in the same direction as the tilt axes. However, D'Silva (1993) points out that the Babcock model predicts time dependent variations in the tilt angles over the course of a solar cycle but no such variations have been observed.

Tilt has been attributed to Coriolis forces acting on plasma draining from the apex of rising flux tubes, as suggested by Schmidt (1968). Models of rising flux tubes by D'Silva and Choudhuri (1993) are able to simulate observed tilt angle behavior if the magnetic field is restricted to between 60 and 160 kG. However, their flux tube model is less predictive outside this range. A more recent study by Kosovichev and Stenflo (2008) show no tilt angle dependency on field strength as would be necessary if the tilt were caused by Coriolis forces.

Thin flux tube models by Weber and Fan (2015) explore the effect of radiative heating on flux tubes near the base of the convective zone. These flux tubes, with magnetic field strengths from 15 kG to 100 kG, trend toward Joy's law tilt angles and other qualitative features observed in active regions. However, results from helioseismology are not supportive of certain aspects of the flux tube model at depth (Warnecke et al. 2015). Recent observations of active regions early in their emergence do not show signs of strong horizontal magnetic fields as would be expected at the top of a rising flux loop (Getling, Ishikawa, & Buchnev 2015). We should continue to question the accuracy of the flux tube model as a way to describe solar surface activity.

Joy's law is inherently noisy and only observable statistically over large enough samples. The scatter in tilt angle is attributed to turbulent convection acting on flux tubes rising through the convective zone to the solar surface. Flux tube simulations by Weber et al. (2013) show that tubes with less flux are more susceptible to convective turbulence, introducing more scatter into the tilt angle of these regions as a result. Recent studies have observed the anti-correlation of scatter in the tilt angle to flux (Stenflo & Kosovichev 2012; Jiang et al. 2014). Due to the noise in Joy's law, it is important to note that recovering the dependence of tilt angle on latitude cannot

be done with a year's worth of data in one hemisphere and that the correlation of tilt angle and latitude varies from cycle to cycle and hemisphere to hemisphere.

While Coriolis forces acting on flows in a rising, expanding flux tube may contribute to the tilt angle, the extent of this force contribution remains undetermined. Divergent flow at the top of supergranular convective cells can also impart a tilt angle to bipolar regions through the Coriolis effect (Schmidt 1968; Weiss 1971). It is difficult to separate whether the tilt angle is determined mainly from flows within the flux tube or flows from convection near the surface. As unorganized flux emerges from the center plume of a supergranule cell, divergent flow at the top pushes flux to the cell boundaries. Footpoint separation distances and tilt angles in either hemisphere can be described by this anti-cyclonic motion at the top of supergranules. This points to the question about the role of large-scale subsurface structures with regard to surface flux emergence (For a detailed discussion, see section 3.5, Cheung & Isobe 2014). Once flux emerges, it is still a point of debate whether near-surface processes organize the flux into sunspot regions or whether the sunspot region was pre-existing as a subsurface structure.

1.7 Statement of Thesis Objectives

This thesis aims to use analysis of the time dependence of sunspot locations and other physical characteristics to provide an improved empirical basis for theoretical modeling of the emergence of small-scale surface magnetic fields and the underlying magnetic dynamo. The particular objectives of the research are to (1) refine Joy's law of sunspots, (2) check the accuracy of the classification of bipolar sunspot regions in accordance with Hale's polarity law, and (3) search for evidence of a second distinct sunspot population indicative of the earliest visible phase of sunspot emergence. Taken together these studies can be used to provide a more complete picture of sunspot behavior, to better constrain models of the dynamo generation and convective emergence of small-scale solar magnetic fields.

2 Recovering Joy’s Law as a Function of Solar Cycle, Hemisphere, and Longitude

It is believed that magnetic fields generated at the base of the convective zone become buoyant and rise as toroidal flux tubes. Oriented in the East–West direction, flux tube loops emerge from the solar surface to form sunspots. Observations of bipolar sunspots, on average, show leading spots closer to the Equator than following spots. Known as Joy’s law, this was first published by Hale et al. (1919) after statistical analysis showed that the mean tilt angle of bipolar sunspots increased with latitude in both hemispheres. Joy’s law has traditionally been interpreted as the Coriolis force operating in the separate hemispheres on motion in the rising magnetic flux tubes. Coriolis forces dissipate once flux tube emergence ends and tilt should relax to zero, but observations made by Howard (2000) showed tilt trending towards average, nonzero values after emergence. Babcock (1961) proposed that tilt is due to a spiral orientation of initial magnetic-field lines prior to emergence. Tilt angle dependence on the latitude has been confirmed by many authors (Howard 1991; Wang & Sheeley 1991; Sivaraman, Gupta, & Howard 1993, 1999) and provides constraints on the magnetic-field strength of the flux tubes which emerge to form the observed active regions (D’Silva & Howard 1993; Schüssler et al. 1994).

We analyze the tilt angles independently by hemisphere. Since the transport of magnetic fields in Babcock–Leighton dynamo models (Babcock 1961; Leighton 1964, 1969) is partly achieved through a meridional-circulation cell seated in an individual hemisphere, the Northern and Southern Hemispheres can become decoupled to some degree (Dikpati & Gilman 2001; Chatterjee, Nandy, & Choudhuri 2004). While it is obvious from the butterfly diagram that some degree of cross-hemispheric coupling prevents the hemispheres from becoming grossly out of phase (at least for solar cycles observed since the late 1800s), nevertheless, hemispheric phase lags are observed. For example, the polar-field reversals in the Northern and Southern Hemispheres occurred half a year apart during Cycle 23 (Durrant & Wilson 2002; Norton & Gallagher 2010), and the Northern Hemisphere led the Southern by 19 months in the declining phase of Cycle 20 (Norton & Gallagher 2010), while hemispheres have been observed to be up to two years out of phase.

In addition to temporal phase lags between the hemispheres, it is common that one hemisphere dominates the other in the production of sunspot numbers and sunspot area (Temmer et al. 2006). McIntosh et al. (2013) suggest that hemispheric asymmetry is a normal ingredient of the solar cycle and has important consequences in the structuring of the heliosphere. Charbonneau (2007) finds a “rich variety of behavior characterizing the two-hemisphere dynamo solution” including intermittency (a cessation of sunspot production similar to the Maunder Minimum) operating independently in separate hemispheres. Data analysis separated into hemispheres is critical to avoid blurring a signal that may be distinct in isolated hemispheres.

A tipping ($m = 1$ mode) or warping ($m > 1$ mode) of the toroidal magnetic band in the solar interior with respect to the equatorial plane in one or both hemispheres due to an MHD instability, as proposed by Cally, Dikpati, and Gilman (2003) and observed by Norton and Gilman (2005), would impart initial tilt angles dependent on longitude prior to a flux rope’s rise through the convection zone. An $m = 0$ instability is expected for toroidal fields stronger than 50 kG on average, whereas $m > 0$ is more likely for weaker toroidal fields. The growth of the tipping or deformation, and whether it is symmetric or asymmetric across the Equator, depends in part upon the width of the toroidal band (Cally, Dikpati, & Gilman 2003). A toroidal field tipped with respect to the Equator would not produce a different mean tilt angle averaged over longitude and latitude for a given cycle, but it would increase the scatter of the mean tilt angle. It could also explain why the tilt does not relax to zero after the active region has fully emerged, as observed by Kosovichev and Stenflo (2008) and summarized nicely as follows: “It may be that Joy’s law reflects not the dynamics of the rising flux tube, but the spiral orientation of the toroidal magnetic field lines below the surface as suggested by Babcock (1961).” We argue that Joy’s law is due to a combination of both the Coriolis force’s acting on the rising flux as it rises as well as an initial tilt imparted to the flux rope from the toroidal geometry that it retains. We search for a dependence of tilt angle on longitude as well as a dependence of noise in the mean tilt angle as a function of solar-cycle strength. It also appears that the tilt angle is inherently noisy, presumably due to the turbulent convection that is encountered by the flux ropes during their rise. However, Stenflo and Kosovichev (2012) argue that the many examples of large bipolar active regions with tilts that differ from the expected Joy’s law angle by 90° are not simply regions buffeted by turbulent convection, but instead are regions from a different flux system that coexists at any given latitude.

2.1 Data

We use sunspot data derived from white light images taken daily from 1917 to 1985 at Mount Wilson Observatory¹. The data allow for observations of solar cycles 16 through 20 in their entirety. The first 4 years of solar cycle 15 and the last year of solar cycle 21 were not observed at Mt. Wilson. Sunspot area and umbral position

¹ftp://ftp.ngdc.noaa.gov/STP/SOLAR_DATA/SUNSPOT_REGIONS/Mt_Wilson_Tilt/

information were digitized from the white light images by Howard, Gilman, and Gilman (1984) and further refined by Howard, Gupta, and Sivaraman (1999).

Sunspots were grouped by proximity if they lay within 3° latitude or 5° longitude of another spot in a particular group. The mass center of the group was computed, then the portion to the east (west) was defined as the leading (following) portion of the group. Howard (1991) determined the tilt angle, γ , of a sunspot group using $\tan \gamma = \Delta\theta(\Delta\lambda \cos \theta)$, where θ is the central latitude of the sunspot group and $\Delta\theta$ and $\Delta\lambda$ represent the latitudinal and longitudinal differences, respectively, between the area-weighted centers of the leading and following regions.

No lifetime information is available from this data set since groups were not tracked for more than two consecutive days. See Howard, Gilman, and Gilman (1984) and Howard, Gilman, and Sivaraman (1999) for detailed descriptions of image digitizing and data reduction techniques for the observed bipolar sunspot regions.

2.2 Recovering Joy's Law

Furthering work by Howard (1996) and others, we examine bipolar active region tilt angles observed at the Mt. Wilson Observatory. We also record tilt angle dependence on hemisphere, solar cycle, latitude, and longitude (dependence on longitude is discussed in Section 2.4). In Figure 2.1, mean tilt-angle values as a function of latitude for each hemisphere are shown averaged over Solar Cycles 16 to 21 for data collected at the Mt. Wilson Observatory between 1923 and 1985. Cycle 15 began in 1913, but Mt. Wilson observations for this data did not begin until 1917, near solar maximum of this cycle. We excluded Cycle 15 from this analysis, as it is an incomplete representation of a solar cycle. Mt. Wilson data are not available for the end of Solar Cycle 21 from January 1986 to September 1986. However, the monthly smoothed sunspot number had dropped to around 12.2 by January 1986. At most, this would have amounted to approximately 110 spots *versus* the 4000 pairs in this cycle. After removing single sunspots from analysis, the effect on overall results would have been negligible; therefore, Cycle 21 is included. The only regions excluded were individual spots, *i.e.* groups that did not have at least one sunspot in both the leading and following portions of a group. These were indexed in the Mt. Wilson data with a tilt angle of zero. Dasi-Espuig et al. (2010) thoroughly investigated entries with a zero tilt angle and found only one data point that corresponded to a true tilt value of zero; all others were single sunspots whose tilt angle could not be defined. The sample standard deviation of each latitudinal bin is divided by the square root of the bin population number and overplotted as standard error bars.

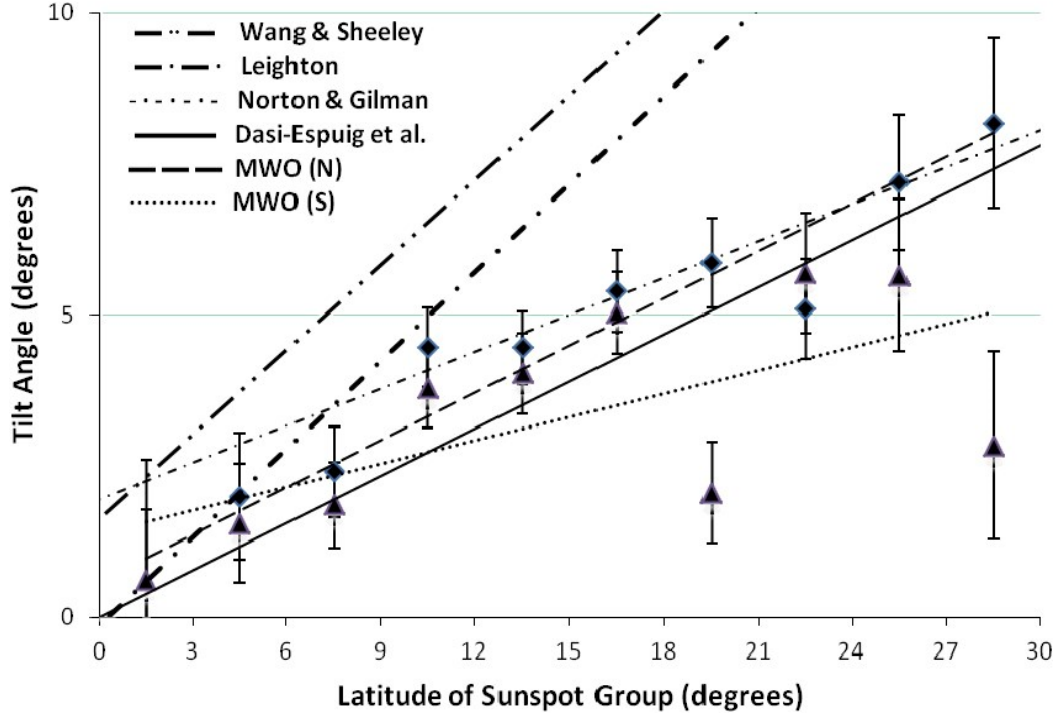


Figure 2.1 Tilt angle as a function of latitude, Northern (diamond) and Southern (triangle) Hemispheres, for Solar Cycles 16 to 21. Data were binned in 3° of latitude. Standard errors of the mean are overplotted as error bars. Common Joy's law equations are plotted for reference: Wang and Sheeley (1991), Equation (2.1), dashed-dot-dot; Leighton (1969), Equation (2.2), large dash-dot; Norton and Gilman (2005), Equation (2.3), small dash-dot; Dasi-Espuig et al. (2010), Equation (2.4), solid. Linear fit Equation (2.5) for Northern Hemisphere data (dash) and Equation (2.6) for Southern Hemisphere data (dot) are also shown.

Empirical Joy's law equations from previous works are also plotted in Figure 2.1 as described by Wang and Sheeley (1991) as Equation (2.1), Leighton (1969) as Equation (2.2), Norton and Gilman (2005) as Equation (2.3), and Dasi-Espuig et al. (2010) as Equation (2.4):

$$\sin \gamma = 0.48 \sin \theta + 0.03 \quad (2.1)$$

$$\sin \gamma = 0.5 \sin \theta \quad (2.2)$$

$$\gamma = 0.2 \theta + 2.0 \quad (2.3)$$

$$\gamma = (0.26 \pm 0.05) \theta \quad (2.4)$$

where γ is tilt angle and θ is latitude. Southern Hemisphere latitudes are considered positive for plotting purposes. Tilt angles in both hemispheres are considered positive if the leading spot is closer to the Equator than the following spot.

In order to understand Equations (2.1)–(2.4), some background on data and analysis is in order. Equation (2.1) was formulated by Wang and Sheeley (1991) after an analysis of National Solar Observatory/Kitt Peak data, utilizing 2710 magnetograms of bipolar magnetic regions (BMRs) collected during Solar Cycle 21. Tilt angles were determined by hand, analyzing magnetogram prints at a time of approximate peak flux for each BMR. Averages were flux weighted and taken over sine-latitude bins of width 0.05 (approximately 3°). Equation (2.2) was formulated by Leighton (1969), who approximated Joy’s law from measurements by Brunner (1930). Norton and Gilman (2005) implemented Joy’s law as part of a sunspot behavior model, and Equation (2.3) is the best fit to an average of tilt angle as a function of latitude for over 650 active regions observed in *Michelson Doppler Imager* (MDI) data from 1996–2004 (Norton & Gilman 2004). Equation (2.4) was determined by Dasi-Espuig et al. (2010) using available Mt. Wilson data, including the latter part of Solar Cycle 15 to most of Cycle 21. The data were binned by 5° latitude and area-weighted in an effort to reduce scatter, and linear fits were forced through the origin for Equation (2.4).

We find a linear fit for the relationship of the northern and southern average tilt angles as a function of latitude to be:

$$\gamma_N = 0.26 \theta + 0.58 \quad (\text{or } \sin \gamma_N = 0.271 \sin \theta + 0.010) \quad (2.5)$$

$$\gamma_S = 0.13 \theta + 1.38 \quad (\text{or } \sin \gamma_S = 0.425 \sin \theta + 0.024) \quad (2.6)$$

The values of the binned, average tilt angles observed at the higher latitudes are not well fit by the Wang and Sheeley (1991) or previous historical Joy’s law equations. We propose an updated Joy’s law with a lower slope between 0.13–0.26, as seen in Equations (2.5) and (2.6) for the Northern and the Southern Hemisphere determined using Mt. Wilson data from Cycles 16 to 21. The linear correlation coefficient for Equations (2.5) and (2.6) are 0.96 and 0.65 for the Northern and Southern Hemispheres, respectively. The correlation coefficient ($-1 \leq r \leq 1$) measures the strength of the linear relationship between two variables and is defined as the covariance of the two variables divided by the product of their standard deviations. Values of -1 and 1 indicate a perfect inverse or direct relationship, respectively. We correlate the binned, mean tilt angle and latitude.

The hemispheric, linear fits to Joy’s law are more consistent with the result of Dasi-Espuig et al. (2010), who report a lower slope value of 0.26–0.28, than with the equations from the 1990s and prior that had higher slopes. We also propose that the Joy’s law equation should not be forced through the origin. It is reasonable that the slope reported by Dasi-Espuig et al. (2010) is higher than the slope reported here because they force the fit through the origin, which we do not. We justify our approach as being purely observational. If we did force the fit through the origin, our slopes in Equations (2.5) and (2.6) would increase to be 0.29 and 0.20 in the Northern and Southern Hemispheres, respectively. The data here consistently demonstrate that Joy’s law does vary by hemisphere. It is possible that the mechanisms responsible for tilt

angles in each hemisphere have a canceling effect on tilt near the Equator and therefore are not an accurate indication of Joy's law by hemisphere.

The results of Dasi-Espuig et al. (2010), showing that tilt angle is variable as a function of solar cycle, are noteworthy. Our initial attempts to recover Joy's law for each hemisphere and solar cycle were frustrating due to the fact that Joy's law only appears weakly (Figure 2.2). Cycle 16 had a low population (<25) in the first ($0-3^\circ$) and last ($27-30^\circ$) bins, resulting in large error bars. These bins were subsequently removed from all individual cycle plots for consistency. The data are poorly fit by a linear function in most cases. The linear correlation coefficients range from $r = 0.18$ (Cycle 17 North, Cycle 19 South) to $r = 0.86$ (Cycle 20 North). The large amount of scatter and high noise apparent in Joy's law is interesting, because it indicates that a stochastic process is competing with the mechanism that determines the tilt angles. The stochastic process dominating Joy's law on the short time scale is considered to be turbulent convection imparting random tilt angles to the rising flux tubes (Fisher, Fan, & Howard 1995; Weber et al. 2013). We agree with Dasi-Espuig et al. (2010), who state that "no clear difference could be determined between the slopes of Joy's law from cycle to cycle," as can be seen in Figure 2.2; therefore, we use the mean tilt value from each hemisphere for each cycle to analyze the hemispheric differences.

It is possible that the recovery of a mean bipolar region tilt angle and scatter for a given solar cycle can be used as a diagnostic for that cycle, *i.e.* the strength of the cycle as indicated by Dasi-Espuig et al. (2010) or the geometry/orientation of the toroidal fields from which the flux ropes begin their initial rise (Babcock 1961; Norton & Gilman 2004). Simulations by Weber et al. (2013) of thin flux tubes rising through solar-like turbulent convection show how much the tilt-angle scatter increases with decreasing flux and field strength. Therefore, quantifying the scatter in Joy's law can constrain the flux and field strength within the context of their model; *i.e.* a larger scatter is indicative of flux tubes dominated by convection instead of magnetic buoyancy. In addition, since smaller average tilt angles minimize the amount of active-region flux that becomes the poloidal field, a smaller average tilt angle leads to a weaker polar cap mean field strength (Petrie 2012).

We are uncertain why specific bins in the Southern Hemisphere showed such different behavior from the other bins. We found that late in all solar cycles (except Solar Cycle 20) aberrant activity occurred at the $18-21^\circ$ latitudes. In particular, the Southern Hemisphere during Cycle 19 is very disorganized, with the high-latitude bins of $18-21^\circ$ (304 regions, 24 %) and $24-27^\circ$ (150 regions, 12 %) having negative mean tilt values, meaning that these bipolar regions have a following spot closer to the Equator than the leading spot. The Southern Hemispheric tilt angles for Cycle 19 are responsible for the low mean tilt angles for the whole Sun in Cycle 19 as reported by Dasi Espuig et al. (2010, see their Table 2.1). It would be of interest to study this in more detail and better understand the conditions favorable for aberrant configurations, *i.e.* anti-Hale and negative tilt angles, to occur.

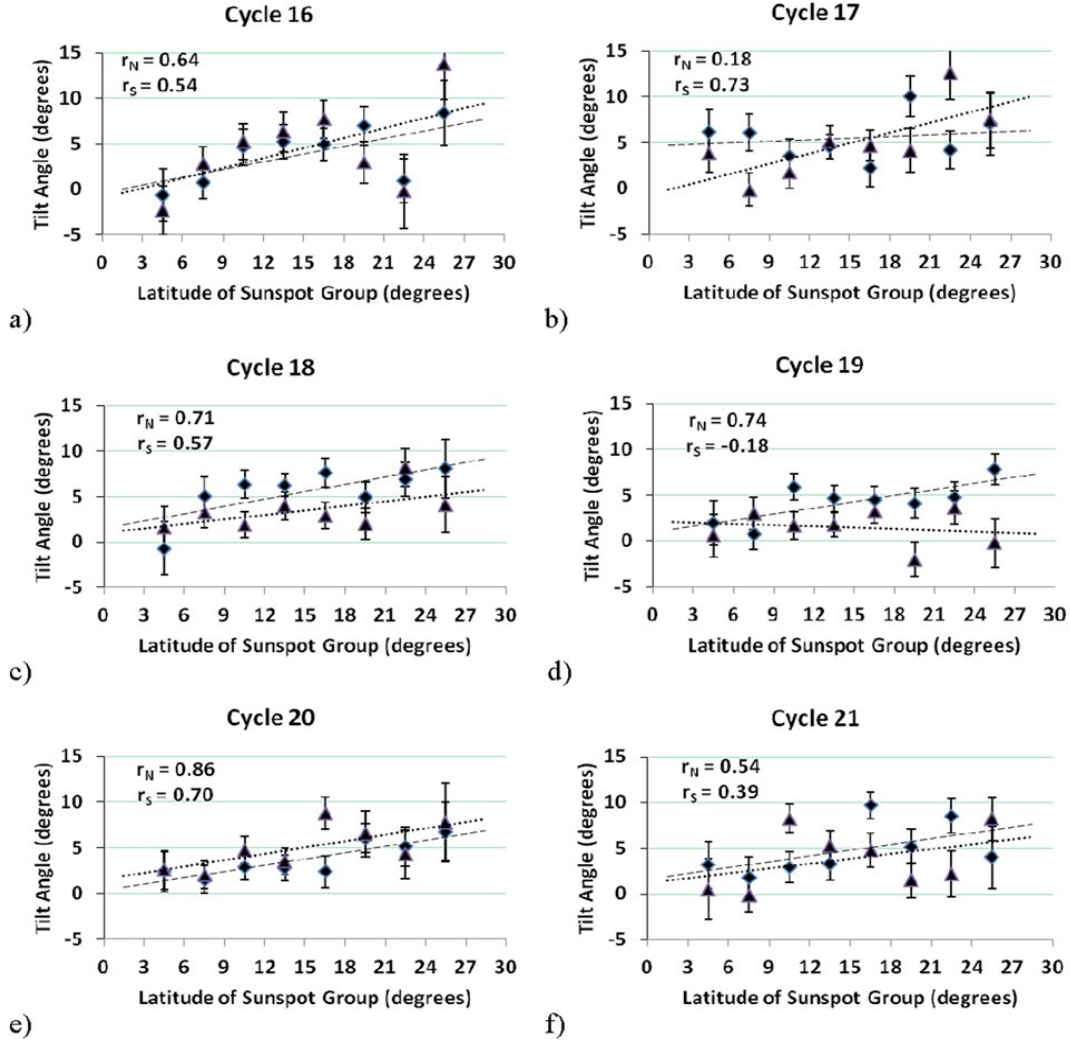


Figure 2.2: Tilt angle as a function of latitude for the Northern (diamond) and Southern (triangle) Hemispheres for Solar Cycles 16–21 are shown in panels (a)–(f), respectively. Data were binned in 3° of latitude. Standard errors of the mean are overlotted as error bars. Linear fits to Northern (dash) and Southern (dot) Hemisphere data are shown with linear correlation coefficients [r_N , r_S] included in the legends.

2.3 Joy's Law as a Function of Hemisphere

The average tilt angle and standard error of the mean for each hemisphere for Solar Cycles 16 to 21 are given in Table 2.1. The standard error of the mean was calculated as the sample standard deviation divided by the square root of the sample number. Differences in Joy's law between hemispheres are poorly determined (below the two- σ level) for Cycles 16, 17, 20, and 21. However, Cycles 18 and 19 as well as the data averaged over all cycles show a significant difference between hemispheres. These findings are indicative that Joy's law varies by hemisphere and by solar cycle.

Table 2.1: Mean tilt angle in degrees for Northern [γ_N] and Southern Hemisphere [γ_S] with standard deviation of mean [σ_γ] for Solar Cycles 16 to 21. The difference of hemispheric mean tilt angle and statistical significance are also shown.

Solar Cycle	$(\bar{\gamma} \pm \sigma_{\bar{\gamma}})_N$	$(\bar{\gamma} \pm \sigma_{\bar{\gamma}})_S$	$\Delta\bar{\gamma} = \bar{\gamma}_N - \bar{\gamma}_S $	$\frac{\Delta\bar{\gamma}}{\sqrt{\sigma_{\bar{\gamma}_N}^2 + \sigma_{\bar{\gamma}_S}^2}}$
16	$3.8^\circ \pm 0.73$	$4.4^\circ \pm 0.81$	0.6	0.3
17	$5.4^\circ \pm 0.70$	$4.0^\circ \pm 0.71$	1.4	1.4
18	$5.7^\circ \pm 0.61$	$2.9^\circ \pm 0.60$	2.8	3.3
19	$4.6^\circ \pm 0.53$	$1.8^\circ \pm 0.59$	2.8	3.5
20	$3.5^\circ \pm 0.60$	$4.8^\circ \pm 0.66$	1.3	1.5
21	$5.0^\circ \pm 0.67$	$4.4^\circ \pm 0.68$	0.6	0.6
16 – 21	$4.7^\circ \pm 0.26$	$3.6^\circ \pm 0.27$	1.1	3.0

Using the results in Table 2.1, we attempt to answer the following questions: Is there a significant difference between Northern and Southern Hemispheric mean tilt? The last row of Table 2.1 indicates that, yes, there is a significant difference of mean tilt at a three- σ level. Do the hemispheric differences in mean tilt values change from cycle to cycle? We find an average value of $\Delta\bar{\gamma}$ over all six cycles equal to 1.5 with a statistical significance of nearly four- σ (3.9). Therefore, we are convinced that there is significant variation in hemispheric mean tilts from cycle to cycle.

We agree with Dasi-Espuig et al. (2010) that a revision of Joy’s law is necessary. Their conclusion that a relationship exists between cycle strength and mean tilt is intriguing, and we attempted to confirm this result. We used the values reported by Goel and Choudhuri (2009) of total sunspot area in micro-hemispheres by solar cycle and hemisphere [A_N , A_S] for Cycles 15 through 21. Cycle 15 data were only available from just prior to solar maximum until the end of the cycle. The minimal effects of data missing from the last nine months of Cycle 21 are discussed in Section 2.2. Sunspot area is used as a proxy for cycle strength (Solanki & Schmidt 1993). Areas were calculated from Royal Greenwich Observatory data. We compare total sunspot area to mean tilt separated by hemisphere and solar cycle in Table 2.2. Assuming that a larger total sunspot area indicates a stronger cycle and that hemispheric differences exist within each cycle, we find evidence of the same inverse relationship as Dasi-Espuig et al. (2010) such that a stronger cycle produces less average tilt.

Table 2.2: Sunspot area [10^4 μ -hemispheres], mean tilt angle [γ], mean tilt angle normalized by mean latitude γ/λ , and area-weighted mean tilt angle normalized by mean latitude $(\gamma/\lambda)_\omega$ values are provided for Northern and Southern Hemispheres and total Sun for Solar Cycles 15–21. The correlation of mean tilt with sunspot area was measured as the correlation coefficient [r] for each hemisphere and total-Sun values. Cycle 15 data were only available after solar maximum.

	Solar Cycle							r
	15*	16	17	18	19	20	21	
A_N	4.3	4.7	6.0	7.4	10.6	6.9	7.5	
$\bar{\gamma}_N$	4.1°	3.8°	5.4°	5.7°	4.6°	3.5°	5.0°	0.25
$\bar{\gamma}_N/\bar{\lambda}$	0.35	0.27	0.36	0.37	0.26	0.24	0.33	−0.17
$(\bar{\gamma}_N/\bar{\lambda})_\omega$	0.45	0.29	0.50	0.46	0.30	0.32	0.40	−0.29
A_S	3.6	3.9	6.0	7.0	7.4	4.9	7.8	
$\bar{\gamma}_S$	3.7°	4.4°	4.0°	2.9°	1.8°	4.8°	4.4°	−0.45
$\bar{\gamma}_S/\bar{\lambda}$	0.27	0.32	0.28	0.20	0.12	0.35	0.29	−0.67
$(\bar{\gamma}_S/\bar{\lambda})_\omega$	0.43	0.43	0.27	0.29	0.11	0.33	0.28	−0.83
A_{tot}	7.9	8.6	12.0	14.5	18.0	11.9	15.3	
$\bar{\gamma}_{tot}$	3.9°	4.2°	4.7°	4.3°	3.4°	4.1°	4.7°	−0.16
$\bar{\gamma}_{tot}/\bar{\lambda}$	0.31	0.30	0.32	0.29	0.20	0.29	0.31	−0.64
$(\bar{\gamma}_{tot}/\bar{\lambda})_\omega$	0.44	0.35	0.39	0.38	0.23	0.32	0.34	−0.75

In Figure 2.3, the area-weighted mean tilt values normalized by mean latitude (see $(\bar{\gamma}/\bar{\lambda})_\omega$ in Table 2.2) are plotted as a function of total sunspot area for Solar Cycles 15 to 21 for the Northern and Southern Hemispheres as well as the total Sun. Dasi-Espuig et al. (2010) used area-weighting to give larger and, therefore, less scattered groups more influence on mean tilt. The mean latitude of sunspot emergence decreases and approaches zero as the solar cycle progresses. Normalizing by latitude removes that latitudinal bias and allows for the inclusion of incomplete cycles in our analysis. Linear regression lines are fit to normalized mean tilt and sunspot area for each hemisphere. Correlation coefficients [r] are found to be $r_N = -0.29$, $r_S = -0.83$, $r_{tot} = -0.75$ for the Northern Hemisphere, Southern Hemisphere, and total-Sun values.

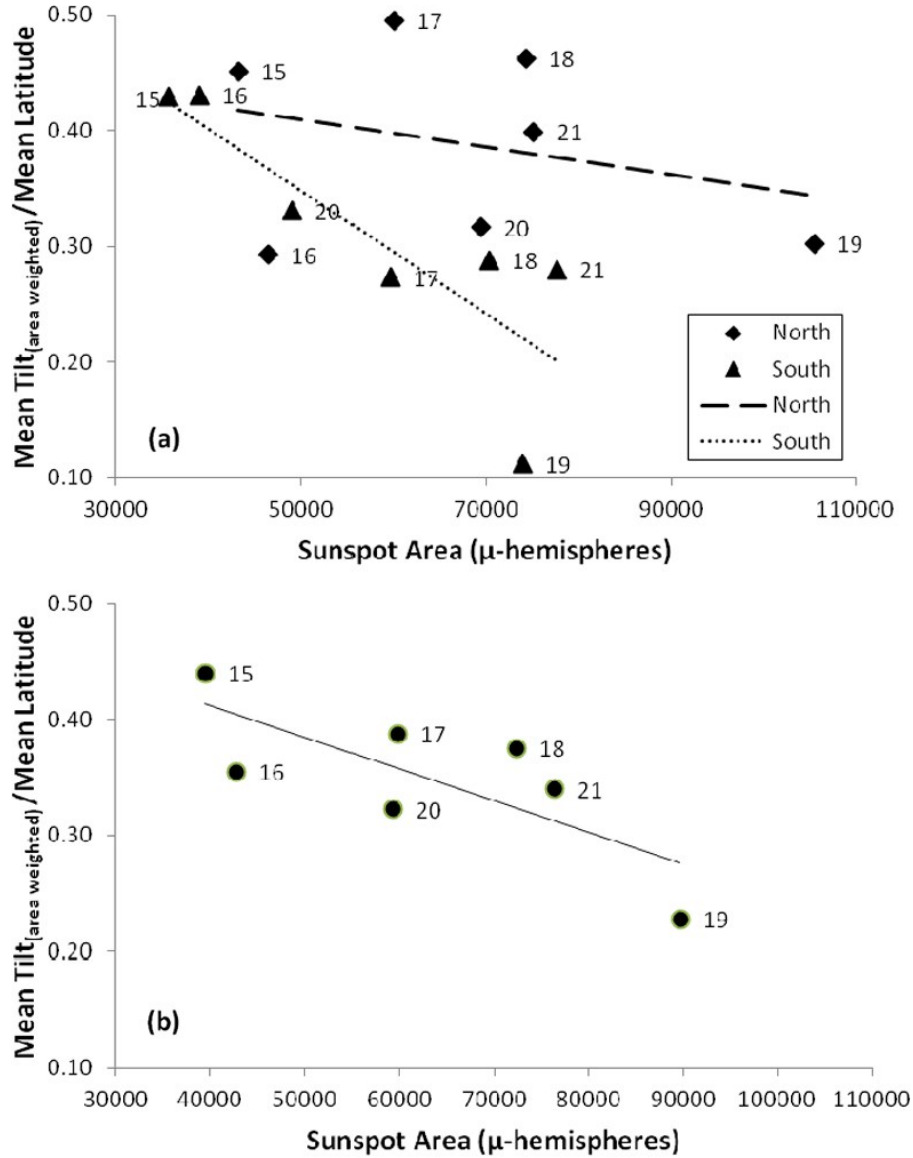


Figure 2.3: Area-weighted mean tilt angle normalized by mean latitude (degrees) as a function of sunspot area [μ -hemispheres] for Cycles 15 to 21. Panel (a) shows Northern Hemisphere (diamond, dashed line) and Southern Hemisphere (triangle, dotted line), and panel (b) shows the total-Sun sunspot area divided by two. Linear correlation coefficients [r] for each hemisphere and total Sun are $r_N = -0.29$, $r_S = -0.83$, $r_{\text{tot}} = -0.75$.

There is an inverse correlation of area-weighted mean tilt to sunspot area and, by proxy, cycle strength in the Southern Hemisphere. The probability is 2.1 % that the linear correlation coefficient of $r_S = -0.83$ in the South is due to chance. Total-Sun values also suggest an inverse relationship of area-weighted mean tilt angle values with cycle strength, the correlation coefficient $r_{\text{tot}} = -0.75$ having a 5.0 % probability of chance. The correlation between mean tilt and cycle strength in the Northern

Hemisphere is insignificant. The smallest chance probabilities of 2.1 % and 5.0 % for the Southern Hemisphere and total-Sun correlations are at or below the usual significance level of 5 %, and therefore we confirm that there exists a statistically significant negative correlation between area-weighted mean tilt value and cycle strength as measured by sunspot area in the Southern Hemisphere and the whole-Sun data.

2.4 Joy's Law as a Function of Longitude: Searching for Evidence of a Tipped Toroidal Field in Tilt Angle Data

If toroidal magnetic fields at the base of the convection zone in each hemisphere were tipped with respect to the equatorial plane, as proposed in theory by Cally, Dikpati, and Gilman (2003) and observations (Norton & Gilman 2005), then flux tubes would begin their rise through the convection zone with a tilt dependent on longitude. This might be observable as a pattern when tilt angles in each hemisphere are studied as a function of longitude. It is well established that active longitudes appear during each solar cycle and certain longitudes host active regions repeatedly over time (De Toma, White, & Harvey 2000). If an $m = 1$ instability were present, we would expect to see a sinusoidal pattern.

To reveal longitudinal structure, possibly relating to the orientation of the toroidal field in each hemisphere, we separated tilt data by hemisphere and solar cycle. Active-region tilt angles as a function of longitude were plotted for the Northern and Southern Hemispheres for all solar cycles, with data binned into 20° longitudes, then averaged. Plots for Cycles 18–20 are presented in Figure 2.4(a)–(f). We expected an $m = 1$ sinusoidal pattern suggestive of a tipped toroidal field in each hemisphere. We attempted to fit the data with sinusoidal curves representing $m = 1$ through $m = 8$ patterns with various amplitudes. No fit to the data was statistically significant. Therefore, we report no longitudinal dependence in Joy's law.

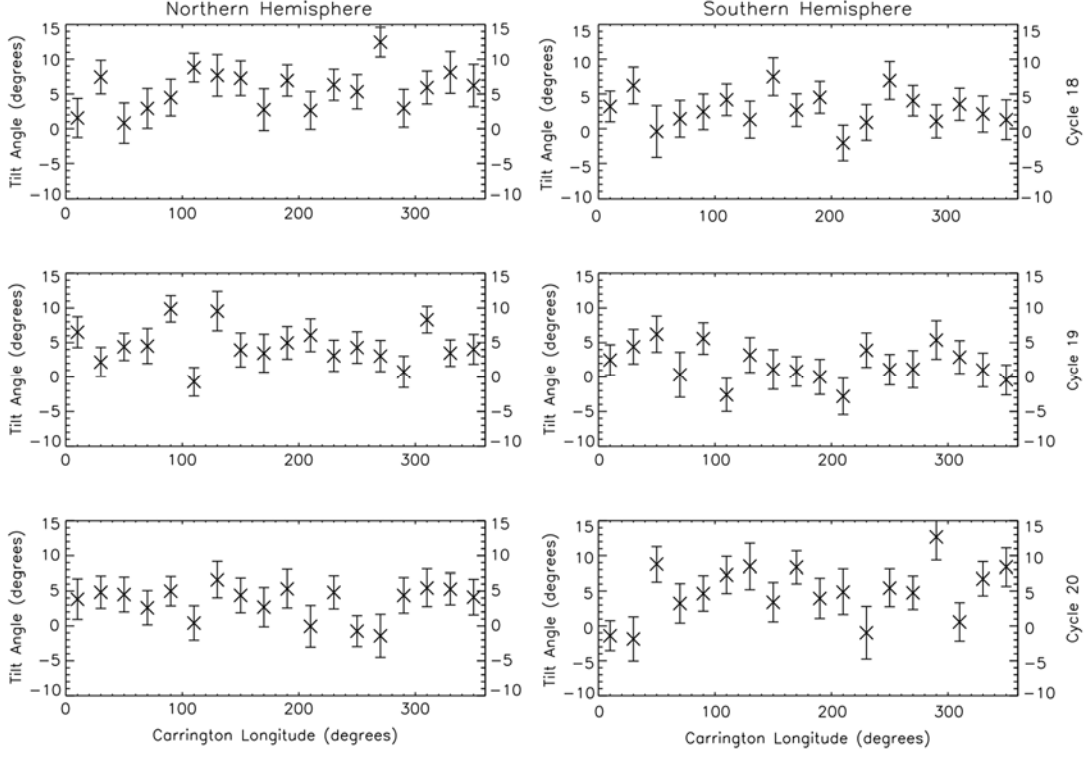


Figure 2.4: Tilt angle as a function of longitude. Solar Cycles 18 – 20. Northern (a) – (c) and Southern Hemispheres (d) – (f). Data were binned 20° in longitude. Standard deviations of tilt angle for all sunspot groups in each longitudinal bin are overplotted as error bars.

If a tipped toroidal field were only present for one to two years during a solar cycle, this might prevent a tilt-angle dependence on longitude to be decipherable when averaging over ≈ 11 years. However, it may be possible to see an increased scatter in the tilt-angle values for a solar cycle that has a tipped toroidal field compared to a cycle without one. For this reason, we determined the standard deviation (not the standard deviation of the mean) for the average tilt angle as a function of hemisphere and cycle (see Table 2.3). The standard-deviation values have a very small range, from 29.3 – 31.2° , even though the strength of the cycle, shown as sunspot area, varies a great deal. The errors of the standard deviation values shown in Table 2.3 range from 0.53 – 0.81° . The small range of standard deviation values indicates that the source of scatter in the tilt angles is due to a process that is nearly identical from one cycle and hemisphere to the next. The values shown in Table 2.3 do not support the presence of a tilting or deformation of the toroidal band in the solar interior since there is no difference in scatter of observed tilt angles at the surface between one cycle and the next. We agree with Fisher, Fan, and Howard (1995) that the very small range of the standard deviations of the tilt angle (referred to as rms tilt in their article) are consistent with a process such as the buffeting by convection that is persistent in scale as a function of longitude and latitude and similar from one cycle to the next.

Table 2.3: Cycle strength in terms of the sunspot area [$10^4 \mu$ -hemispheres] and the standard deviation [σ_γ] (not the standard deviation of the mean) in the mean tilt angle for the bipolar regions of the Northern and Southern Hemispheres for Cycles 16–21.

Cycle	16	17	18	19	20	21
A_N	4.7	6.0	7.4	10.6	6.9	7.5
σ_γ	29.6°	30.5°	30.0°	31.2°	29.6°	29.8°
A_S	3.9	6.0	7.0	7.4	4.9	7.8
σ_γ	30.6°	31.0°	30.4°	29.6°	29.3°	29.7°

2.5 Discussion

We determined that the mean tilt angle observed in Solar Cycles 16 to 21 was significantly different in the Northern and Southern Hemispheres. Hemispheric differences up to 2.8° in average tilt angle persist across solar cycles. We suggest a revision to Joy’s law equations with a weaker dependence on latitude (slopes of 0.26 and 0.13 for the Northern and Southern Hemispheres were found) and more attention paid to the differences between hemispheres and cycles. We did not force the linear fit through the origin as Dasi-Espuig et al. (2010) did in their analysis. It is possible that bipolar active regions at the Equator have mean tilt angles of zero because the sampling is an aggregate of flux activity from both hemispheres. If we do force the fits through the origin, we find slopes of 0.29 and 0.20 for the Northern and Southern Hemispheres, compared to 0.26 reported by Dasi-Espuig et al. (2010). Weber et al. (2013) simulate rising flux tubes, including the effect of convection, and produce an expected slope for Joy’s law dependent upon the strength of the source toroidal field and total flux in the tube. Our slope values of 0.29 and 0.20 in the Northern and Southern Hemispheres are consistent with field strengths of 15 kG in the interior and flux ropes containing between 10^{20} and 10^{21} Mx.

We confirm the results of Dasi-Espuig et al. (2010) that whole-Sun mean tilt angles, weighted by area and normalized by latitude, for Cycles 16 to 21 show a statistically significant negative correlation with cycle strength (see Figure 2.3b). A tilt-angle dependence upon cycle strength is a feedback mechanism in which the Sun can regulate sunspot-cycle amplitudes; *i.e.* a stronger cycle produces a smaller tilt angle and therefore a weaker poloidal seed field for the $n + 1$ cycle (Cameron & Schüssler 2012). Jiang et al. (2010) study the effect of meridional-flow perturbations and find that larger perturbations reduce the tilt angle of bipolar magnetic regions and

thus diminish its contribution to the polar field. The perturbations are caused by near-surface inflows towards the active-region band in each hemisphere, and the perturbation amplitude increases with stronger magnetic cycles. This mechanism may explain the observed anti-correlation between tilt angle and cycle strength. However, some doubts are cast on the results, because the Northern Hemisphere did not exhibit a statistically significant negative correlation with cycle strength, while the Southern Hemisphere did (see Figure 2.3a). We hope that this result reinforces the importance of isolating data by hemisphere.

We searched for a non-axisymmetric mechanism at work by analyzing tilt angles as a function of longitude (see Figure 2.4 for Cycles 18–20). We attempted to fit the data with sinusoidal curves representing $m = 1$ through $m = 8$ patterns with various amplitudes. No fit to the data was statistically significant. Therefore, we find no evidence that tilt angles vary regularly in longitude. A toroidal field tipped with respect to the East–West direction would introduce a significant scatter into Joy’s law if the flux rope retained some of the original tilt imparted to it from the source toroidal field. Therefore, we calculated the standard deviation of the average tilt angle from each cycle and hemisphere. The values exhibited a narrow range from 29.3 – 31.2° even though the cycle strengths varied greatly (see Table 2.3). This does not support the presence of a tilting or deformation of the toroidal field but is consistent with a process such as the buffeting by convection that is persistent in scale in latitude and longitude and similar from one cycle to the next.

Moreover, a bias towards reporting positive results regarding Joy’s law may have impeded progress on this topic that would benefit from identifying time periods in which Joy’s law cannot be recovered. These would be times in which the stochastic processes of turbulent convection dominate the tilt-producing mechanism thought to be the Coriolis force. The work by Weber et al. (2013) is a great step towards the ability to interpret the scatter of bipolar region tilt angles in any period of the solar cycle to constrain the toroidal field strength in the interior and the flux residing in the thin flux tubes. The standard deviation values of the average tilt angle shown in Table 2.3 are consistent with Weber et al. (2013) simulations of flux tubes containing 10^{21} Mx and forming from a toroidal field with a strength of 50 kG.

3 **Re-Examining Sunspot Tilt Angle to Include Anti-Hale Statistics**

The ~ 11 year pattern of sunspot activity begins at high latitudes (near $\pm 30^\circ$) to form a latitudinal band of activity. The unsigned mean latitude of sunspot location decreases over time. This is observed as a drift in the hemispheric latitudinal bands towards the equator later in the cycle. Late cycle sunspots finally appear near the equator while the next solar cycle sunspots begin emerging at high latitudes. A diagram of sunspot latitude as a function of time over the course of a solar cycle resembles butterfly wings, as first noted by Maunder and Maunder (1922). We show a version of the butterfly diagram in Figure 3.1 using the Debrecen Photoheliographic Data (DPD) described in the next section. Carrington (1858) first noticed that the average latitude of sunspot emergence becomes increasing equatorward as the solar cycle progresses. Maunder and Maunder (1922) said that the diagram “seems to suggest three butterflies pinned down to a board with their wings extended. Heads, bodies and legs have disappeared, but the outstretched wings remain. Each pair of wings is distinct from the next; there is a clear V-shaped gap between each of the two specimens.”

Observations of magnetic flux (Hale et al. 1919) reveal sunspot groups have opposite polarities for leading and following spots with respect to solar rotation. The majority of the time, the leading spot of a bipolar magnetic region (BMR) has the opposite polarity to leading spots in the other hemisphere. With every solar cycle, the hemispheres alternate the dominant leading sunspot polarity as seen in Figure 3.2, courtesy of David Hathaway at NASA Marshall Space Flight Center. Hale’s law, as it is often called, denotes that if the northern hemisphere has a BMR configuration where the leading spot is positive and the following spot is negative, then the southern hemisphere would have the leading spot as negative and the following spot as positive. BMRs that have the opposite orientation from the expected polarities are considered anti-Hale.

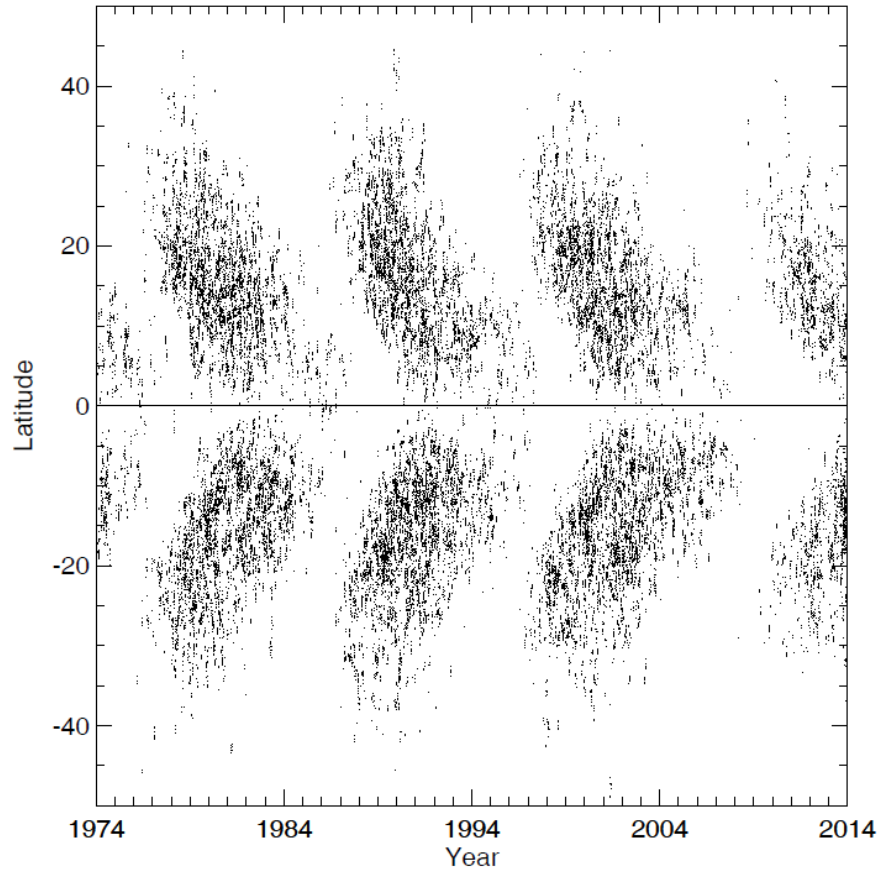


Figure 3.1: Latitude of bipolar sunspots as a function of time from daily DPD observations. Portions of Solar Cycles 20 and 24 are visible at the left and right edges of the diagram, respectively, while all of Cycles 21-23 are shown.

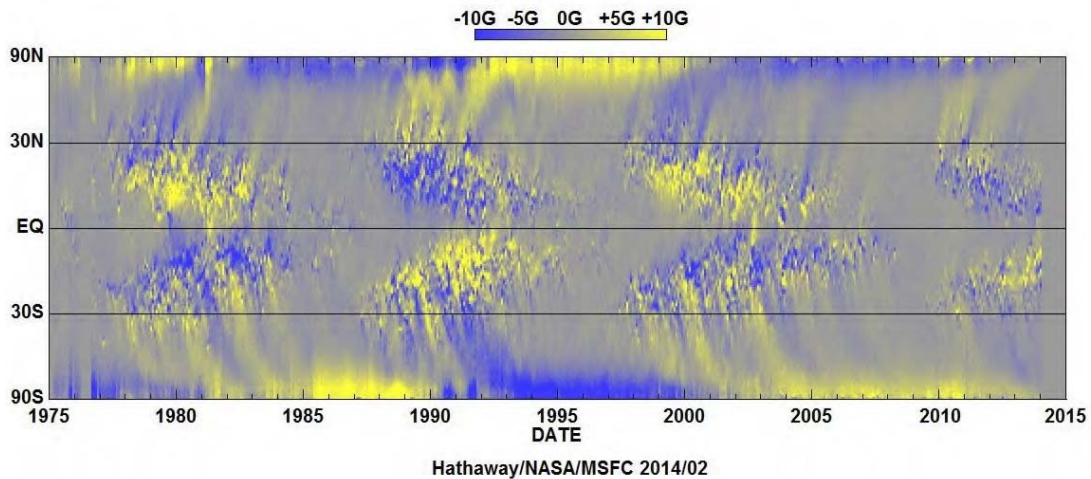


Figure 3.2: Diagram of the magnetic field of the Sun. Yellow represents positive (outward) flux, blue represents negative (inward) flux. Hale's law can be observed. Courtesy of NASA/MSFC/David Hathaway.

Leading spots, on average, are closer to the equator than following spots. The difference in the latitudinal location of the leading and following spots is related as a tilt in the angle between the equator and a line drawn between bipolar sunspot groups. Joy's law describes how BMRs on the solar surface are tilted with respect to the east-west equator of the Sun, with average tilt angle increasing as a function of increasing latitude. Sunspot tilt angle may inform us about the process by which bipolar magnetic activity originates and rises to the surface. The large scatter in tilt angles makes it difficult to recover Joy's law for a single solar cycle or individual hemisphere (McClintock & Norton 2013). There is some indication that the slope of Joy's law is anti-correlated with the strength of a solar cycle (Dasi-Espuig et al. 2010), although this is still under debate.

Historical data used for the determination of BMR tilt angle have not included magnetic polarity information to correctly identify anti-Hale regions. Anti-Joy regions (those with the follower spot closer to the equator than the leading spot) are not necessarily anti-Hale (Tlatov et al. 2013). The existence of significant numbers of anti-Hale spots has been argued as evidence that our current understanding of sunspot formation is incomplete, if not flawed. Stenflo and Kosovichev (2012) speculate that anti-Hale spots were caused by the existence of toroidal flux bands in opposite orientation at the same latitudinal in the interior.

Tilt angle has been historically determined using white light observations from which magnetic polarity and anti-Hale information cannot be extracted. Observational studies of BMRs include polarity information, but many of the BMR studies include regions that are not sunspots since they do not have an umbra and penumbra seen in continuum intensity. The BMRs in these studies include smaller active regions without sufficient flux to form sunspots or former sunspot regions that have broken apart. One example is the work of Wang and Sheeley (1989) who observed 2706 BMRs with fluxes $\geq 3 \times 10^{20}$ Mx from daily magnetograms obtained at the National Solar Observatory (NSO) during Solar Cycle 21 between 1976-1986. Using the expected polarity for that cycle, they classified 113 BMRs as anti-Hale or approximately 4%. Stenflo and Kosovichev (2012) using MDI/SOHO magnetograms confirmed 4% of mid-size to large BMRs between 1995-2011 were anti-Hale; however, smaller regions unlikely to form sunspots exceeded 25%.

Others have reported similar low percentages of anti-Hale regions; 3.1% (Richardson 1948) and <5% (Smith & Howard 1967). However, these studies included in their total number of regions those that were not sunspots, regions that were unipolar, and poorly observed regions. (Note: tilt angles were not determined for the unipolar regions, but they were counted as part of the total number of regions to determine a percentage.) Khlystova and Sokoloff (2009) noted that their determination of 4.9% anti-Hale of bipolar sunspot regions might be low due to regions not properly recorded as anti-Hale in the data. Harvey (1992) used Mount Wilson sunspot polarity drawings and NSO full-disk magnetograms to propose that anti-Hale regions at high latitudes may be an indication of the next solar cycle starting earlier than previously established. This is an obvious problem if a single date is used to separate one cycle

from another. We avoid this problem by separating the distinct cycles as a function of time and latitude so that high-latitude new cycle spots can be correctly identified and not mistaken for anti-Hale regions.

Maunder and Maunder (1904) noticed that the Southern hemisphere was producing spots on and across the Equator for Solar Cycle 12. He states “Though the diagram shows clearly that there is but a single spot-zone in either hemisphere in each of these two cycles, a zone which moves in general accordance with Spörer’s curves, it reveals a striking and unexpected fact – namely, that the southern current not only reaches the equator, but crosses it. The limit which bounds spot-distribution in the southern hemisphere on the equatorial side can be traced not only as far as the equator, but beyond it.” Spörer’s curves represent the progressive migration of sunspot mean latitude toward the Equator over the course of a solar cycle (Spörer 1890). Throughout this paper, we make a distinction between the magnetic and heliographic equators. Zolotova et al. (2009) define the magnetic equator as the difference in latitude of sunspot production between the hemispheres. We define magnetic equator in a similar fashion using only sunspot group latitudes. We explore whether a percentage of anti-Hale regions near the Equator are due to Northern polarity spots appearing below the heliographic equator or vice versa.

3.1 Data

The Debrecen Photoheliographic Data (DPD),² spanning dates from 1974 January 2 to the present, consist of daily white light images taken primarily at the Heliophysical Observatory of the Hungarian Academy of Sciences (Győri et al. 2011). Our collection from 1974 January 2 to 2014 February 27 is based on 38,852 daily measurements of tilt angle and latitude (Figure 3.1). We average latitude and tilt over the life of each region, resulting in 6968 sunspot regions. At the time of publication, data were still under preparation for 1980 to 1985 due to missing plates. Note that the Hungarian Academy of Sciences houses a similar data set using hourly MDI observations known as SOHO/MDI-Debrecen Data (SDD) with dates ranging from 1996 May 19 to 2010 December 31, although we are not utilizing the SDD data in this paper because they only contain one cycle and do not currently offer advantages over the DPD data other than an hourly cadence and coverage uninterrupted by poor atmospheric conditions. The SDD data use the polarity of sunspots only “to separate to the following or leading portion of the group independently from the geometrical position of spots” and do not indicate “whether the polarities of the leading and following part follows the Hale’ polarity law or not, the leading part is always that part which is in the leading position according to its longitude.”³ The SDD data has the potential to report on Hale’s polarity law and record a full 360° range of tilt angles. We hope this paper emphasizes the importance of anti-Hale statistics in order to encourage catalogues like SDD or

²<http://fenyi.solarobs.unideb.hu/DPD/index.html>

³ftp://fenyi.solarobs.unideb.hu/pub/SDD/additional/tilt_angle/Readme.txt

STARA⁴ (another sunspot catalogue using MDI and HMI data) to include polarity information with full tilt angle ranges.

Li and Ulrich (2012) collected data from 1974 to 2012 using primarily Mount Wilson Observatory daily sunspot records and daily averaged magnetograms as well as MDI/SOHO magnetograms from 1996 to 2010. Approximately 30,600 sunspot tilt angles were recorded with magnetic polarity information. Only sunspot data were included, meaning there were no smaller magnetic regions that were not visible in white light images included in their sample. Instead of plotting daily values, we average latitude and tilt over the life of each sunspot region, which provides a data set of 8377 bipolar sunspot regions. See Li and Ulrich (2012) for all details and methodology, which include the assigning of ellipsoidal boundaries and centroids of polarity for active regions.

Magnetic information in historical data sets (Table 3.1) may have been used to identify that a certain spot group was bipolar, but not to establish a true magnetic tilt angle based on the dominant leading polarity for the hemisphere and solar cycle (i.e., tilt angles in historical data are limited to $\pm 90^\circ$ not $0-360^\circ$). Data of this type are flawed because anti-Hale regions are not recorded as such. All data in Table 3.1 report tilt angles in the southern hemisphere as positive if the leading sunspot is closer to the equator than the following spot, regardless of the polarity of the leading sunspot. It was only the combination of magnetic polarity information with sunspot data by Li and Ulrich (2012) that allows for the reporting and analysis of anti-Hale sunspot activity.

Table 3.1: Data Containing Tilt Angle Measurements without Anti-Hale Information.

Data	Dates	Cadence
Mount Wilson (MW)	1917-1985	daily
Kodaikanal (KK)	1906-1987	daily
Debrecen Photoheliographic Data (DPD)	1974-2014	daily
SOHO/MDI-Debrecen Data (SDD)	1996-2010	hourly
SDO/HMI-Debrecen Sunspot Data (HMIDD)	2010-2013	hourly

3.2 Adding Tilt Angle to Butterfly Diagrams

Variations in the way the butterfly diagram is plotted can illustrate characteristics of the solar cycle beyond the simple fact that sunspots move equatorward over time. For example, if sunspot area is included, as shown in Figure 3.3 and originally produced by Hathaway et al. (2003), then details regarding the times of greatest sunspot area

⁴<http://www.nso.edu/staff/fwatson/STARA/catalogue>

production are evident roughly in the center of the butterfly wings. Ternullo (2007, 2010) further studied the density of sunspot area as a function of time and latitude and found that in any hemisphere the activity is split into two or more distinct activity waves drifting equatorward. We explore whether the depiction of the bipolar sunspot region tilt angles as plotted in the classical butterfly diagram format can tell us anything more about the solar dynamo.

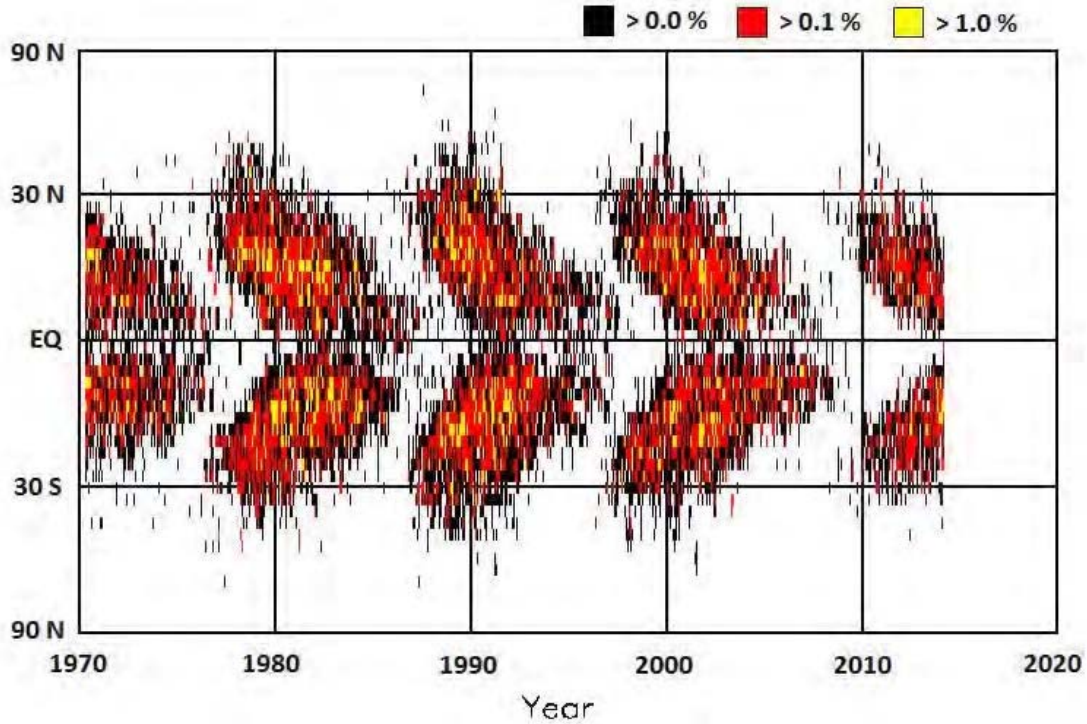


Figure 3.3: Daily mean sunspot area per each solar rotation plotted as a function of time and latitude. Areas are binned in 50 equal-area latitude strips. The relative area of the sunspot group is illustrated with black, red, and yellow as areas of increasing size. Courtesy of NASA/MSFC/David Hathaway.

Using magnetic polarity information, Li and Ulrich (2012) defined tilt angle from the west to produce a range of -180° to 180° . We define tilt angle in similar fashion, measuring tilt angle counterclockwise from the north to produce a full range of 360° as well (Figure 3.4), rather than the traditional tilt angle range of -90° to 90° used in other data sets, such as those listed in Table 3.1. Our tilt angles have the same range as Li and Ulrich, however by comparison we would define an angle of 90° by Li and Ulrich as 0° in our orientation from the north.

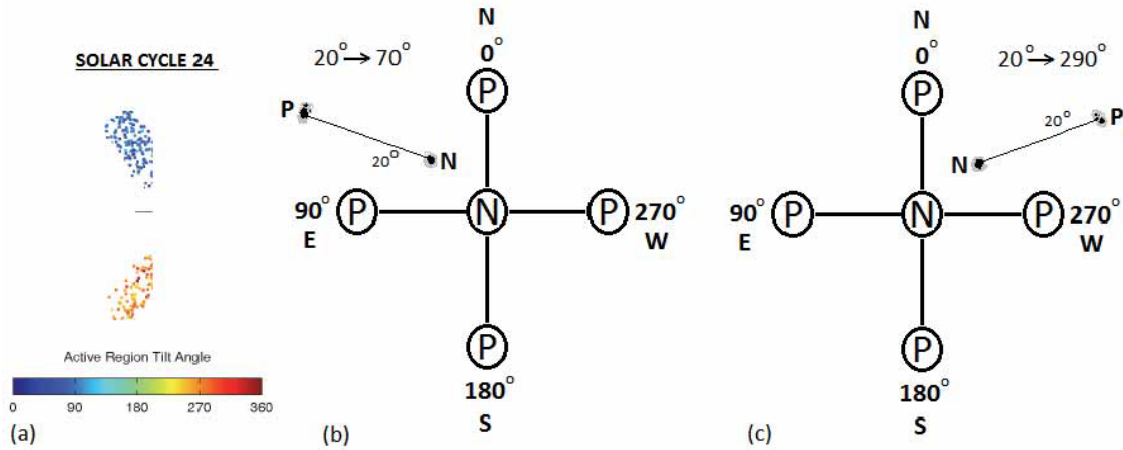


Figure 3.4: “P” is positive polarity, “N” is negative. (a) An example of expected tilt angles for Solar Cycle 24. We would expect tilt angles to average slightly less than 90° and slightly more than 270° for this cycle. (b) The dominant leading polarity in the northern hemisphere for Solar Cycle 24 is negative. A northern hemisphere tilt angle of 20° from the equator would be 70° . (c) A southern hemisphere tilt angle of 20° from the equator would be 290° . Li and Ulrich (2012) defined tilt angle from the west to produce a similar range of 360° .

Examples of expected tilt angles for Solar Cycle 24 are included in Figure 3.4 for reference. We define anti-Hale tilt angles in Solar Cycles 20, 22, and 24 for the northern (southern) hemisphere as between 0° and 180° (180° and 360°). For Cycles 21 and 23, anti-Hale in the northern (southern) hemisphere is between 180° and 360° (0° and 180°). We would expect tilt angles in Cycle 24 for example to average slightly less than 90° in the Northern hemisphere and slightly more than 270° in the Southern hemisphere according to our definition of tilt angle.

Solar Cycles 20 to 24 are plotted from Li and Ulrich data to include tilt angle as measured counterclockwise from the north (Figure 3.5). The latitude of the sunspot group is an average of area-weighted latitude determinations of leading and following sunspot umbrae. Solar Cycles 20, 22, and 24 have a negative (positive) leading sunspot in the northern (southern) hemisphere. Solar Cycles 21 and 23 are reversed to where the northern (southern) hemisphere has a positive (negative) leading sunspot.

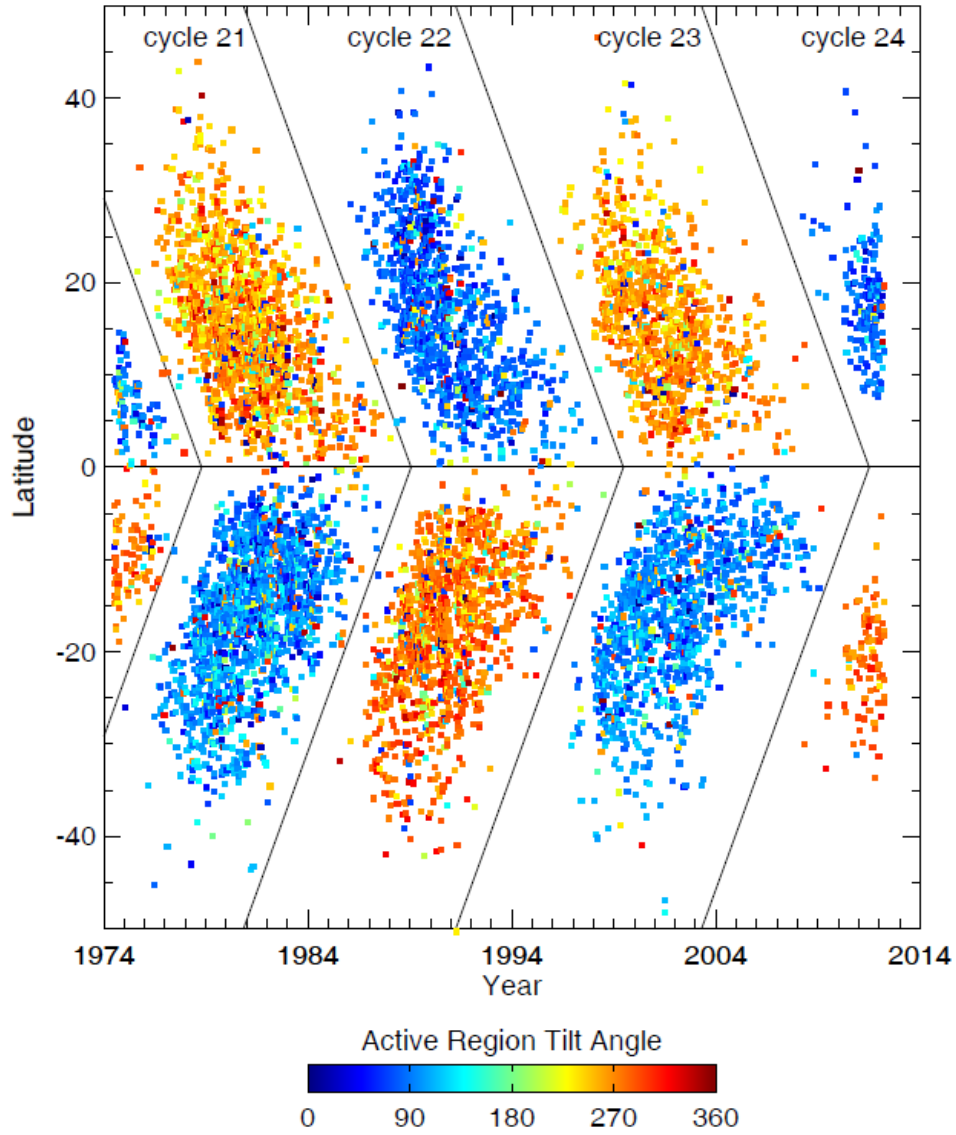


Figure 3.5: Tilt angles from Li and Ulrich (2012) data averaged by bipolar sunspot region and plotted as a function of time and latitude. Tilt measured counterclockwise from the north. Slope ($\pm \frac{1}{60}$) and location of solar cycle boundaries chosen manually for best fit. A portion of Solar Cycle 20 is visible at the left edge of the diagram.

The boundary between the hemispheres is defined by the heliographic equator and the boundaries between cycles for the southern/northern hemispheres are defined by $60 \times ylat = \pm(xdate - xint)$, where $ylat$ is latitude, $xdate$ is a function of the number of days from 1974 January 1 and $xint$ is the point of intersection at the equator.⁵ We visually determined the slope, $\frac{1}{60}$, as a value that could easily demarcate all of the cycles while $xint$ was visually determined separately for the best fit for each cycle as

⁵ $xdate = 365.25(year - 1974) + DOY$

determined by the plot of all regions. Values and dates are listed in Table 3.2. We explicitly denote the solar cycle boundaries in the paper because the determination of anti-Hale regions depends on it.

Table 3.2: Solar Cycle Boundary Information Used to Determine Anti-Hale Activity

Solar Cycle	Minimum	xint	Date
20	...	1	1974 Jan 1
20/21	1976 Jun	1750	1978 Oct 16
21/22	1986 Sep	5500	1989 Jan 21
22/23	1996 May	9300	1999 Jun 18
23/24	2008 Jan	13700	2011 Jul 5

Solar Cycles 20 to 24 are plotted from DPD data to include tilt angle as measured counterclockwise from the north (Figure 3.6). Latitude of the sunspot group is an average of area-weighted latitude determinations of leading and following sunspot umbrae. Sunspot groups near the equator are assigned a hemisphere as determined by mean latitude, regardless of leading spot polarity. DPD data are limited to a tilt angle range of 180° , so we used the expected polarity orientation for that solar cycle to assign a range of 0 to 180° to the appropriate hemisphere and 180° to 360° to the other hemisphere. Anti-Hale information is therefore not represented in either hemisphere for any solar cycle.

We use mean and median of tilt angles plotted over sunspot butterfly diagrams to confirm that tilt angle time dependence is a function of sunspot latitude (Li & Ulrich 2012). We first binned all data points in 300 day intervals, then found mean and median tilt angles of each bin using

$$\text{mean}(\gamma) = \arctan\left(\frac{\sum \sin \gamma}{\sum \cos \gamma}\right) \quad (3.1)$$

$$\text{median}(\gamma) = \arctan\left(\frac{\text{median}(\sin \gamma)}{\text{median}(\cos \gamma)}\right) \quad (3.2)$$

where γ represents tilt angle.

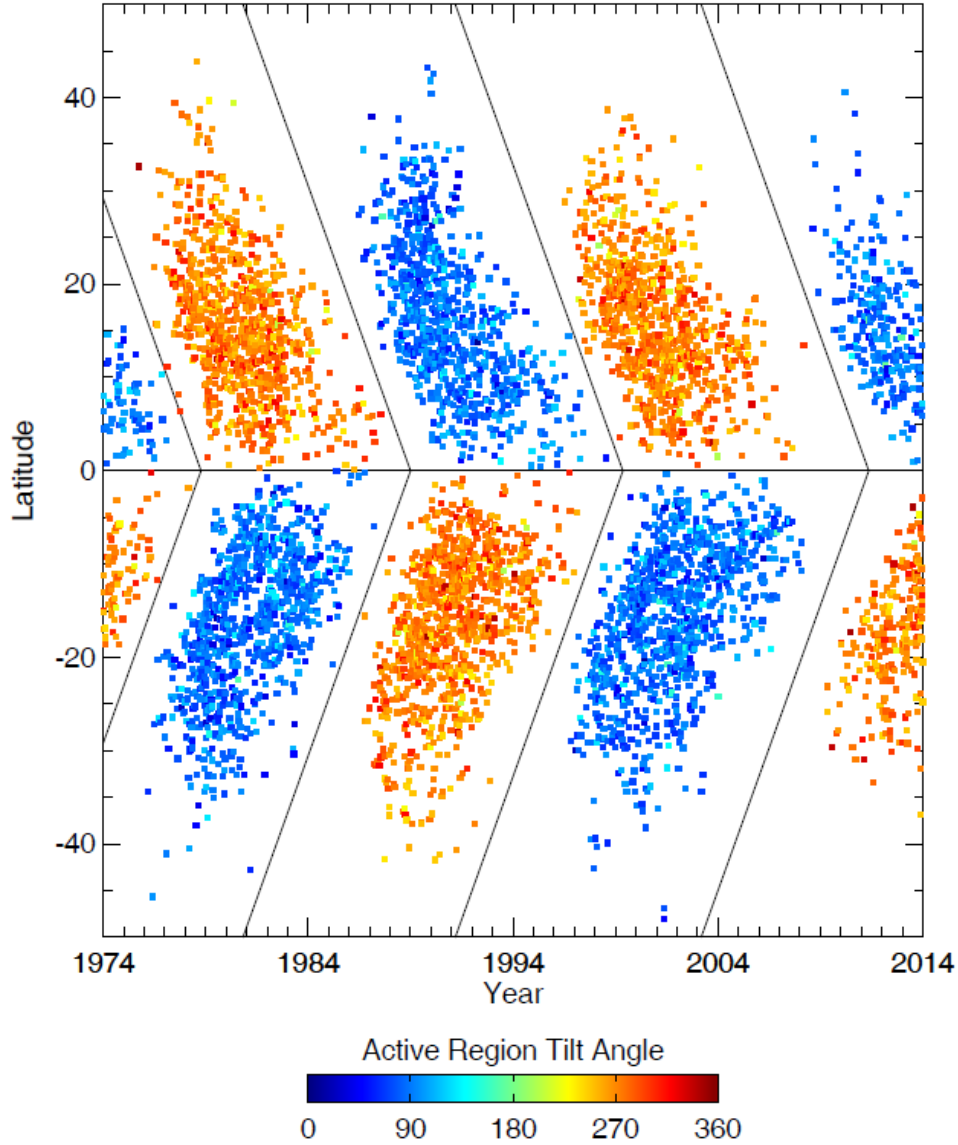


Figure 3.6: Tilt angles from DPD data averaged by bipolar sunspot region and plotted as a function of time and latitude. Tilt measured counterclockwise from the north and assigned a range of either $0-180^\circ$ or $180^\circ-360^\circ$ based on the expected polarity orientation for each hemisphere in that solar cycle. Portions of Solar Cycle 20 and 24 are visible at the left and right edges of the diagram, respectively, with all of Cycles 21-23 presented.

Mean (solid) and median (dashed) of each bin are plotted over the butterfly diagram of all sunspots in Figure 3.7(a). We also determined mean latitude and tilt angle for each active region, binned those values in 300-day intervals, and found mean and median of each bin (Figure 3.7(b)) using Equations (3.1) and (3.2). The sunspot latitude is given on the left vertical axis with a range of $0-40^\circ$. The tilt angle mean and

median (lines) are shown on the right vertical axis with a range of 0-20°. It should be noted that the tilt angles were not separated by cycle boundaries in Figure 3.7. The 300-day bins near solar minimum will contain overlapping cycles for data shown in these figures. Mean or median tilt angle is not useful near solar minimum and were therefore excluded from the plots. Tilt angle decreases as sunspots migrate from high to low latitudes in each solar cycle, as expected from Joy's law. Note that the decrease of tilt angle over time is not smooth, but discontinuous, possibly an indication of the distinct dynamo waves as mentioned by Ternullo (2007, 2010). Standard deviation, $s(\gamma)$, as set by,

$$s(\gamma) = \sqrt{\frac{(\overline{\sin \gamma})^2 + (\overline{\cos \gamma})^2}{n}} \quad (3.3)$$

of all sunspot observations (solid) and active region means (dash) for the Northern (red) and Southern (blue) hemispheres are shown in Figure 3.7(c). The peak of tilt angle scatter occurs as expected between solar cycles when polarities in both hemispheres are changing 180° in accordance with Hale's law.

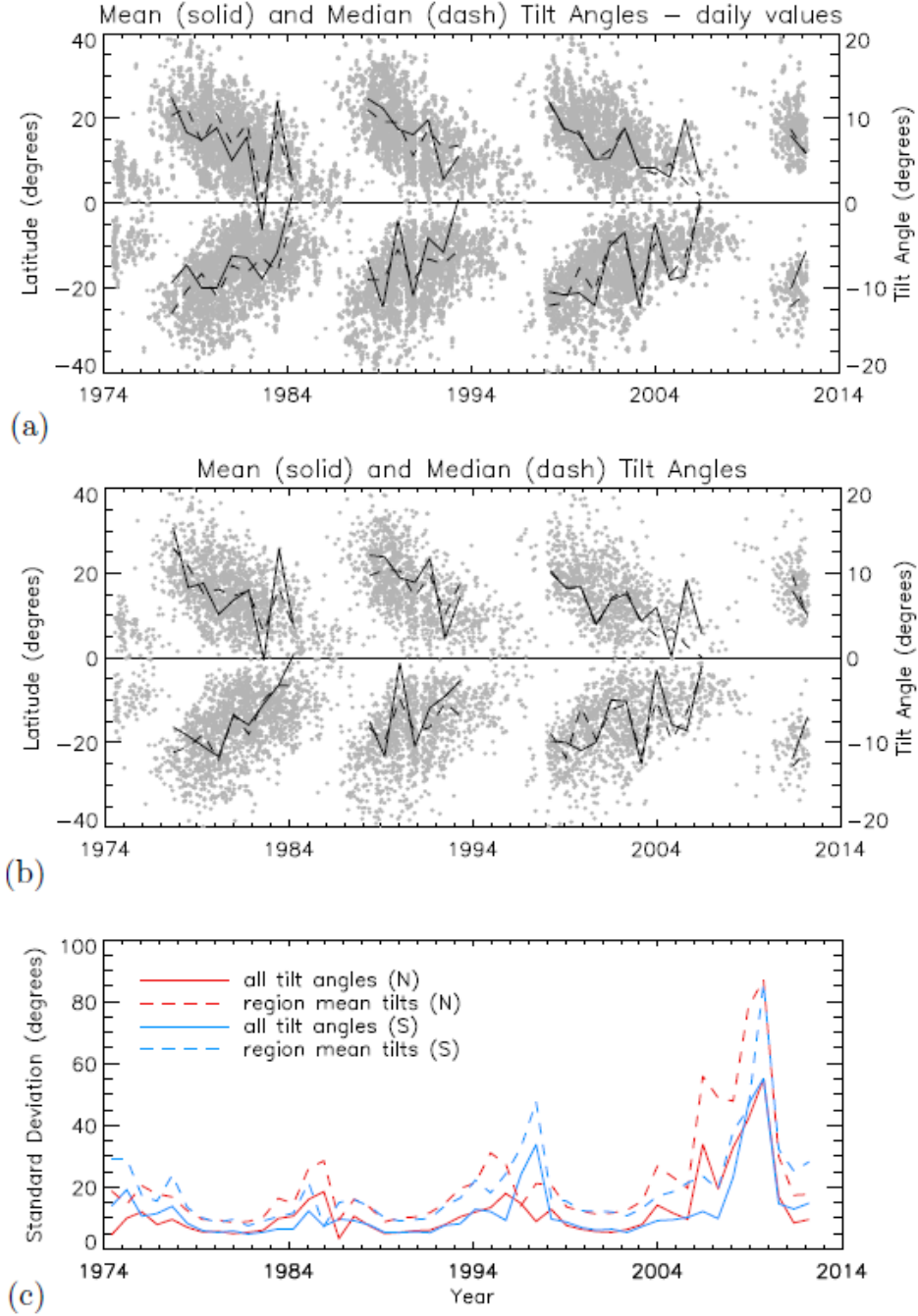


Figure 3.7: In panels (a) and (b), mean (solid) and median (dash) tilt angles binned in 300 day intervals are plotted over the sunspot butterfly diagram. Latitudes (tilt angles) are given in the left (right) vertical axis. The horizontal straight line indicates the equator. In panel (a), sunspot tilt angles and latitudes are recorded for each day (daily) that the sunspot group is present on the disk. In panel (b), the average tilt and latitude for that group is recorded only once during its passage across the disk. In panel (c), standard deviation of all sunspot observations (solid) and active region means (dash) for the northern (red) and southern (blue) hemispheres are shown.

3.3 Anti-Hale Regions

Li and Ulrich data are used to plot anti-Hale bipolar sunspot regions from 1974 to 2012 as a function of time and latitude (Figure 3.8). Tilt angles were averaged over the lifetime of each region. With fewer data points, a larger pixel size than previous figures is assigned to make color variations more visible.

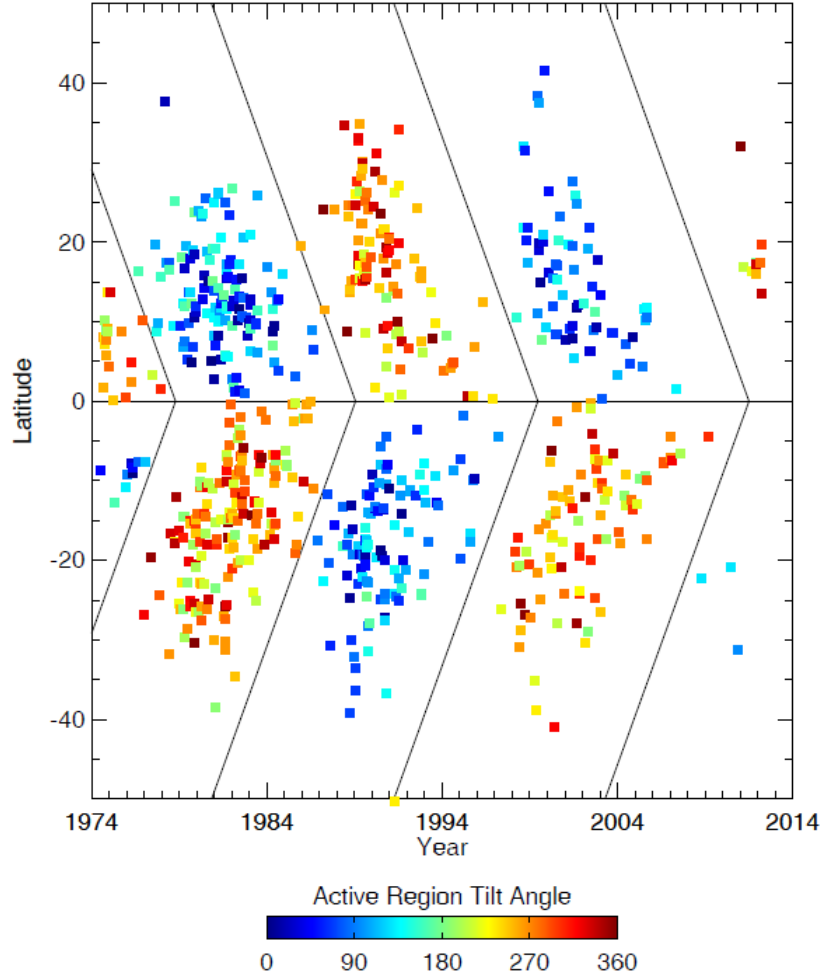


Figure 3.8: Anti-Hale tilt angles from Li and Ulrich (2012) data averaged by bipolar sunspot region and plotted as a function of time and latitude. Tilt measured counterclockwise from the north. Portions of Solar Cycle 20 and 24 are visible at the left and right edges of the diagram, respectively, with all of Cycles 21-23 presented. With fewer data points, larger pixel size assigned to make color variations more visible.

The percentage of bipolar sunspot regions that are anti-Hale from 1974 to 2012 are shown in Table 3.3. See Table 3.2 for solar cycle boundary definitions. The total

sunspot area by hemisphere for Solar Cycles 20 to 23 from the archives of the Greenwich Royal Observatory⁶ is in 10^4 micro-hemispheres. Sunspot area is used as a proxy for cycle strength (Solanki & Schmidt 1993). Solar Cycles 20 and 24 only include partial bipolar sunspot data at the end and beginning of those cycles, respectively, which could explain the high percentage of anti-Hale in the northern hemisphere for Solar Cycle 20. Of 8377 bipolar sunspot regions, 705 (8.4%) were anti-Hale. We found anti-Hale percentages of 9.0%, 8.7%, and 7.2% for Solar Cycles 21, 22, and 23 respectively, with 14.8% for Cycle 20 and 4.0% for Cycle 24.

Table 3.3: Anti-Hale (AH) Information by Solar Cycle and Hemisphere with Total Area

Cycle (yr) Length	Year of Minimum	Northern Hemisphere			Southern Hemisphere			Total AH
		N	AH	Σ Area ^a	N	AH	Σ Area ^a	
20 (partial)	(1964.8)	(107)	(19.6%)	6.94	(96)	(9.4%)	4.91	14.8%
21 (10.3)	1976.5	1547	8.4%	7.51	1710	9.5%	7.77	9.0%
22 (10.0)	1986.8	1150	9.0%	6.38	1287	8.5%	7.24	8.7%
23 (12.2)	1996.9	1004	6.6%	5.61	1178	7.8%	6.45	7.2%
24 (partial)	2008.1	(193)	(4.7%)	...	(105)	(2.9%)	...	4.0%
Total	...	4001	8.2%	...	4376	8.6%	...	8.4%

^atotal sunspot area in 10^4 micro-hemispheres

Figure 3.9(a) shows that the percentage of anti-Hale regions binned yearly are relatively consistent over time except near the end of each cycle. This could be a result of activity occurring at low latitudes, thus interacting across the equator. The number of anti-Hale regions (red) closely tracks the number of bipolar sunspot regions divided by 10 (black) in Figure 3.9(b). Similar tracking occurs when mean latitude of bipolar sunspot regions (black) and anti-Hale (red) are plotted, with the standard deviation as error bars (Figure 3.9(c)). Zolotova et al. (2009) defined the magnetic equator as the difference in the latitudinal centroids of the sunspot locations in the hemispheres. Our data are limited to sunspot groups, of which we take the yearly mean latitude in each hemisphere and average the two values to define the magnetic equator (blue). Note that the magnetic equator is deflected southward at all times except for the beginning of Solar Cycle 24. Zolotova et al. (2009) also calculated the magnetic equator from Royal Greenwich Observatory USAF/NOAA data showing that the magnetic equator was located a few degrees south of the heliographic equator.

⁶<http://solarscience.msfc.nasa.gov/greenwch.shtml>

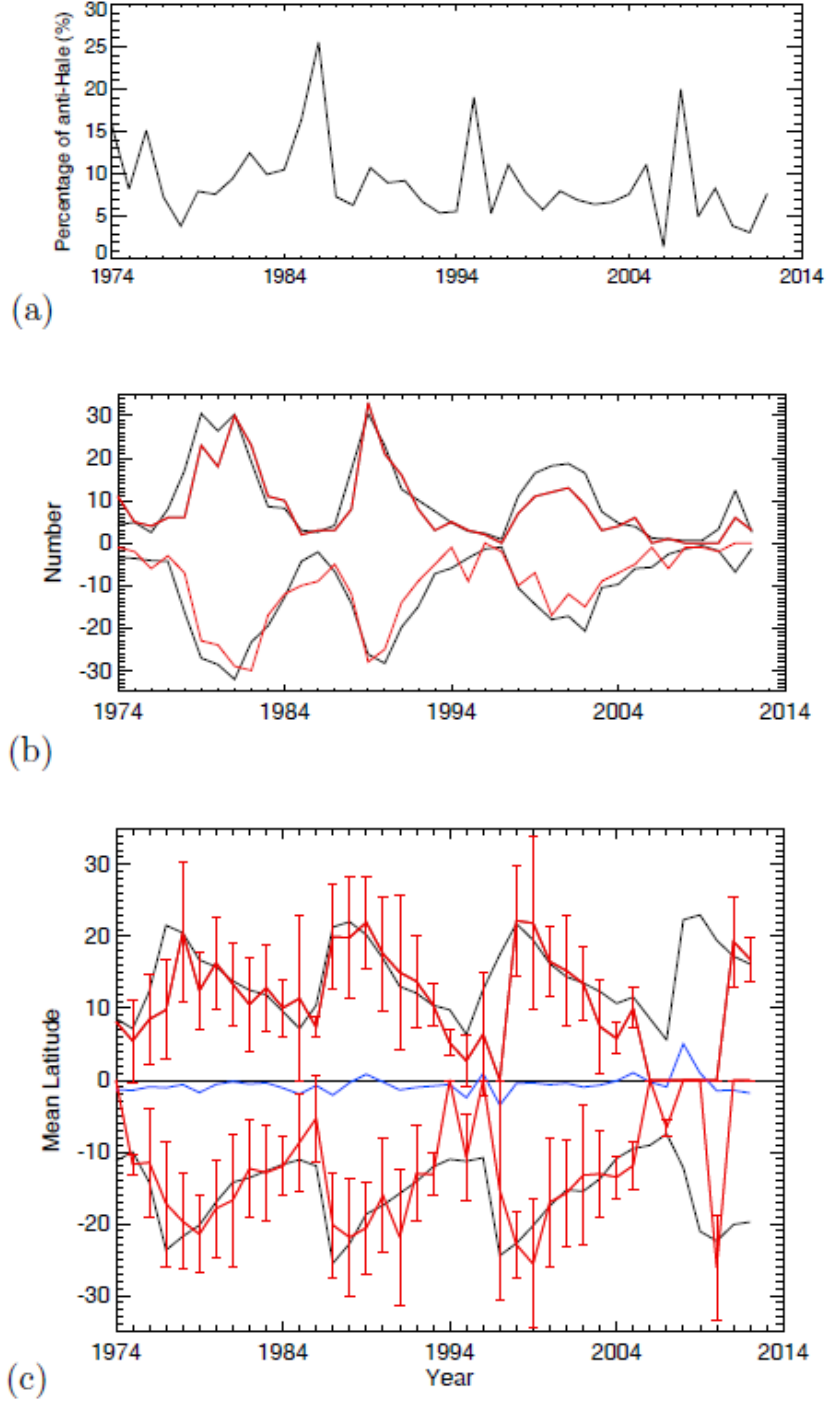


Figure 3.9: Yearly binning of Li and Ulrich (2012) data plotted over time. (a) The percentage of bipolar sunspot regions that are anti-Hale. (b) The number of bipolar sunspot regions divided by 10 (black) and anti-Hale regions (red). (c) Mean latitude of bipolar sunspot regions (black) and anti-Hale (red). Standard deviation of anti-Hale bins plotted as error bars. The magnetic equator (blue) is defined as the difference in the latitudinal centroids of the sunspot locations in the hemispheres. Note that the magnetic equator is deflected southward of the heliographic equator at all times except for the beginning of Solar Cycle 24.

Tilt angles with polarity (0 - 360°) were binned in 10° bins. The number of sunspots for each bin is shown in Figure 3.10 as total (solid). We plotted anti-Hale tilt angles normalized by the total number of sunspots (dot) and normalized by the total number of anti-Hale spots (dash). Anti-Hale tilt angles are part of a broader distribution of all tilt angles and show a weak dependence on being tilted 180° from their expected Joy's law angle. The reason for this could be two-fold: (1) that east-west orientations of active regions are preferred and (2) the active regions contributing to the 90° and 270° peaks are the late-cycle, near-equator sunspot groups that are classified as anti-Hale because the magnetic equator is offset from the heliographic equator.

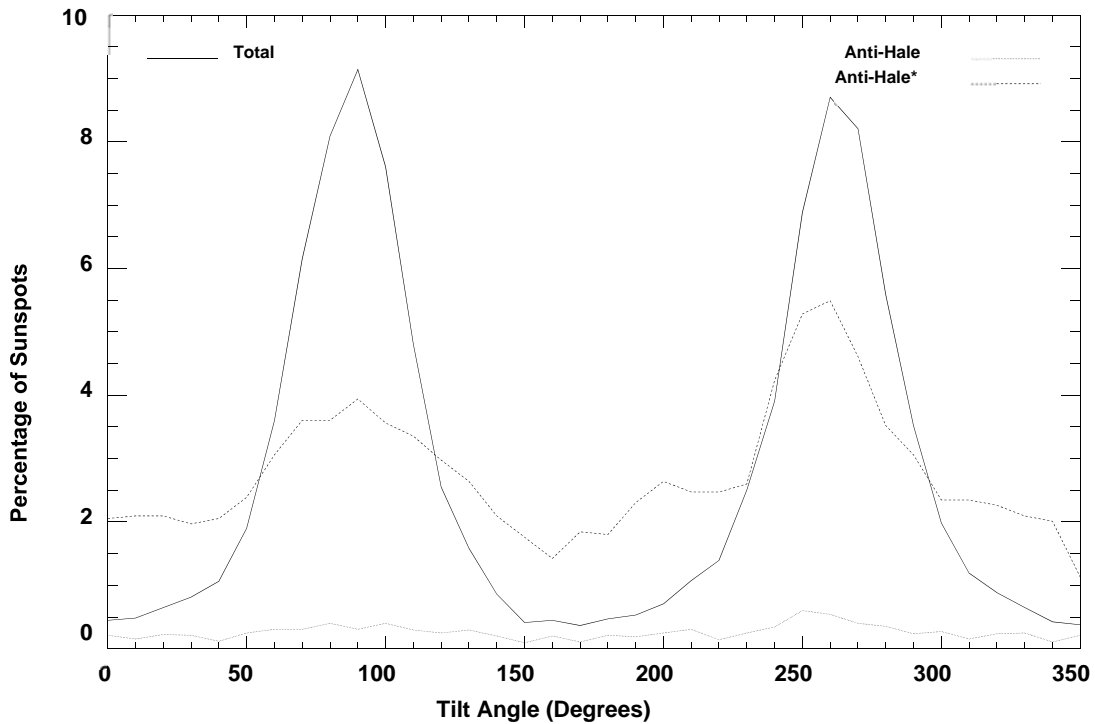


Figure 3.10: Tilt angles (0 - 360°) binned in 10° intervals. Distribution of all sunspot tilt angles (solid), anti-Hale numbers normalized by the total of all tilt angles (dot), and anti-Hale* normalized by the total of anti-Hale only (dash).

Li and Ulrich (2012) located sunspots on magnetograms to determine sunspot magnetic area in micro-hemispheres (MSH). Figure 3.11(a) shows the size distribution function of sunspot area for all bipolar sunspots (asterisk, solid) and anti-Hale sunspots (diamond, dotted). The distributions for all sunspots and anti-Hale sunspots are similar to the log-log shape reported by Baumann and Solanki (2005) and Bogdan et al. (1988). The percentage of anti-Hale spots for any given size is roughly 10% as seen in Figure 3.11(b).

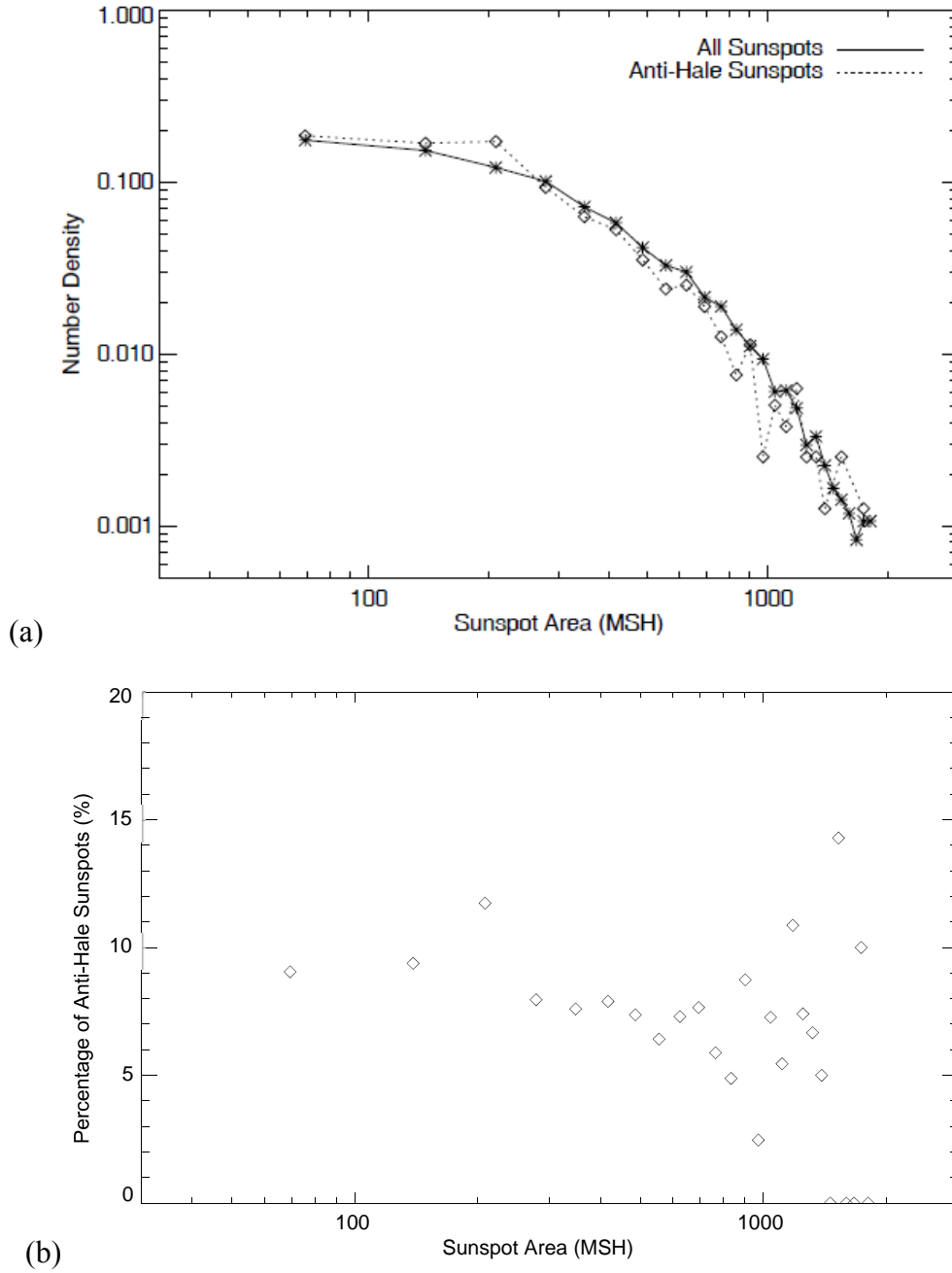


Figure 3.11: (a) Size distribution function of sunspot magnetic areas in micro-hemispheres (MSH) for all sunspot groups (asterisk, solid) and anti-Hale sunspots (diamond, dot) on a log-log scale. (b) Percentage of anti-Hale sunspots as a function of sunspot magnetic area in micro-hemispheres (MSH) plotted to log-normal scale.

3.4 Equatorial Regions

We examine the tilt angle of sunspots close to the equator, comparing DPD tilts without anti-Hale information (Figure 3.12(a)) to Li and Ulrich tilt angles that include anti-Hale (Figure 3.12(b)). We focus attention within 5° of the equator between 1974–2007. No bipolar regions were within 5° of the equator for the Li and Ulrich data after solar minimum in 2008 January. Although the DPD data are incomplete at the time of publication and some sunspots are present in Figure 3.12(b) that are not found in Figure 3.12(a), it can be noted that tilt angles near the equator in Figure 3.12(a) are at times miscalculated because the algorithm utilized in the DPD data set does not allow for any tilt angles outside the $\pm 90^\circ$ range. In Figure 3.12(b), one can find anti-Hale sunspots in any given cycle shown as data points that are 180° opposite the dominant color. Within 5° of the equator, 65 out of 470 (13.8%) bipolar sunspot regions are anti-Hale. This percentage is slightly lower if sunspots at all latitudes are included. From 1974 to 2012, 8.4% of all Li and Ulrich tilt angles are anti-Hale. We therefore assume DPD data have incorrect tilt angles since anti-Hale are not recorded as such.

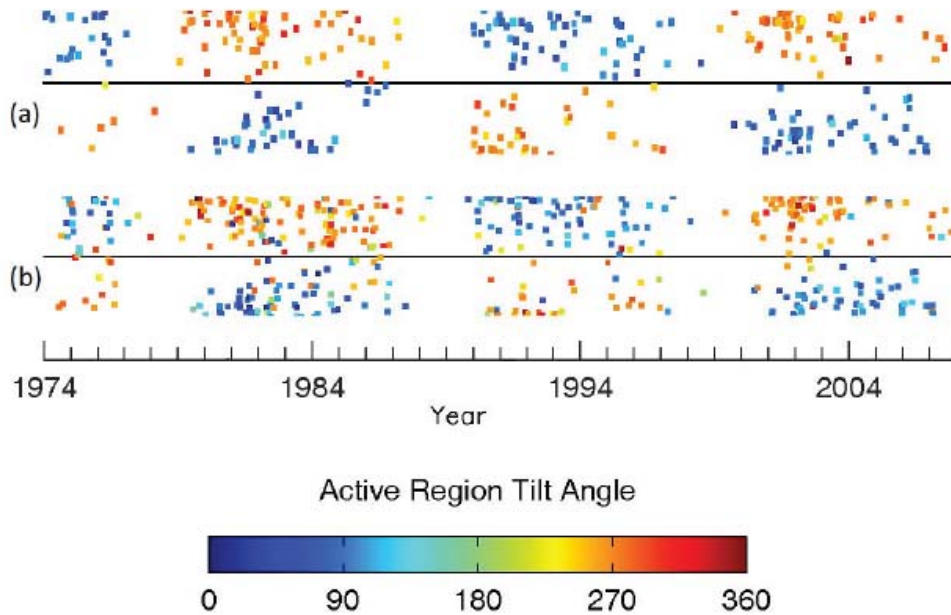


Figure 3.12: Bipolar sunspot regions within 5° of equator from 1974 to 2007. (a) DPD data are incomplete at the time of publication, most significantly from 1980 to 1985. (b) Li and Ulrich data. Panels (a) and (b) are cropped from Figures 6 and 5, respectively.

A southward-deflected magnetic equator in relation to the heliographic equator for the past 40 years (Zolotova et al. 2009), also seen in Figure 3.9(c), causes an increase in the number of sunspots that are categorized as anti-Hale late in cycle because northern hemispheric polarity sunspots are appearing south of the

heliographic equator. That the magnetic equator is shifted in relation to the heliographic equator can explain the increase in percentage of anti-Hale spots late in solar cycle. Others (McIntosh et al. 2013; Norton et al. 2014) have investigated the asymmetry of the hemispheres by studying photospheric magnetism and also found that the northern hemisphere has been leading the southern hemisphere in Cycle 24. As mentioned in the discussion of Figure 3.10, equatorial regions that appear as anti-Hale, because they are northern hemispheric regions emerging slightly south of the heliographic equator contribute to the slight peaks at 90° and 270° in the anti-Hale tilt angle distributions.

In addition to assigned tilt angle range, other differences between DPD data and those of Li and Ulrich become apparent in Figure 3.12. Data-point density differences could be attributed to weather at each of the sites precluding agreement on any given day. The DPD conversion to digitized data, although nearly complete, is not finished. DPD data identified the active regions by NOAA number while Li and Ulrich relied on Mount Wilson numbering until 1990, switching to NOAA in 1991, which could explain the higher number of data points before 1991 in Figure 3.12(b) when compared to Figure 3.12(a).

3.5 Other Efforts to Include Tilt Angle in Butterfly Diagrams

Plotting quantities as a function of latitude and time has illustrated many physical processes of the sunspot cycle. Because tilt angle as a function of latitude is noisy as seen in Joy's law, it is unclear whether including tilt angle in the butterfly diagram can be useful. Previous efforts include Tlatov et al. (2013), who used weighted MDI data to plot tilt angle information over butterfly diagrams that used color to indicate sunspot area. Large sunspot areas were defined as larger than 300 millionths of the solar hemisphere (MSH) and small areas as between 50 and 300 MSH. In Figure 3.13(a), mean tilt angles for large sunspot areas are oriented as expected with positive (negative) mean tilt angles in the northern (southern) hemisphere. Data represented by double circles have a mean tilt value that is indistinguishable from zero. Smaller sunspot areas (Figure 3.13(b)) have mean tilt angles at high latitudes mostly oriented away from what we would expect. Mean tilt values are noisier in the smaller sunspots (Figure 3.13(b)) and are not well determined at the beginning of cycles or near the equator. Perhaps it is only useful inasmuch that readers are able to understand that Joy's law is not well behaved or statistically easy to recover for a single hemisphere and solar cycle. Tlatov et al. (2013) claims that these results are indicative of two distinct dynamo processes occurring, one that generates large sunspots and another that generates small sunspots. Overplotting tilt angle on the butterfly diagram was productive in their efforts after separating the large and small sunspots.

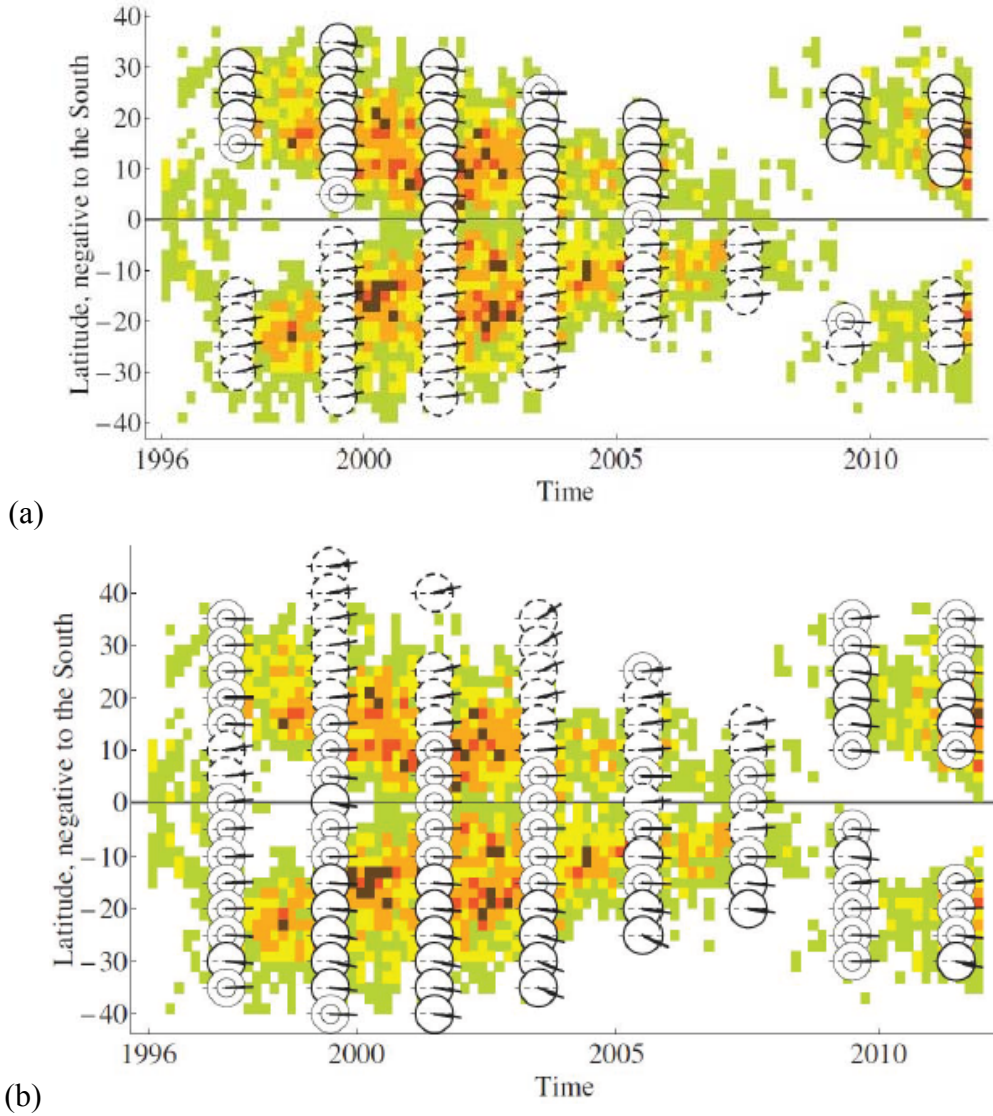


Figure 3.13: Figure of Solar Cycle 23 ($B_{min} = 10$ G) reproduced with permission from Tlatov et al. (2013). The underlying butterfly diagram with color representing area does not change in (a) and (b). (a) Tilt angles are represented for larger sunspots with areas $S > 300$ MSH from weighted MDI data. (b) Tilt angles are represented for smaller sunspots with areas $50 < S < 300$ MSH for non-weighted MDI data. Circles indicate mean tilt angle. Solid (dashed) circles indicate positive (negative) mean tilt angle. Zero tilt does not belong to the confidence interval, unless a double circle is present. Tilt is positive (negative) if the tilt is clockwise (counterclockwise), regardless of hemisphere.

It appears that there is a contradiction in the literature, as follows. Kosovichev and Stenflo (2008) do not find a dependence of tilt angle value on sunspot flux. (Note that sunspot flux and size are highly correlated.) Weber et al. (2013) simulations show that the tilt angle scatter increases for lower flux regions but the mean tilt angle does

not vary significantly with flux. Jiang et al. (2014) present Kodaikanal and Mt. Wilson Observatory tilt angle data binned according to sunspot size. They find that “the average tilt angles have a weak trend to increase with the sunspot group size, while the standard deviations significantly decrease” with sunspot group size. However, Tlatov et al. (2013) find that smaller sunspots show more scatter and consistently have average tilt angles that are anti-Joy (not anti-Hale). The contradiction may in part have its source in the different data used to determine group size: Tlatov et al. (2013) uses MDI magnetograms to determine area while Jiang et al. (2014) use white-light intensity from ground-based observations. Kosovichev and Stenflo (2008) also use MDI magnetograms, so the disagreement between Tlatov et al. (2013) and Kosovichev and Stenflo is difficult to understand.

We disagree with Tlatov et al. (2013) as we do not think there are two distinct dynamo processes occurring. We also disagree with Kosovichev and Stenflo (2008) that anti-Hale spots indicate the presence of oppositely directed toroidal bands occurring simultaneously in the same hemisphere. Rather, we agree with Weber et al. (2013) simulations showing that the convective flows interact with the rising thin flux tubes to produce anti-Hale regions. Weber et al. (2013) find “that 6.9% emerge with polarities that violate Hale’s law, in comparison to the $\approx 4\%$ as found via observations” of Wang and Sheeley (1989) and Stenflo and Kosovichev (2012). We agree with Weber et al. (2013) observations that the anti-Hale spots “arise as a result of flux tubes emerging in the opposite hemisphere from which they originated, or as a result of the flux tube becoming so distorted by convection that the legs of the emerging loop can become reversed.”

X. Sun and T. Hoeksema (Sun et al. 2015) are using tilt angle information from the DPD data set to illustrate how flux transport on the solar surface reverses the polarity of the Sun’s poles.

3.6 Discussion

We compared the statistics of a sunspot tilt angle catalog that utilizes magnetic polarity information to assign tilt angles from $0\text{--}360^\circ$ (Mount Wilson and MDI, Li & Ulrich 2012) to a traditional tilt angle catalog in which the range of values is $\pm 90^\circ$ (DPD). Because historical tilt angle databases have not been capable of including anti-Hale information due to the lack of magnetograms or the unwillingness to incorporate the magnetogram information into a functional database, we paid particular attention to the anti-Hale statistics of bipolar sunspot regions. We summarize our findings as follows.

1. We find that $8.4\% \pm 0.8\%$ of sunspot groups are anti-Hale from 1974-2012 as recorded in the Li and Ulrich data, so we assume DPD data have incorrect tilt angles for these regions since anti-Hale values are not possible in the DPD value range. The number of anti-Hale sunspots were found to be 9.0%, 8.7%,

and 7.2% of the total number of sunspot groups in Solar Cycles 21, 22, and 23, respectively. Our reported 8.4% value of anti-Hale regions is higher than previous studies. This could simply be due to Wang and Sheeley (1989) and Stenflo and Kosovichev (2012) using active regions that were not sunspots whereas we only use sunspots. The number of anti-Hale regions at any given time is simply a fraction (see Figure 3.9(b)) of the total number of sunspots present, excepting the end of each cycle when spots are very near the equator (see point 4, this section) and the expected polarity or source hemisphere is unknown.

2. The average latitudes of anti-Hale regions are the same as all other sunspots for any given time in a solar cycle, meaning the average latitude of anti-Hale spots becomes more equatorward as the cycle progresses. The size distribution of anti-Hale sunspots is the same as the log-normal distribution of all sunspots. No area preferences emerge for anti-Hale regions.
3. We find that anti-Hale are just part of a broader distribution of tilt angles, possibly as a result of convective zone turbulence as previously proposed by many researchers. However, the misclassification of anti-Hale near the Equator is due to the heliographic equator not aligning with the magnetic equator. This is visible in the tilt angle distribution as a slight tendency for the anti-Hale regions to be tilted 180° from their expected Joy's law tilt angle.
4. Joy's law cannot be observed by eye in the tilt-butterfly diagrams (Figures 3.5 and 3.6) but must be teased out statistically by averaging over significant periods of time. This is evident by the lack of a smooth gradient in the color representing tilt angle in the butterfly wings when examining one hemisphere and one cycle. Even after averaging and binning, the trend in tilt angle shows discontinuous behavior in that the mean or median tilt angle will decrease on average for a period of years then increase again suddenly. This may be related to distinct dynamo waves that occur within the solar cycle (Ternullo, 2007).
5. Sunspots very near the equator are often assigned incorrect tilt angles due to the magnetic equator being offset a few degrees. For example, sunspots that have a northern hemispheric magnetic polarity and appear just below the heliographic equator (presumably because the northern hemisphere is ahead in the sunspot cycle and has reached the Equator first) are assigned tilt angles as if they are produced from the southern hemisphere polarity. Figure 3.9(a) shows an increase in anti-Hale near the end of each solar cycle. Within 5° of the equator, 65 out of 470 (13.8%) bipolar sunspot regions are anti-Hale. The end of Solar Cycle 20 produced 14.8% anti-Hale when sunspot activity is concentrated near the equator.

Example: an active region (NOAA11987/HARP3784) straddles the equator but its central latitude is calculated to be 2° in the southern hemisphere on 2014 February 24

(Figure 3.14(a)). DPD reported a tilt angle on that date to be -15.26° . According to our definition, shown in Figure 3.4, the tilt angle should be 15.26° . The magnetogram in Figure 3.14(b) shows a magnetic orientation consistent with a northern hemisphere BMR for this solar cycle. It is probably that this region, slightly south of the equator, originated from magnetic dynamo activity in the northern hemisphere since the Northern hemisphere is leading the southern hemisphere and reached the equator first. Conversely, this region could have originated from dynamo action in the southern hemisphere with polarity orientation and tilt angle opposite from that anticipated via Joy's law and Hale's law. We suggest the former is more plausible. We propose assigning this region to the northern hemisphere based on tilt and polarity, with a caveat regarding latitude. Also note that this active region has a significant tilt angle, not a zero tilt angle as predicted by many versions of Joy's law that forces the tilt to be zero at the equator. The practice of forcing Joy's law to zero at the equator is not supported by observations. Doing so makes a huge difference in the slopes as reported in the literature and we find that there are, as often as not, BMRs with significant tilts at the equator.

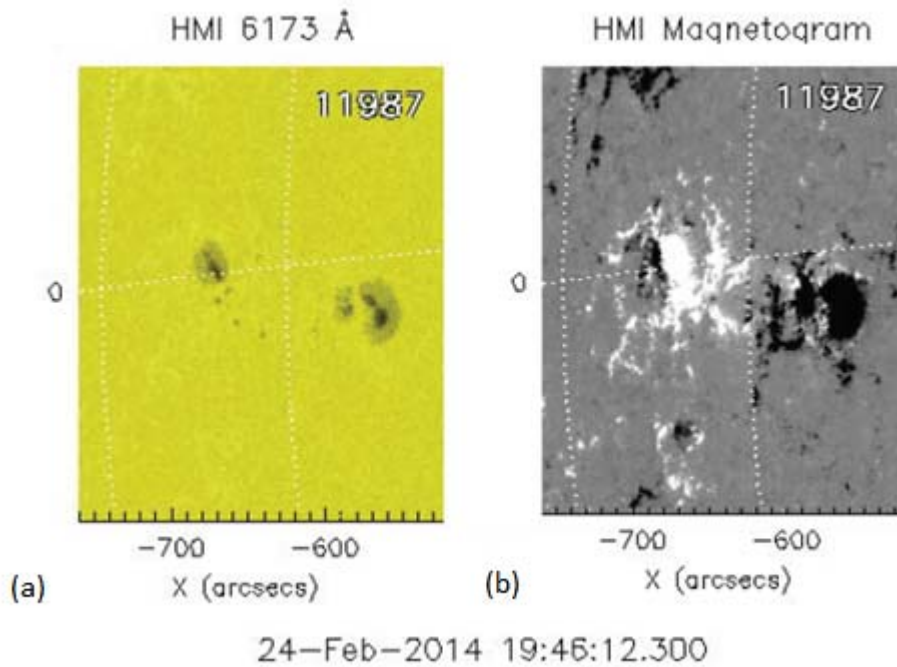


Figure 3.14: (a) White light intensity image and (b) magnetogram on 2014 February 24 of bipolar sunspot group NOAA11987 straddling the equator. The leading polarity of NOAA11987 is indicative of a northern hemisphere orientation for this solar cycle. DPD reported a tilt of umbral activity as -15.26° whereas a northern hemisphere bipolar region of this orientation would be reported with a positive tilt angle.

6. The tilt angles of sunspot groups and associated scatter in the tilt angle values are crucial for the build-up and reversals of the polar fields in surface flux transport simulations (Cameron et al. 2010; Cameron & Schüssler 2012).

Recent efforts by Jiang et al. (2014) have shown that the tilt angle scatter constitutes a significant random factor in the variability of cycle strength. Therefore, we anticipate that the inclusion of the 8.4% of anti-Hale sunspots in surface flux transport models may allow for even greater cycle to cycle amplitude variability.

From points 1 and 2, we conclude that the physical processes that produce anti-Hale regions are the same processes that produce sunspots obeying Hale's polarity rules. Knowing that tilt angles have a high scatter, we conclude that the tails of the tilt angle distribution function are quite wide and therefore 8.4% of all spots can have angle $\pm 90^\circ$ from the expected orientation. Of course, many questions about tilt angles and anti-Hale activity remain unanswered. There is, as always, more work to do.

4 Tilt Angle and Footpoint Separation of Small and Large Bipolar Sunspot Regions Observed with HMI

Magnetic fields generated at the base of the Sun's convective zone are thought to form toroidal flux tubes that become buoyant and rise to the surface (Parker 1955; Charbonneau & MacGregor 1997; Charbonneau 2005). Sunspots often appear where the flux loops break the surface. On average, bipolar sunspots show leading spots to be closer to the Equator than following spots. Hale et al. (1919) first published observations of this phenomenon, now known as Joy's law, after statistical analysis showed that the mean tilt angle of bipolar sunspots increased with latitude. Joy's law has traditionally been interpreted as the Coriolis force operating on divergent plasma at the apex of a rising magnetic flux tube. Rough calculations of the Coriolis effect on a rising flux tube by D'Silva and Choudhuri (1993) measured a deflection in the tilt angle from an E-W orientation over time in terms of the rotational frequency of the Sun and emergence latitude. The subsurface pitch angle of the toroidal field has also been proposed as a cause of tilt angle prior to the rise of flux tubes through the convection zone (Babcock 1961).

Numerical simulations of toroidal flux loops (Fan et al. 1994) show a dependence of the tilt angle on the emerging latitude and field strength (B) where $B > 20$ kG. Negative tilt angles start to occur when $B < 20$ kG, where the weak field strength and low flux (10^{20} Mx) host a converging flow at the apex in contrast to the standard divergent flow model (Weber et al. 2013). The thin flux tube approximation has been used to study rising magnetic loops in the convection zone and to explore the tilt angles and latitudes of emergence (Spruit 1981; Moreno-Insertis 1986). Studies show that the strength of the toroidal magnetic field should be around 30 - 100 kG in addition to indicating that the Coriolis force could explain the tilt angle described by Joy's law (D'Silva & Choudhuri 1993; Caligari et al. 1995). See Fan (2009) for a review of these topics, including models of toroidal flux tubes rising with and without the influence of convective zone turbulence. Weber et al. (2013) also compared flux tube simulations and found that tilt has a dependence on magnetic field strength in the flux tubes but no dependence on the total flux in the tube.

Thin flux tube models that include convection and radiative diffusion predict shorter rise times through the convective zone (Weber & Fan 2015), producing tilt

angles consistent with observed active regions. These simulations are able to reproduce tilt angles consistent with Joy's law without the need for anchored footpoints in the overshoot region. However, tilt angle scatter for magnetic field strengths ≤ 40 kG are higher than observations.

Fisher et al. (1995) found that tilt was proportional to latitude and magnetic flux in the tube and inversely related to the magnetic field strength in the initial toroidal flux tube at the base of the convection zone. This version of Joy's law includes flux and initial field strength because aerodynamic drag balances the Coriolis force for rapidly emerging regions and magnetic tension balances the Coriolis force for slowly emerging regions. However, Kosovichev and Stenflo (2008) studied MDI magnetograms and found no evidence of a Joy's law dependence on magnetic flux or for a relaxation of the tilt angle toward zero after emergence. Introducing magnetic field line twist stabilizes the cohesion of the rising tubes but also affects the tilt angle (Fan 2008). Since sunspot area and sunspot flux are highly correlated, area is used as a proxy for flux in order to study the relationship between the tilt angle and flux. Jiang et al. (2014) binned Kodaikanal and Mt. Wilson Observatory tilt angle data according to sunspot size and found a weak correlation between mean tilt angle and sunspot group size, while the standard deviations significantly decrease with sunspot group size.

The amount of scatter in the tilt angles of bipolar regions provides information about the magnetic structures that produce sunspots. Wang and Sheeley (1989) analyzed 2710 bipolar magnetic regions (BMRs) and found no noticeable dependence of tilt angle on flux but higher deviations from the mean tilt angle for weaker BMRs. Longcope and Choudhuri (2002) explained the departures of tilt angle from Joy's law during emergence as caused by upper convective zone turbulence. Tilt angle scatter about Joy's law introduced by convection increases as flux decreases in thin flux tube models by Weber et al. (2013). Illarionov et al. (2015) showed the significant scatter in bipolar regions with areas less than 300 MSH (including ephemeral regions without sunspot activity). A transition occurs between 300 and 400 MSH where the distribution of larger regions becomes dominated by sunspot activity with substantially less tilt angle scatter and more tilt angles that follow Joy's law.

It has been proposed that the magnetic field could become so weak below the surface that convective zone turbulence dominates the flux tube. Fan et al. (1994) suggested a mechanism of dynamic disconnection where a submerged portion of an emerged flux tube collapses after achieving hydrostatic equilibrium, disconnecting the tilt angle from the influence of the initial toroidal field pitch angle. Schrijver and Title (1999) proposed subsurface reconnection of the untethered legs of the flux tube at depth to explain surface activity during decay. Longcope and Choudhuri (2002) rule out dynamic disconnection at shallow depths in their model of rising flux tubes. Schüssler and Rempel (2005) modify the dynamic disconnection model based on strong, buoyancy-driven upflow and radiative cooling in a rising flux loop prior to emergence, finding disconnection depths around 5 Mm and disconnection times less than 3 days.

As a flux loop ends its emergence and the footpoints stop separating, as observed in the photosphere as the centroid locations of the two polarities, Coriolis forces should end and the tilt angles should relax toward zero due to magnetic tension restoring field lines to an E-W orientation. If the field is significantly frozen into the plasma and the differential rotation force is not strong enough, then the region maintains the tilt angle established prior to the end of emergence. The higher cadence of recently collected sunspot data presents a more complete picture of the tilt angle and footpoint separation over the lifetime of active regions. A limited study of six active regions by Pevtsov et al. (2003) using Solar and Heliospheric Observatory (SOHO)-MDI data reported separation distances around 25 Mm but generally increasing over time. Fan (2009) discussed the post-emergence evolution of subsurface fields (section 8.3) and observed that the photospheric portion of the footpoints stop separating at 100 Mm which cannot be explained in the Ω -loop model.

In order to better understand the complexities of Joy's law, it is helpful to keep the following in mind.

1. The pitch angle of the toroidal field beneath the surface may be a cause of the tilt angle prior to the rise of flux tubes through the convection zone.
2. Coriolis forces act on flows from the expanding plasma in the apex of the flux tubes rising through the bulk of the convection zone. Coriolis forces increase with latitude and conversely should decrease near the Equator.
3. The high scatter in the tilt angle is attributed to the interaction of a rising flux tube with convection. After emergence, subsurface convection should no longer impart scatter in tilt over the lifetime of the region.
4. A disconnection of the flux tube from the source field would cause the tilt angle to no longer be affected by the initial pitch angle but instead relax to the angle held by the legs at the disconnection depth.

4.1 Data

Images taken by the Helioseismic and Magnetic Imager on board NASA's Solar Dynamics Observatory were used to calculate bipolar sunspot tilt angles for HMI - Debrecen Data (HMIDD)⁷ from 2010 April 30 to the present. The calculation methods employed were an extension of those used by Györi et al. (2011) on the SOHO/MDI - Debrecen Data (SDD). After correcting for limb darkening and flat field effects, Sunspot Automatic Measurement (SAM) software determined the penumbra borders from the first contour having a local maximum in an averaged gradient along contour (AGAC) with the umbra border contour having the global maximum in the AGAC.

⁷<http://fenyi.solarobs.unideb.hu/ESA/HMIDD.html>

Umbral area is defined by the number of pixels within the umbral border and reported in the HMIDD as millionths of solar hemispheres (MSH). Within the umbra border, the centroid of the pixels weighted by intensity determined the umbral latitude and longitude of the spots.

Line-of-sight magnetic field information and umbral area measurements were used to calculate the mean latitude and longitude of the leading and following sunspot groups. The HMIDD data used the polarity of sunspots only to separate the following and leading groups and do not indicate whether Hale’s polarity rule is observed or not. After grouping sunspots by polarity, only longitude determines which group is considered the leading group.⁸ The HMIDD calculation of the tilt angle included the area-weighted latitude, area-weighted longitude, and latitude of the centroid of the entire bipolar region (Baranyi 2015, Eq. 1). The latitude and longitude of the leading and following spot groups were determined by averaging the positions of all of the individual spots (weighted by area) within their respective group. We calculate the separation in degrees from the latitude and longitude of the leading and following spot groups and convert to Mm by equating 1° in separation with 12.13 Mm on the solar surface.

HMIDD data report tilt angles as positive in either hemisphere if the leading spot group is closer to the Equator than the following group. Joy’s law would be observed in the tilt angle as a function of the unsigned latitude. However, we emphasize that near-Equator measurements of the tilt are incomplete since bipolar regions are assigned a hemisphere by latitude without regard to polarity (McClintock & Norton 2014). At the time of publication, the HMIDD data only contained the beginning of Solar Cycle 24 when sunspot activity occurs at higher latitudes.

4.2 Bipolar Sunspot Behavior during Emergence and Decay

Trends in tilt angle are difficult to observe in individual active regions and become more apparent in larger samples. We identify 1151 NOAA regions in the HMIDD data and determine that 1111 regions had at least one umbral tilt angle reported. We use the umbral calculations of the latitude and longitude for the leading and following sunspot groups to determine footpoint separation, which we report as the distance between the centroids of the opposite polarities in the photosphere. NOAA active regions often contain new emergence activity after previous umbral activity has stopped. We exclude new activity in a particular NOAA region if the umbral activity was not reported for more than 24 hours. To minimize the foreshortening distortion of active regions observed near the limb, we limit the data to observations taken within 0.7 solar radii from the center of the Sun’s disk. The hourly cadence of HMIDD data allow for binning of the tilt angle, total umbral area, and footpoint separation over 8 hour intervals for each active region.

⁸http://fenyi.solarobs.unideb.hu/pub/SDO/additional/tilt_angle/Readme.txt

Individual active region information is recorded at various stages of development and decay depending on where the activity occurs on the solar surface in relation to the observation sight lines. It would not be as useful to observe tilt angle behavior over the lifetime of an active region unless we calibrate the data to an active region characteristic that is observable in each region. The onset of emergence would be an ideal reference point, but requiring regions to emerge on disk significantly limits the number of viable regions for study and emphasizes the emergence period over decay. The observational data of an active region that emerges on disk are more likely to exclude decay information, especially for longer-lived regions, as the regions rotate out of sight.

The umbral area bin with the maximum value establishes the end of emergence and the beginning of sunspot decay for that region, creating a suitable common reference point across all of the active regions and placing equal emphasis on emergence and decay observations. Data which start or end with peak umbral area for a region are excluded as these regions most likely began their decay prior to appearing on disk or did not complete their emergence period before vanishing off disk due to solar rotation away from the observational line of sight. According to this restriction and all previously stated parameters, the number of viable regions to date available for study is limited to 235.

Muñoz-Jaramillo et al. (2015) reconcile the area and flux distributions of the photospheric magnetic structures from multiple sunspot and active region databases into a composite of Weibull and log-normal distributions for flux below 10^{21} Mx and above 10^{22} Mx, respectively. They suggest that two separate mechanisms are “giving rise to visible structures on the photosphere: one directly connected to the global component of the dynamo (and the generation of bipolar active regions), and the other with the small-scale component of the dynamo (and the fragmentation of magnetic structures due to their interaction with turbulent convection)” Muñoz-Jaramillo et al. (2015, p.18). Muñoz-Jaramillo et al. show that a shift in the HMI sunspot data from a Weibull distribution ($< 10^{21}$ Mx) to a log-normal distribution ($> 10^{22}$ Mx) occurs around 90 MSH in the umbral area. We use 90 MSH to separate tilt angle and footpoint separation data by peak umbral area into two data sets. A substantial number of regions fall below this threshold, so we use 45 MSH to distinguish between small and midsize regions less than 90 MSH in peak umbral area.

For each active region with a maximum umbral area (UA_{max}) of less than 45 MSH, we sort tilt angle into 8-hour bins and find the median of each bin. We do the same for the mean footpoint separation and mean umbral area. The median serves as a better measure of the center for low-sampled degree measurements that might include positive and negative values, however, the mean is preferred for non-negative measures of the separation and area. The time at which the peak umbral area is observed is noted such that all data before (after) that time are considered as emergence (decay). The tilt, separation, and area values corresponding to the time of maximum umbral area are plotted at the $t=0$ point along the x-axis, see Figure 4.1. We repeat the

process to create two more data sets of midsize ($45 \leq UA_{max} < 90$ MSH) and large ($UA_{max} \geq 90$ MSH) regions. Error bars are overplotted as the standard error of the mean. We excluded bins more than 72 hours (96 hours) from time zero for small and midsize (large) regions due to low sampling sizes at these times.

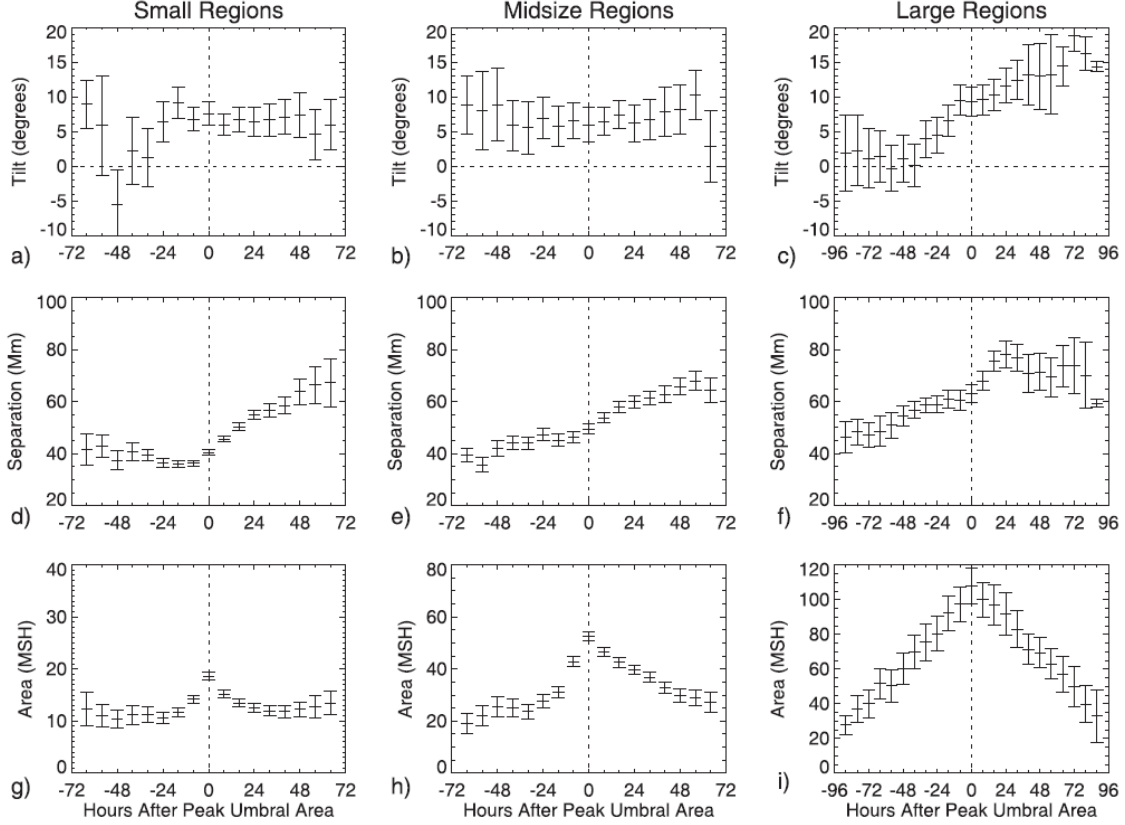


Figure 4.1: Umbral tilt angle, footpoint separation, and total umbral area binned in 8-hour intervals are plotted in reference to the maximum umbral area (UA_{max}). Regions are separated into small ($UA_{max} < 45$ MSH), midsize ($45 \leq UA_{max} < 90$ MSH), and large regions ($UA_{max} \geq 90$ MSH). (a) Median tilt angle of small, (b) midsize, (c) and large regions. (d) Mean footpoint separation of small, (e) midsize, (f) and large regions. (g) Mean total umbral area for small, (h) midsize, (i) and large regions. Standard error of the mean overplotted as error bars.

At the peak in umbral area, tilt angles are least noisy and typical for early cycle (higher latitude) activity. Midsize regions have the lowest median tilt angle (5.9°) compared to small (7.6°) and large regions (9.3°), see Table 4.1. Given the concentration of all of the regions at higher latitudes (Table 4.1), it is not useful to normalize the tilt angle for latitude until an entire solar cycle is observed. The dip in small region tilt angles around -48 hours (also visible in the separation and area plots) is likely an indication of regions that are smaller than average for this group beginning

their emergence with negative tilt angles. For two days before and after the peak area, the median tilt angles of midsize regions remain fairly constant, whereas the large regions show tilt angles occurring near zero earlier in the emergence period before steadily increasing over 4-5 days well into decay. Higher variations are observed for all of the area classifications closer to the onset of emergence and toward the end of the decay period. It is not unexpected to see more variability in the median tilt angles of small regions, especially at the beginning of their lifetimes when the influence of external factors such as convective turbulence is greater. Larger organized regions are more resistant to convective turbulence as seen in the more stabilized tilt angles.

Table 4.1: Tilt Angle, Area, and Latitude at Maximum Umbral Area (UA_{max})

	Small ($UA_{max} < 45$ MSH)	Midsize ($45 \leq UA_{max} < 90$ MSH)	Large ($UA_{max} \geq 90$ MSH)
Median Tilt	7.6°	5.9°	9.3°
Mean Area	18 MSH	52 MSH	107 MSH
Median Latitude	16.7°	16.1°	15.2°
n (viable)	149	60	26
N (original)	618	261	232

Tilt angle increases in larger regions during emergence and decay but remains relatively steady for the small and midsize regions. We cite this as evidence of supergranular convective flows influencing the formation and evolution of smaller regions. It may be that the evolution of larger regions is better explained by the Ω -loop model, whereas smaller regions begin to form bipoles primarily from supergranular convection, although this does not preclude smaller regions from evolving beyond the supergranule model into larger regions. This remains a topic of interest beyond the scope of our study.

All of the regions demonstrate a 3-4 day period of increase in footpoint separation with the onset of this period varying by region size. Approximately 3 days before the umbral area peaks and lasting a day into decay, large regions increase in separation from around 45 to 75 Mm. Midsize regions show a 30 Mm increase over 4 days as well, although the separation values are shifted downward slightly (40-70 Mm) and forward in time by about a day. Small regions maintain 35-40 Mm in separation throughout the observed portion of the emergence period, then begin a 3 day period of increase in separation at the onset of decay, peaking near 70 Mm. Near -6 hours, small regions organize around 35 Mm in separation with almost no variation. This coincides with the beginning and end of two trends in separation for these regions: the onset of a steady increase in separation after a period of relatively constant mean separation values.

Otsuji et al. (2011) studied the footpoint separation distances of 101 active regions, including in their sample many smaller flux regions that would not have been used in our study. Their results are similar in scale to our determinations of separation distances for small regions near the end of the emergence period. Discrepancies in mean separation distances between the two reports can be attributed to their inclusion of smaller flux regions as well as the shorter observational periods in their analysis. Our results from section 4.3 for very small regions compare more favorably.

The footpoint separation for small regions during the observed portion of the emergence phase remains relatively constant before beginning a period of separation at the start of decay, whereas the larger regions begin their separation prior to decay. We suggest that these smaller regions have not yet accumulated enough flux to overcome the influences of supergranular convection before decay begins. The divergent flow at the top of a supergranule cell pushes the flux to the cell boundaries as described by Schmidt (1968) while the magnetic structure of the bipole begins to dictate the size and shape of the supergranule cell. Smaller regions cannot begin their separation phase until the supergranular cell that aided in its formation begins to dissipate, typically after 1-2 days (Hirzberger et al. 2008). We suggest that larger regions are less influenced by supergranular convection during the emergence phase and simply separate beyond the typical size of a supergranule cell as a result.

The mean peak umbral areas for small regions (≈ 18 MSH) and midsize regions (≈ 52 MSH) skew significantly lower in their respective area bins (Table 4.1). Muñoz-Jaramillo et al. (2015) determined that smaller sunspot regions (< 90 MSH) display a Weibull distribution that also skews toward lower umbral areas. An empirical distribution of HMI data (Figure 4.2) shows the transition at 90 MSH from the Weibull distribution of smaller regions to a log-normal distribution for larger regions.

Including BMRs in the discussion extends the observation of tilt angle behavior to smaller regions that may or may not include sunspots. It should be noted that BMR areas are reported to be up to 44 times larger than sunspot areas in the same active region (Chapman et al. 2011). Figure 4.3 shows a BMR distribution of the area and tilt angle from MDI data at higher latitudes ($|\theta| \geq 10^\circ$) where the color intensity indicates the number of bipoles relative to the total number of bipoles with the same areas. Two distinct distributions are visible due to the substantial amount of tilt angle scatter for BMRs less than 300 MSH as well as the trend toward negative tilt angles for smaller regions.

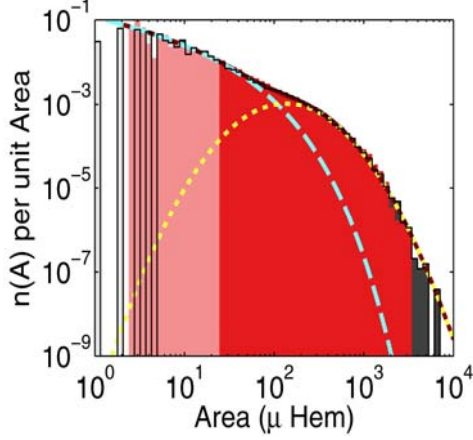


Figure 4.2: Empirical distribution of HMI sunspot areas (red), with Weibull (dashed blue line) and log-normal distributions (dotted yellow line) fitted to the darker red shade. Note the transition in distributions near 90 MSH. Reproduced with permission from Muñoz-Jaramillo et al. (2015).

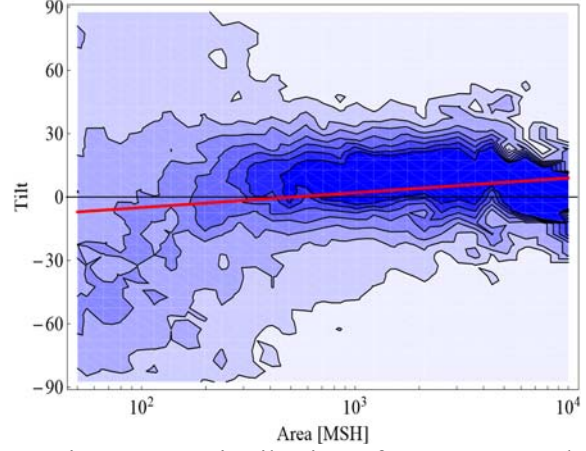


Figure 4.3: Distribution of BMR area and tilt angle from MDI data (1998-2007, latitudinal zone $|\theta| \geq 10^\circ$). Color intensity indicates the number of bipoles relative to the total number of bipoles with the same areas. The red line corresponds to the linear least-square fit. Reproduced with permission from Illarionov et al. (2015).

4.3 Very Small Bipolar Sunspot Regions

We have already seen evidence of smaller regions emerging with negative tilt angles (Figure 4.1a), particularly regions with shorter emergence periods and areas which are lower than average. We limit our observations to very small peak umbral areas (< 9 MSH) in the HMIDD data. Since these regions do not last as long, we are more likely to observe the entire life of the region within 0.7 solar radii from the center of the Sun's disk. The behavior of very small active regions gives insight into how all active regions behave when they are first forming with smaller areas. Due to the shorter lifetimes of these regions, we can apply the same binning techniques previously described but at a higher cadence of 2 hours.

The median tilt angle, mean separation, and mean area are binned every 2 hours and calibrated to the time of peak umbral area according to previously described methods. The standard error of the mean is overplotted as error bars for the tilt, separation, and area in Figure 4.4. Given the previous parameters established for viable active regions as well as the size restriction to less than 9 MSH, our sample is small ($n = 12$) but still worthy of inclusion in the discussion. Median tilt angles are anti-Joy (negative) at first, increasing to expected values in the decay period for activity at a median latitude of 16.1° . Footpoint separation increases from 20 Mm to about 35 Mm in a 14 hour span ($\approx 298 \text{ m s}^{-1}$), which is more rapidly than larger regions during the previously observed 3-4 periods of steady increase ($\approx 87 \text{ m s}^{-1}$). The umbral area averages between 3 and 5 MSH throughout the lifetimes of these regions.

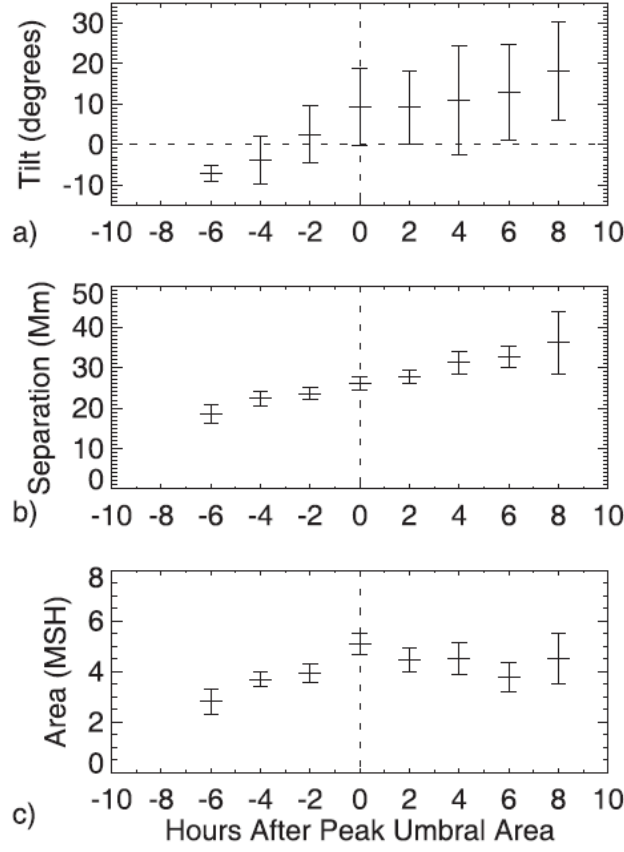


Figure 4.4: (a) Median umbral tilt angle, (b) mean footpoint separation, and (c) total umbral area binned in 2 hour intervals are plotted in reference to the peak umbral area for regions of less than 9 MSH peak umbral area. Standard error of the mean overplotted as error bars.

Using MDI magnetograms, Tlatov et al. (2013) noted the anti-Joy behavior (negative tilt angles) of BMRs with areas less than 300 MSH at higher latitudes that was not observed in larger regions. Chapman et al. (2011) report an average facular-to-sunspot ratio of approximately 44 to 1. As a rough conversion of total umbral area to BMR area, 5 MSH in the umbral area equates to 220 MSH in the BMR area, which is less than the 300 MSH threshold set by Tlatov et al. (2013). This permits a comparison of tilt angle results for our respective observations of smaller regions. It appears that anti-Joy tilt angles occur in smaller regions during the emergence period and then rotate toward positive values as the decay period begins. Coriolis forces from the divergent plasma flow in the apex of a rising flux tube deflect E-W oriented bipoles toward the positive mean tilt angles typically reported. In contrast, any existing convergent flows would deflect toward negative tilt angles. The apex of a flux tube nearing emergence in the upper convective zone with weak toroidal field strength (15-30 kG) and low flux (10^{20} Mx) hosts a converging flow (Fan et al. 1994; Weber et al. 2013), producing tilt away from expected Joy's law angles.

4.4 Discussion

When the peak umbral area is used to sort sunspot regions by size and to define the emergence and decay periods for each region, evidence of two size distributions emerges in the tilt angle behavior. After a period of near-zero tilt angles during emergence, a consistent increase in the large region ($UA_{max} \geq 90$ MSH) tilt angle begins 48 hours before peak umbral area and lasts several days into the decay period. Regions smaller than 90 MSH show more consistency in tilt during this same time frame. It may be that larger regions eventually accumulate enough flux to form a new dynamic, with Coriolis forces acting on plasma draining from the apex of a more organized flux tube. At some point during the accumulation of flux as larger regions emerge, Coriolis force induced tilt overtakes the influence of toroidal fields oriented in the E-W direction such that the increase in tilt angle persists into the decay period.

We attribute the negative tilt angles in small regions ($UA_{max} < 45$ MSH) seen at -48 hours as evidence of new activity emerging with weaker initial field strengths (Weber et al. 2013) and consistent with other observational studies of smaller active regions (Tlatov et al. 2013; Illarionov et al. 2015). Our preliminary observations of very small regions ($UA_{max} < 9$ MSH) at a higher cadence indicate the presence of negative tilt angles during emergence. As the current solar cycle progresses, further study of small regions in the HMIDD data will be of interest.

A sustained period of increase in footpoint separation lasting several days occurs for all regions, but the onset of that period varies with region size. Small regions ($UA_{max} < 45$ MSH) do not increase in separation until the end of the emergence period, whereas larger regions begin several days earlier. Separation distances during the observed portion of the emergence period for small regions are consistently near 35-40 Mm, with almost no variation in the binned values near the peak in umbral area. We attribute this behavior to the influence of supergranular convective cells as suggested by Schmidt (1968) and discussed below. These small regions then steadily increase in separation during the first three days of decay, separating to at least 70 Mm. Midsize ($45 \leq UA_{max} < 90$ MSH) and large regions ($UA_{max} \geq 90$ MSH) were observed to steadily increase in separation from 40 to 70 Mm and 45 to 75 Mm, respectively, from the start of the observed emergence period and lasting into decay. It should be noted that our observations of bipolar sunspot separation distances early in the emergence period are approximately 40 Mm, which are larger than the ≈ 25 Mm distances reported by Pevtsov et al. (2003) for BMRs. This can be attributed in part to magnetic bipoles forming before the umbral intensity signature necessary for measuring bipolar sunspot separation distances is reached.

Dynamo theories of the solar magnetic cycle use the pitch angle of subsurface toroidal fields as a source of the initial tilt in active regions prior to emergence (Babcock 1961; Leighton 1969), however, pitch angle is not sufficient to explain all tilt angle behavior on the surface. Schmidt (1968) suggests that the Coriolis forces from a divergent supergranular flow influences the tilt angle. He states that “the horizontal Coriolis force needs a day of unimpeded uniform motion to rotate the

resulting displacement by 6 degrees. Such motion can be found in a supergranulation cell which seems to last for 1 day (cf. Simon and Leighton, 1964). The same timescale holds for the appearance of a new active center” Schmidt (1968, pp. 96-97). In modeling magnetic activity in the convective zone, Weiss (1971) considered Coriolis-induced cyclonic motion formed by the divergent flow at the top of convection cells, also noting the concentration of magnetic flux around the perimeters of the convection cells. The supergranule divergent flow and the resultant anti-cyclonic motion push magnetic flux to the boundaries of the cell and build up tilt angles as long as the flow persists. The footpoint separation sizes of very small regions or regions early in the emergence period are reasonably comparable to the observed distribution of supergranule diameter sizes (Hirzberger et al. 2008). The separation velocities of the bipolar portion of very small regions are consistent with observed supergranular divergent flows of around 300 m s^{-1} (Rieutord & Rincon 2010; Langfellner et al. 2015). It is likely that many active regions begin their emergence period with small umbral areas and that supergranular divergent flows influence the initial tilt angle and separation distances in these just forming regions.

We cite the distinct variations in tilt angle and footpoint separation behaviors by region size as confirmation that two distributions of sunspot sizes exist. In order for a rising flux tube model to adequately describe all of the magnetic activity as it appears on the surface, some artificial assumptions are necessary. As more detailed observational data of magnetic regions become available, questions arise about the flux tube model. Getling et al. (2015) discuss difficulties in comparing rising-tube model to observations and how a convective mechanism using in situ amplification and structuring of magnetic fields by convection avoids these difficulties. The rising flux tube model may be sufficient to describe the formation of larger bipolar sunspot regions, whereas the initial tilt angle and footpoint separation of smaller regions are heavily influenced by supergranular convection. Further research into the cause of tilt angles in either sunspot size distribution is worth pursuing, especially the probability that a portion of the larger region distribution may be the result of smaller regions accumulating enough flux to expand beyond the influence of supergranular convection.

5 Conclusion

The results contained within this thesis are a product of observational research into Joy's law and possible causes which is research summarized in the following papers: McClintock & Norton 2013; McClintock, Norton & Li 2014, and McClintock & Norton 2016. In this chapter, we present a summary of the main results from each published work, our overall findings, and suggestions for future research.

5.1 Summary

We observed the mean tilt angle of bipolar sunspots in Solar Cycles 16 to 21 and found differences of up to 2.8° between the hemispheres and across the cycles. Revisions to Joy's law should include a weaker dependence on latitude, with more emphasis on the differences between the hemispheres and cycles. Forcing the linear fit through the origin (Dasi-Espuig et al. 2010) artificially distorts the slope and is not supported by observations. We do confirm a statistically significant negative correlation of cycle strength with area-weighted tilt angles normalized by latitude, as previously determined by Dasi-Espuig et al. (2010). It is important to note that there are times during the solar cycle when Joy's law cannot be determined, perhaps due to convective turbulence dominating the mechanism which produces tilt. Our observations of tilt angle as a function of longitude did not yield evidence of a non-axisymmetric mechanism affecting tilt angles.

A recently reported discrepancy in Joy's law determined from white light observations versus magnetogram data should be noted here. Wang et al. (2015) found that the slope of Joy's law increases more steeply for tilt angle measurements obtained from Mount Wilson magnetogram data as measured by Li and Ulrich versus sunspot tilt angles taken from Debrecen Photoheliographic Data. This discrepancy could be due to the contribution of plage areas that tend to have greater tilt inclinations than adjacent sunspot groups. We would expect to see the same increase in the slope of Joy's law if we were to include plage regions in our determinations of tilt angle. It may also be that some tilt angles based on older white-light images without magnetic information are inaccurate due to polarity grouping errors (Baranyi 2015, Wang et al. 2015).

While Joy's law is observed statistically over sufficiently large samples, the tilt angles of individual sunspot regions are noisy over their lifetimes and often identified as anti-Hale. We determined that $8.4\% \pm 0.8\%$ of sunspot groups are anti-Hale from 1974-2012, which is higher than previous studies (Wang & Sheeley 1989; Stenflo & Kosovichev 2012). For Solar Cycles 21, 22, and 23, the anti-Hale percentages of the total number of sunspots groups per cycle were 9.0%, 8.7%, and 7.2%, respectively. Although we broadened our range of tilt angle to include a representation of anti-Hale activity, Joy's law cannot be observed by eye over the life time of a particular solar cycle in our tilt-butterfly diagrams.

Latitudinal measurements of Anti-Hale regions over the course of a solar cycle follow the behavior of Hale regions, appearing at higher latitudes first then moving towards the equator as the cycle progresses. Size distributions of Hale and Anti-Hale spots are similar as well. It may be that anti-Hale spots are an extension of previously determined tilt angle distributions. We suggest that previous classifications of sunspot activity near the equator as Hale (or anti-Hale for that matter) should be questioned unless consideration is given to the orientation of the magnetic equator in relation to the heliographic equator at the time of observation. Surface flux transport simulations depend on scatter in the tilt angle values to contribute a random factor in the variability of cycle strength (Jiang et al. 2014). Including the 8.4% of anti-Hale sunspots in these models may result in greater amplitude variability from cycle to cycle.

While the cadence of individual sunspot observations has improved dramatically with the launch of the Solar Dynamics Observatory in February 2010, the rotation of the solar surface still poses a challenge to our line-of-sight observations over time. Active regions frequently do not appear and disband entirely on disk, leaving significant time segments of an active region's evolution unobservable. We used peak umbral area to sort sunspot regions by size and to define the emergence and decay periods for each region. After calibrating regions by peak umbral area, two size distributions emerge in the tilt angle behavior. A consistent increase in the median tilt angles for larger regions ($UA_{max} \geq 90$ MSH) begins during decay, whereas the median tilt angles of smaller regions ($UA_{max} < 90$ MSH) are fairly consistent over the same observational period. The behavior of the larger regions suggests that enough flux has accumulated to form a new dominating factor in tilt angle production, such as Coriolis forces acting on plasma draining away from the apex. Evidence of negative tilt angles in very small regions during emergence is consistent with previous studies and attributable to weaker initial field strengths.

A sustained period of increase in footpoint separation lasting several days occurs for all regions. This period begins near the end of emergence for smaller regions, occurring earlier for larger regions. Leading up to this sustained period of increase in separation, the distances of smaller regions are consistently near 35-40 Mm. We cite this as the influence of supergranular convective cells as previously suggested by Schmidt (1968) and Weiss (1971). Divergent flow at the top of a convection cell concentrate flux at the perimeter of a cell and build up tilt angle through Coriolis-induced cyclonic motion. Footpoint separation sizes and separation

velocities of very small regions are reasonably consistent with observed supergranule distributions (Hirzberger et al, 2008; Rieutord & Rincon 2010; Langfellner et al. 2015). Many active regions emerge at first with small umbral areas and it is reasonable to expect supergranular divergent flows to influence the initial tilt angle and separation distances in these just forming regions. Further research may reconcile the two sunspot size distributions as parts of an evolutionary process overall in bipolar sunspot formation, whereas a supergranular convection model better describes sunspot behavior until enough flux has accumulated to warrant consideration of the traditional rising flux tube model.

Much of our understanding of the convective dynamo process on other solar-type main sequence stars originated with solar physics research. Only recent advances in instrumentation have allowed for useful observations of magnetic activity in nearby stars. Observations of other low-mass stars show that more toroidal magnetic field is generated as a fraction of the total magnetic field when a tachocline develops as opposed to the star being fully radiative or fully convective (Donati et al. 2008; Morin et al. 2008, 2010). This confirms that the convective process, in part if not in full, drives the dynamo process. The behavior of small-scale magnetic activity can tell us something about the origins of global magnetic fields in the Sun, other main sequence stars, and stellar magnetic fields in general. See Brun et al. (2015) for a more detailed discussion of the solar magnetic dynamo in a stellar context.

Any dynamo theory explaining the regeneration of solar magnetic fields should account for Joy’s law, anti-Hale activity and the effect of turbulent convection on the twist in flux ropes rising through the convective zone. A complete model must consider the tilt or twist in these magnetic flux ropes that, when ejected from the Sun via mass coronal ejections, can remove helicity from the star. It may be that the flux tube concept is part of a larger, more complex model of the dynamo producing magnetic activity on the solar surface. We therefore must consider alternative theories for magnetic field production across all scales, such as the effect of divergent flows at the top of supergranules on newly emerging flux. Understanding the behavior and causes of Joy’s law brings us one step closer to a more comprehensive picture of the magnetic field generator at work in the Sun and other stars.

5.2 Overall Findings

This thesis has determined that the analysis of sunspot behavior can be significantly improved using an updated version of Joy’s law and rigorous statistical analysis of modern solar imaging datasets. In particular, we established that Joy’s law has a weaker latitude dependence than previously concluded and that anti-Hale activity occurs more frequently than what has traditionally been reported. Our findings indicate that Joy’s law varies significantly between solar cycles and across solar hemispheres. We also found evidence for the existence of small spot features not following Joy’s law, part of a second distinct sunspot population that may represent an early phase of sunspot emergence. In overall terms, this thesis has discovered increased complexity

in bipolar sunspot emergence, type and time-dependent behavior compared to previous studies, and demonstrates that analysis of sunspot observations continues to provide ways to advance the empirical basis for theoretical modeling of small-scale solar flux tubes and underlying magnetic dynamo processes.

5.3 Future Research

Our research suggests that measurements of Joy’s law should be approached more carefully if we wish to use it as a diagnostic of magnetic field production. Additional research regarding the tilt angle of bipolar sunspot groups or bipolar magnetic regions should distinguish between the hemispheres as it may be that separate dynamos are at work in each hemisphere. Verification of the accuracy of historical tilt angle data should continue as new questions arise about the measurement techniques employed to determine tilt angles from white-light images (Baranyi 2015; Wang et al. 2015). We also hope that the practice of forcing a linear fit of latitude to tilt angle through the origin is discontinued as it is inconsistent with observations. Even after separating by hemisphere, it may be that one linear fit is no longer an adequate description of Joy’s law. The availability of more detailed (i.e. higher cadence) tilt angle data will permit further refinements of Joy’s law in the future.

It is also important to recognize the existence of anti-Hale activity and how it has historically been under-reported in tilt angle databases – if at all. With the improvements to solar observatories so as to include magnetic information when determining the tilt angle of bipolar regions, anti-Hale regions can be further analyzed and incorporated into future dynamo models. The opportunity to observe active regions at a higher cadence for a significant portion of their lifetimes may yield some information about how active regions evolve and what role anti-Hale activity plays in their evolution.

The likelihood of the nesting effect, described as the emergence of bipoles within existing active regions (Harvey & Zwaan 1993), may impact the statistical measurements of Joy’s law. We took steps to minimize nesting effects in our study of bipolar sunspot regions using HMI data by excluding regions with significant new flux emerging within an already active region. However, the occurrence of this phenomenon on smaller scales can still alter the determination of the end of the emergence period. Examination of the nesting effects on Joy’s law is much more feasible with the higher cadence data sets becoming more available and should be investigated further.

As the solar dynamo is responsible for all magnetic flux events, not just sunspot regions, it would be useful to compare our examination of sunspot characteristics to a similar comprehensive analysis of bipolar magnetic regions. Given that not all bipolar magnetic regions produce sunspots, it would be of special interest to see how the tilt angle of magnetic regions evolves over the emergence and decay periods and whether there are any significant differences with our sunspot tilt angle results. A statistical

analysis of the behavior of anti-Hale magnetic regions separated into hemispheres by the magnetic equator would be a valuable comparison to our results for anti-Hale sunspot groups, especially if any significant discrepancies between the two populations are discovered.

As higher-cadence observations of magnetic events become available due to advances in space-based instrumentation, we anticipate the ability to study smaller active regions during their emergence and decay periods. Coupled with improving helioseismic observational techniques and instrumentation, a better understanding of how much impact convective flows in supergranules have on the evolving tilt angle and footpoint separation of emerging flux can be achieved. Given the recent questions about the rising flux tube model as a complete description of how surface magnetic activity is produced, it is the study of the relationship between supergranules and emerging flux that holds great interest for the future of solar magnetic dynamo research. As improved datasets become available over complete solar cycles, future work can more thoroughly analyze the extent to which small sunspot regions with anti-Joy tendencies can be explained as a supergranular precursor to the more familiar flux tube construct of bipolar sunspots. Such an evolutionary sequence can in turn provide additional empirical constraints on our theoretical understanding of sunspot formation and the Sun's magnetic fields.

Bibliography

- BABCOCK, H. W. (1961). The Topology of the Sun's Magnetic Field and the 22-YEAR Cycle. *The Astrophysical Journal*, **133**, 572.
- BARANYI, T. (2015). Comparison of Debrecen and Mount Wilson/Kodaikanal sunspot group tilt angles and the Joy's law. *Monthly Notices of the Royal Astronomical Society*, **447**, 1857-1865.
- BAUMANN, I., & SOLANKI, S. K. (2005). On the size distribution of sunspot groups in the Greenwich sunspot record 1874–1976. *Astronomy & Astrophysics*, **443**, 1061-1066.
- BOGDAN, T. J., GILMAN, P. A., LERCHE, I., & HOWARD, R. (1988). Distribution of sunspot umbral areas-1917-1982. *The Astrophysical Journal*, **327**, 451-456.
- BRAY, R. J., & LOUGHHEAD, R. E. (1964). Sunspots.
- BRUN, A. S., GARCÍA, R. A., HOUDEK, G., NANDY, D., & PINSONNEAULT, M. (2015). The Solar-Stellar Connection. *Space Science Reviews*, **196**, 303-356.
- BRUNNER, W. (1930). Regularities in the formation of sunspots to groups. *Astronomical releases the Swiss Observatory Zurich*, **13**, 67-74.
- CALIGARI, P., MORENO-INSERTIS, F., & SCHUSSLER, M. (1995). Emerging flux tubes in the solar convection zone. 1: Asymmetry, tilt, and emergence latitude. *The Astrophysical Journal*, **441**, 886-902.
- CALLY, P. S., DIKPATI, M., & GILMAN, P. A. (2003). Clamshell and tipping instabilities in a two-dimensional magnetohydrodynamic tachocline. *The Astrophysical Journal*, **582**, 1190.
- CAMERON, R. H., JIANG, J., SCHMITT, D., & SCHÜSSLER, M. (2010). Surface flux transport modeling for solar cycles 15-21: Effects of cycle-dependent tilt angles of sunspot groups. *The Astrophysical Journal*, **719**, 264.

- CAMERON, R. H., & SCHÜSSLER, M. (2012). Are the strengths of solar cycles determined by converging flows towards the activity belts? *Astronomy & Astrophysics*, **548**, A57.
- CARRINGTON, R. C. (1858). On the distribution of the solar spots in latitudes since the beginning of the year 1854, with a map. *Monthly Notices of the Royal Astronomical Society*, **19**, 1-3.
- CHAPMAN, G. A., DOBIAS, J. J., & ARIAS, T. (2011). Facular and sunspot areas during solar cycles 22 and 23. *The Astrophysical Journal*, **728**, 150.
- CHARBONNEAU, P. (2005). Dynamo models of the solar cycle. *Living Reviews in Solar Physics*, **2**, 1-83.
- CHARBONNEAU, P. (2007). Cross-hemispheric coupling in a Babcock–Leighton model of the solar cycle. *Advances in Space Research*, **40**, 899-906.
- CHARBONNEAU, P., & MACGREGOR, K. B. (1997). Solar interface dynamos. II. Linear, kinematic models in spherical geometry. *The Astrophysical Journal*, **486**, 502.
- CHATTERJEE, P., NANDY, D., & CHOUDHURI, A. R. (2004). Full-sphere simulations of a circulation-dominated solar dynamo: Exploring the parity issue. *Astronomy & Astrophysics*, **427**, 1019-1030.
- CHEUNG, M. C., & ISOBE, H. (2014). Flux emergence (theory). *Living Reviews in Solar Physics*, **11**, 1-128.
- D'SILVA, S., & CHOUDHURI, A. R. (1993). A theoretical model for tilts of bipolar magnetic regions. *Astronomy and Astrophysics*, **272**, 621.
- D'SILVA, S., & HOWARD, R. F. (1993). Limits on the magnetic field strength at the base of the solar convection zone. *Solar physics*, **148**, 1-9.
- DASI-ESPUIG, M., SOLANKI, S. K., KRIVOVA, N. A., CAMERON, R., & PEÑUELA, T. (2010). Sunspot group tilt angles and the strength of the solar cycle. *Astronomy & Astrophysics*, **518**, A7.
- DE TOMA, G., WHITE, O. R., & HARVEY, K. L. (2000). A picture of solar minimum and the onset of solar cycle 23. I. Global magnetic field evolution. *The Astrophysical Journal*, **529**, 1101.
- DELUCA, E. E., & GILMAN, P. A. (1986). Dynamo theory for the interface between the convection zone and the radiative interior of a star: Part I model equations and exact solutions. *Geophysical & Astrophysical Fluid Dynamics*, **37**, 85-127.

- DIKPATI, M. (2005). Solar magnetic fields and the dynamo theory. *Advances in Space Research*, **35**, 322-328.
- DIKPATI, M., & GILMAN, P. A. (2001). Flux-transport dynamos with α -effect from global instability of tachocline differential rotation: a solution for magnetic parity selection in the Sun. *The Astrophysical Journal*, **559**, 428.
- DONATI, J. F., MORIN, J., PETIT, P., DELFOSSE, X., FORVEILLE, T., AURIÈRE, M., ... & JARDINE, M. M. (2008). Large-scale magnetic topologies of early M dwarfs. *Monthly Notices of the Royal Astronomical Society*, **390**, 545-560.
- DURRANT, C. J., & WILSON, P. R. (2003). Observations and simulations of the polar field reversals in Cycle 23. *Solar Physics*, **214**, 23-39.
- FAN, Y. (2008). The three-dimensional evolution of buoyant magnetic flux tubes in a model solar convective envelope. *The Astrophysical Journal*, **676**, 680.
- FAN, Y. (2009). Magnetic fields in the solar convection zone. *Living Reviews in Solar Physics*, **6**, 1-96.
- FAN, Y., FISHER, G. H., & MCCLYMONT, A. N. (1994). Dynamics of emerging active region flux loops. *The Astrophysical Journal*, **436**, 907-928.
- FISHER, G. H., FAN, Y., & HOWARD, R. F. (1995). Comparisons between theory and observation of active region tilts. *The Astrophysical Journal*, **438**, 463-471.
- GETLING, A. V., ISHIKAWA, R., & BUCHNEV, A. A. (2015). Doubts about the crucial role of the rising-tube mechanism in the formation of sunspot groups. *Advances in Space Research*, **55**, 862-870.
- GETLING, A. V., ISHIKAWA, R., & BUCHNEV, A. A. (2015). Development of active regions: flows, magnetic-field patterns and bordering effect. *Solar Physics*, **291**, 371-372.
- GILMAN, P. A. (2000). Magnetohydrodynamic “shallow water” equations for the solar tachocline. *The Astrophysical Journal Letters*, **544**, L79.
- GOEL, A., & CHOUDHURI, A. R. (2009). The hemispheric asymmetry of solar activity during the last century and the solar dynamo. *Research in Astronomy and Astrophysics*, **9**, 115.
- GYÖRI, L., BARANYI, T., & LUDMÁNY, A. (2011). Photospheric data programs at the Debrecen Observatory. *Proceedings of the International Astronomical Union*, **6**, 403-407.
- HALE, G. E. (1908). On the probable existence of a magnetic field in sun-spots. *The astrophysical journal*, **28**, 315.

- HALE, G. E., ELLERMAN, F., NICHOLSON, S. B., & JOY, A. H. (1919). The magnetic polarity of sun-spots. *The Astrophysical Journal*, **49**, 153.
- HARVEY, K. L. (1992). Proceedings of the National Solar Observatory/Sacramento Peak 12th Summer Workshop on the Solar Cycle. In *ASP Conference Series* (Vol. 27, p. 335).
- HARVEY, K. L., & ZWAAN, C. (1993). Properties and emergence patterns of bipolar active regions. *Solar physics*, **148**, 85-118.
- HATHAWAY, D. H., NANDY, D., WILSON, R. M., & REICHMANN, E. J. (2003). Evidence that a deep meridional flow sets the sunspot cycle period. *The Astrophysical Journal*, **589**, 665.
- HATHAWAY, D. H. (2015). The solar cycle. *Living Reviews in Solar Physics*, **7**, 1-65.
- HIRZBERGER, J., GIZON, L., SOLANKI, S. K., & DUVAL JR, T. L. (2008). Structure and evolution of supergranulation from local helioseismology. *Solar Physics*, **251**, 417-437.
- HOWARD, R. F. (1991). Axial tilt angles of sunspot groups. *Solar physics*, **136**, 251-262.
- HOWARD, R. F. (1996). Solar active regions as diagnostics of subsurface conditions. *Annual Review of Astronomy and Astrophysics*, **34**, 75-109.
- HOWARD, R. F. (2000). Active region magnetic fields. *Journal of Astrophysics and Astronomy*, **21**, 119-125.
- HOWARD, R., GILMAN, P. I., & GILMAN, P. A. (1984). Rotation of the sun measured from Mount Wilson white-light images. *The Astrophysical Journal*, **283**, 373-384.
- HOWARD, R. F., GUPTA, S. S., & SIVARAMAN, K. R. (1999). Measurement of Kodaikanal White-Light Images–II. Rotation Comparison and Merging with Mount Wilson Data. *Solar Physics*, **186**, 25-41.
- ILLARIONOV, E., TLATOV, A., & SOKOLOFF, D. (2015). The Properties of the Tilts of Bipolar Solar Regions. *Solar Physics*, **290**, 351-361.
- JIANG, J., CAMERON, R. H., & SCHÜSSLER, M. (2014). Effects of the scatter in sunspot group tilt angles on the large-scale magnetic field at the solar surface. *The Astrophysical Journal*, **791**, 5.
- JIANG, J., İŞİK, E., CAMERON, R. H., SCHMITT, D., & SCHÜSSLER, M. (2010). The effect of activity-related meridional flow modulation on the strength of the solar polar magnetic field. *The Astrophysical Journal*, **717**, 597.

- KARAK, B. B., & BRANDENBURG, A. (2015). Is the small-scale magnetic field correlated with the dynamo cycle? *The Astrophysical Journal*, **816**, 28.
- KELLER, C. U., & STAFF, N. S. O. (1998). SOLIS Instrumentation Aspects. In *Synoptic Solar Physics*, **140**, 539.
- KHLYSTOVA, A. I., & SOKOLOFF, D. D. (2009). Toroidal magnetic field of the Sun from data on Hale-rule-violating sunspot groups. *Astronomy reports*, **53**, 281-285.
- KOSOVICHEV, A. G., & STENFLO, J. O. (2008). Tilt of emerging bipolar magnetic regions on the Sun. *The Astrophysical Journal Letters*, **688**, L115.
- LANGFELLNER, J., GIZON, L., & BIRCH, A. C. (2015). Spatially resolved vertical vorticity in solar supergranulation using helioseismology and local correlation tracking. *Astronomy & Astrophysics*, **581**, A67.
- LEIGHTON, R. B. (1964). Transport of Magnetic Fields on the Sun. *The Astrophysical Journal*, **140**, 1547.
- LEIGHTON, R. B. (1969). A magneto-kinematic model of the solar cycle. *The Astrophysical Journal*, **156**, 1.
- LI, J., & ULRICH, R. K. (2012). Long-term measurements of sunspot magnetic tilt angles. *The Astrophysical Journal*, **758**, 115.
- LIVINGSTON, W., HARVEY, J. W., MALANUSHENKO, O. V., & WEBSTER, L. (2006). Sunspots with the strongest magnetic fields. *Solar Physics*, **239**, 41-68.
- LONGCOPE, D., & CHOUDHURI, A. R. (2002). The orientational relaxation of bipolar active regions. *Solar Physics*, **205**, 63-92.
- LOVE, J. (1999). Reversals and excursions of the geodynamo. *Astronomy and Geophysics*, **40**, 14.
- MAUNDER, E. W. (1904). Note on the distribution of sun-spots in heliographic latitude, 1874-1902. *Monthly Notices of the Royal Astronomical Society*, **64**, 747-761.
- MAUNDER, E. W. (1922). The sun and sun-spots, 1820-1920. *Monthly Notices of the Royal Astronomical Society*, **82**, 534-543.
- MCCLINTOCK, B. H., & NORTON, A. A. (2013). Recovering Joy's law as a function of solar cycle, hemisphere, and longitude. *Solar Physics*, **287**, 215-227.
- MCCLINTOCK, B. H., & NORTON, A. A. (2016). Tilt Angle and Footpoint Separation of Small and Large Bipolar Sunspot Regions Observed with HMI. *The Astrophysical Journal*, **818**, 7.

- MCCLINTOCK, B. H., NORTON, A. A., & LI, J. (2014). Re-examining sunspot tilt angle to include anti-Hale statistics. *The Astrophysical Journal*, **797**, 130.
- MCINTOSH, S. W., LEAMON, R. J., GURMAN, J. B., OLIVE, J. P., CIRTAIN, J. W., HATHAWAY, D. H., ... & SITONGIA, L. (2013). Hemispheric asymmetries of solar photospheric magnetism: radiative, particulate, and heliospheric impacts. *The Astrophysical Journal*, **765**, 146.
- MCCOMAS, D. J., BARRACLOUGH, B. L., FUNSTEN, H. O., GOSLING, J. T., SANTIAGO-MUÑOZ, E., SKOUG, R. M., ... & BALOGH, A. (2000). Solar wind observations over Ulysses' first full polar orbit. *Journal of Geophysical Research: Space Physics*, **105**(A5), 10419-10433.
- MIESCH, M. S. (2012). The solar dynamo. *Philosophical Transactions of the Royal Society of London A: Mathematical, Physical and Engineering Sciences*, **370**, 3049-3069.
- MIESCH, M. S., & TEWELDEBIRHAN, K. (2016). A Three-Dimensional Babcock-Leighton Solar Dynamo Model: Initial Results with Axisymmetric Flows. *Advances in Space Research*.
- MORENO-INSERTIS, F. (1986). Nonlinear time-evolution of kink-unstable magnetic flux tubes in the convective zone of the sun. *Astronomy and Astrophysics*, **166**, 291-305.
- MORIN, J., DONATI, J. F., PETIT, P., DELFOSSE, X., FORVEILLE, T., ALBERT, L., ... & GASTINE, T. (2008). Large-scale magnetic topologies of mid M dwarfs. *Monthly Notices of the Royal Astronomical Society*, **390**, 567-581.
- MORIN, J., DONATI, J. F., PETIT, P., DELFOSSE, X., FORVEILLE, T., & JARDINE, M. M. (2010). Large-scale magnetic topologies of late M dwarfs. *Monthly Notices of the Royal Astronomical Society*, **407**, 2269-2286.
- MUÑOZ-JARAMILLO, A., SENKPEIL, R. R., WINDMUELLER, J. C., AMOUZOU, E. C., LONGCOPE, D. W., TLATOV, A. G., ... & YEATES, A. R. (2015). Small-scale and Global Dynamos and the Area and Flux Distributions of Active Regions, Sunspot Groups, and Sunspots: A Multi-database Study. *The Astrophysical Journal*, **800**, 48.
- NORTON, A. A., CHARBONNEAU, P., & PASSOS, D. (2014). Hemispheric coupling: comparing dynamo simulations and observations. *Space Science Reviews*, **186**, 251-283.
- NORTON, A. A., & GALLAGHER, J. C. (2010). Solar-cycle characteristics examined in separate hemispheres: phase, gnevyshev gap, and length of minimum. *Solar Physics*, **261**, 193-207.

- NORTON, A. A., & GILMAN, P. A. (2004). Magnetic field-minimum intensity correlation in sunspots: A tool for solar dynamo diagnostics. *The Astrophysical Journal*, **603**, 348.
- NORTON, A. A., & GILMAN, P. A. (2005). Recovering solar toroidal field dynamics from sunspot location patterns. *The Astrophysical Journal*, **630**, 1194.
- OSSENDRIJVER, M. (2003). The solar dynamo. *The Astronomy and Astrophysics Review*, **11**, 287-367.
- OTSUJI, K., KITAI, R., ICHIMOTO, K., & SHIBATA, K. (2011). Statistical study on the nature of solar-flux emergence. *Publications of the Astronomical Society of Japan*, **63**, 1047-1057.
- PARKER, E. N. (1955). The Formation of Sunspots from the Solar Toroidal Field. *The astrophysical journal*, **121**, 491.
- PARNELL, C. E., DEFOREST, C. E., HAGENAAR, H. J., JOHNSTON, B. A., LAMB, D. A., & WELSCH, B. T. (2009). A power-law distribution of solar magnetic fields over more than five decades in flux. *The Astrophysical Journal*, **698**, 75.
- PETRIE, G. J. D. (2012). Evolution of active and polar photospheric magnetic fields during the rise of cycle 24 compared to previous cycles. *Solar Physics*, **281**, 577-598.
- PEVTSOV, A. A., MALEEV, V. M., & LONGCOPE, D. W. (2003). Helicity evolution in emerging active regions. *The Astrophysical Journal*, **593**, 1217.
- RICHARDSON, R. S. (1948). Sunspot Groups of Irregular Magnetic Polarity. *The Astrophysical Journal*, **107**, 78.
- RIEUTORD, M., & RINCON, F. (2010). The Sun's Supergranulation. *Living Reviews in Solar Physics*, **7**, 2.
- SCHERRER, P. H., BOGART, R. S., BUSH, R. I., HOEKSEMA, J. A., KOSOVICHEV, A. G., SCHOU, J., ... & ZAYER, I. (1995). The solar oscillations investigation-Michelson Doppler imager. *Solar Physics*, **162**, 129-188.
- SCHERRER, P. H., SCHOU, J., BUSH, R. I., KOSOVICHEV, A. G., BOGART, R. S., HOEKSEMA, J. T., ... & TARBELL, T. D. (2012). The helioseismic and magnetic imager (HMI) investigation for the solar dynamics observatory (SDO). *Solar Physics*, **275**, 207-227.
- SCHMIDT, H. U. (1968). Magnetohydrodynamics of an Active Region. In *Structure and Development of Solar Active Regions* (Vol. 35, p. 95).
- SCHRIJVER, C. J. (1999). Active regions losing their moorings by subsurface RECONNECTION. *Solar Physics*, **188**, 331-344.

- SCHUSSLER, M., CALIGARI, P., FERRIZ-MAS, A., & MORENO-INSERTIS, F. (1994). Instability and eruption of magnetic flux tubes in the solar convection zone. *Astronomy and Astrophysics*, **281**, L69-L72.
- SCHÜSSLER, M., & REMPEL, M. (2005). The dynamical disconnection of sunspots from their magnetic roots. *Astronomy & Astrophysics*, **441**, 337-346.
- SOKOLOFF, D., KHLYSTOVA, A., & ABRAMENKO, V. (2015). Solar small-scale dynamo and polarity of sunspot groups. *Monthly Notices of the Royal Astronomical Society*, **451**, 1522-1527.
- STURROCK, P. A. (2008). Solar neutrino variability and its implications for solar physics and neutrino physics. *The Astrophysical Journal Letters*, **688**, L53.
- SIVARAMAN, K. R., GUPTA, S. S., & HOWARD, R. F. (1993). Measurement of Kodaikanal white-light images. *Solar physics*, **146**, 27-47.
- SIVARAMAN, K. R., GUPTA, S. S., & HOWARD, R. F. (1999). Measurement of Kodaikanal white-light images–IV. Axial tilt angles of sunspot groups. *Solar Physics*, **189**, 69-83.
- SMITH, S. F., & HOWARD, R. (1967). Structure and development of solar active regions. *IAU Sym. II, Kiepenheuer, O., Dordrecht, D. Reidel.(Ed.)*, 33.
- SOLANKI, S. K. (2003). Sunspots: an overview. *The Astronomy and Astrophysics Review*, **11**, 153-286.
- SOLANKI, S. K., & SCHMIDT, H. U. (1993). Are sunspot penumbrae deep or shallow? *Astronomy and Astrophysics*, **267**, 287-291.
- SPOERER, F. W. G. (1890). Prof. Spoerer's researches on Sun-spots. *Monthly Notices of the Royal Astronomical Society*, **50**, 251.
- SPRUIT, H. C. (1981). Motion of magnetic flux tubes in the solar convection zone and chromosphere. *Astronomy and Astrophysics*, **98**, 155-160.
- STENFLO, J. O., & KOSOVICHEV, A. G. (2012). Bipolar magnetic regions on the Sun: global analysis of the SOHO/MDI data set. *The Astrophysical Journal*, **745**, 129.
- SUN, X., HOEKSEMA, J. T., LIU, Y., & ZHAO, J. (2015). On polar magnetic field reversal and surface flux transport during solar cycle 24. *The Astrophysical Journal*, **798**, 114.
- TEMMER, M., RYBÁK, J., BENDÍK, P., VERONIG, A., VOGLER, F., OTRUBA, W., ... & HANSLMEIER, A. (2006). Hemispheric sunspot numbers R_N and R_S from 1945–2004: catalogue and N-S asymmetry analysis for solar cycles 18–23. *Astronomy & Astrophysics*, **447**, 735-743.

- TERNULLO, M. (2007). After a Century with Maunder's Butterfly Diagram. *MEMORIE-SOCIETA ASTRONOMICA ITALIANA*, **78**, 596.
- TERNULLO, M. (2010). The butterfly diagram internal structure. *Astrophysics and Space Science*, **328**, 301-305.
- TLATOV, A., ILLARIONOV, E., SOKOLOFF, D., & PIPIN, V. (2013). A new dynamo pattern revealed by the tilt angle of bipolar sunspot groups. *Monthly notices of the Royal Astronomical Society*, **432**, 2975-2984.
- ULRICH, R. K., & TRAN, T. (2013). The global solar magnetic field—identification of traveling, long-lived ripples. *The Astrophysical Journal*, **768**, 189.
- WANG, Y. M., COLANINNO, R. C., BARANYI, T. & LI, J. (2014). Active-region Tilt Angles: Magnetic versus White-light Determinations of Joy's Law. *The Astrophysical Journal*, **798**, 50.
- WANG, Y. M., & SHEELEY JR, N. R. (1989). Average properties of bipolar magnetic regions during sunspot cycle 21. *Solar physics*, **124**, 81-100.
- WANG, Y. M., & SHEELEY JR, N. R. (1991). Magnetic flux transport and the sun's dipole moment-New twists to the Babcock-Leighton model. *The Astrophysical Journal*, **375**, 761.
- WARNECKE, J., LOSADA, I. R., BRANDENBURG, A., KLEEORIN, N., & ROGACHEVSKII, I. (2015). Bipolar region formation in stratified two-layer turbulence. *Astronomy & Astrophysics*, **589**, A125.
- WEBER, M. A., & FAN, Y. (2015). Effects of Radiative Diffusion on Thin Flux Tubes in Turbulent Solar-like Convection. *Solar Physics*, **290**, 1295-1321.
- WEBER, M. A., FAN, Y., & MIESCH, M. S. (2013). Comparing simulations of rising flux tubes through the solar convection zone with observations of solar active regions: constraining the dynamo field strength. *Solar Physics*, **287**, 239-263.
- WEISS, N. O. (1971). Theories of Large Scale Fields and the Magnetic Active Cycle. In *Solar Magnetic Fields* (Vol. 43, p. 757).
- ZOLOTOVA, N. V., PONYAVIN, D. I., ARLT, R., & TUOMINEN, I. (2010). Secular variation of hemispheric phase differences in the solar cycle. *Astronomische Nachrichten*, **331**, 765-771.
- ZOLOTOVA, N. V., PONYAVIN, D. I., MARWAN, N., & KURTHS, J. (2009). Long-term asymmetry in the wings of the butterfly diagram. *Astronomy & Astrophysics*, **503**, 197-201.

Publications

Refereed Publications

- McClintock, B. H., & Norton, A. A. (2013). Recovering Joy's law as a function of solar cycle, hemisphere, and longitude. *Solar Physics*, **287**, 215-227.
- McClintock, B. H., Norton, A. A., & Li, J. (2014). Re-examining sunspot tilt angle to include anti-Hale statistics. *The Astrophysical Journal*, **797**, 130.
- McClintock, B. H., & Norton, A. A. (2016). Tilt Angle and Footpoint Separation of Small and Large Bipolar Sunspot Regions Observed with HMI. *The Astrophysical Journal*, **818**, 7.

Conference Contributions

- LWS/SDO-3/SOHO-26/GONG-2011 workshop "Solar Dynamics and Magnetism from the Interior to the Atmosphere", Oct. 31-Nov. 4, 2011
Poster by B.H. McClintock and A.A. Norton: *Recovering Joy's Law, Tilt Angle as a Function of Longitude, and Tilt Angle Change during Emergence*